Optical properties and gain characteristics of erbium-doped fiber amplifier(Dissertation_全文)

AUTHOR(S):

Ono, Shunsuke

OPTICAL PROPERTIES AND GAIN CHARACTERISTICS OF ERBIUM-DOPED FIBER AMPLIFIER

SHUNSUKE ONO

OPTICAL PROPERTIES AND GAIN CHARACTERISTICS OF ERBIUM-DOPED FIBER AMPLIFIER

SHUNSUKE ONO

Preface

This thesis is a summary of my works carried out at Kyoto University for three years. In this thesis, my interests are focused on the gain characteristics and the optical properties of silica-based erbium doped fiber (EDF) as an erbium-doped fiber optical amplifier (EDFA). A series of investigations on silica-based EDF gain performance was carried out including numerical simulations and experimental measurements.

In the last decade, the Internet has come into explosively use and become one of the basic infrastructures of our life. EDFA backs up the information infrastructure from the basic physical layer. Now EDFA becomes indispensable key optical device to build up the optical fiber network. On the other hand, as the ultra fast optical network comes to realize, it is much anticipated that there occur several problems associated with the gain performance of EDFA, which lead to the degradation of the optical amplifier performance. These problems are originated from the optical properties of the Er^{3+}-doped glass, and few efforts have been dedicated to study the interactions that have influences on the spectral profile of the gain bandwidth and particularly the relation between the glass composition and the spectroscopy of erbium while the extensive work on the determination of pump wavelength, pumping configuration, improvement of noise performance have been made. Therefore, it is possible to extract more potential abilities of erbium-doped silicate glasses and fibers for advanced EDF by approaching from the material side.

In this present study, the potential abilities and the problems of erbium-doped silica-based fiber were investigated by the means of spectroscopic measurements and numerical simulation that had not been applied to the study on the optical amplifier performance of erbium-doped fiber. With that, this thesis showed the uncultivated field with relation to EDFA and gave the new knowledge on the performance of EDFA.

I wish the results of the present study can contribute to the improvement of the performance of optical amplifier and lead to the development of the basic information infrastructure.

Sakyo, Kyoto
January 2005

Shunsuke Ono

Contents

Chapter 1

General introductions for evolution of optical amplifier and optical transmission systems

1. General introduction for gain media using 1.5 μ m stimulated emission of Er^{3+} ion.

1-1. Erbium-Doped Fiber as Gain Media

The object of this study is to investigate the gain characteristics and optical properties of silica-based erbium doped fiber (EDF) in fiber form to improve the optical amplifier performance of silica-based EDF.

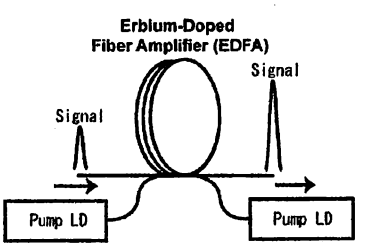

Fig. 1 EDFA (Erbium-Doped Fiber Amplifier)

Erbium-doped fiber amplifier (EDFA) (Fig. 1), erbium-doped waveguide amplifier (EDWA) and erbium-doped fiber ring laser (EDFL) (Fig. 2) are the gain media using 1.5 μ m stimulated emission of Er^{3+} ion. Particularly, silica-based EDFA has been used and known to be as one of the most important key devices in the optical

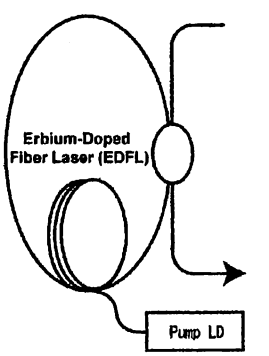

Fig. 2 EDFL (Erbium-Doped Fiber Ring Laser)

telecommunication and optical device areas. [1-9].

Now, in the optical telecommunication area, EDFA has come into wide use in order to amplify the modulated optical pulse signal in the 1.5 μ m wavelength region with pumping laser diode(LD) in the wavelength-division multiplexing (WDM) optical system. So far, many trans-oceanic and terrestrial WDM optical transmission systems using EDFA as repeater have been studied and realized in telecommunication system [10-16].

It would not be too much to say that the EDF as optical amplifier brought the explosive improvement and widespread of the Internet as we know today. This widespread of the usage of EDF as an optical amplifier in optical transmission systems is explicable based on two technical points.

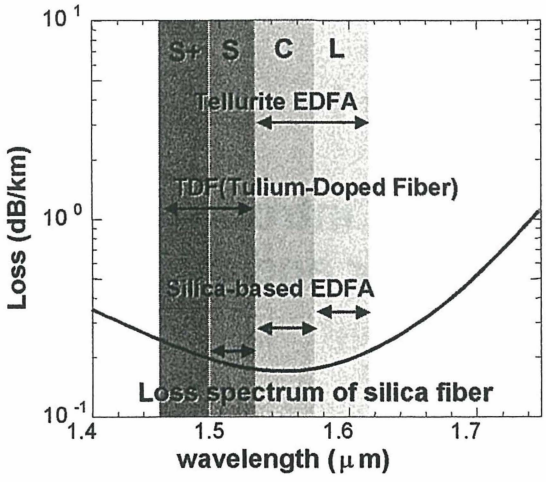

Fig. 3 Loss spectrum of silica-based optical telecom silica-based fiber

One is the favorable suitability of EDF to the optical transmission system silica fiber that has the most low loss region in 1.5 μ m wavelength region as shown in Fig. 3. The other is that erbium-doped fiber has the induced emission at 1.5 μ m from the $^4I_{13/2}$ level of erbium ion pumped by 980nm and/or 1480nm LD to amplify 1.5 μ m optical signal as shown in Fig. 4.

These advantages of silica-based EDF have been made silica-based EDF play major roles in the optical transmission system compared with some other optical amplifiers.

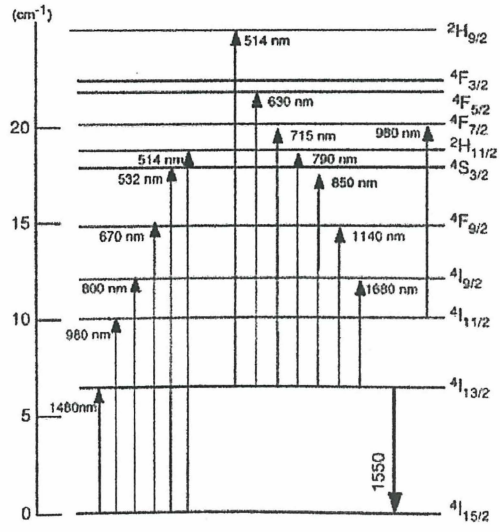

Fig. 4 Optical transition diagram of Er^{3+} ion

Now, in order to exploit the new transmission window of the silica-based telecom fiber, many studies on non-silicate based rare earth-doped optical amplifier are following the evolution in the telecom system by EDFA. Thulium-doped fiber (TDF) is one of the most well known promising fiber glass for the S-band optical amplifier and utilizes stimulated emission between the $^3H_4$ and the $^3F_4$ energy level [17, 18]. The population inversion between the $^3H_4$ and the $^3F_4$ levels is created by the two-step excitation process because the fluorescence lifetime of the upper level $^3H_4$ is shorter compared with that of the lower level $^3F_4$. Therefore, the power conversion efficiency of Tm^{3+} doped fiber is rather low. This becomes one of the barriers to make TDFA cost-efficient optical amplifier in the optical transmission system. Also the suitability of TDF to the silica-based telecom fiber is not so good as that of EDF. This becomes one of the problems to be solved for the realization of TDFA in optical transmission system.

1-2. Evolution of Rare Earth-Doped Glass

The invention of the EDFA in the late 1980s was one of the major events of optical communication system. Before the emergence of EDFA, optical telecommunication system in the 1980s required the optical signals to be converted back into electronic signals at the each repeater. EDFA removes this step from photo-electric conversion process in many repeaters in the system. This simplification of amplification scheme should be pointed out for the most remarkable contribution of EDFA to the improvement of the optical transmission system. In early 1960s, a study on glasses doped with rare earth ion, which leads to the much-anticipated emergence of EDFA and other rare earth doped amplifiers today, was started by E. Snitzer. He proposed rare earth-doped fiber cavity laser firstly and showed the shape of the optical fiber amplifiers and lasers what we know today [19-22].

Nevertheless, for many years rare-earth doped fibers remained relatively obscure with performance far inferior to that offered by "bulk" forms. This changed in the mid 1980s, with the realization of rare-earth doped single-mode high silica fibers with low loss. In 1985, S. B.

Poole suggested that optical fiber amplifier could be realized with the fibers doped with the rare earth ion [23]. A research group of Southampton University showed that optical fibers doped with the rare earth erbium ion can exhibit laser gain at a wavelength near 1.55 μ m [24-26].

In 1987, the first erbium-doped optical fiber amplifier was made [27].

In 1989, the erbium-doped optical fiber amplifier was pumped by 1480nm InGaAsP semiconductor laser and could obtain 12.5dB in 1.55 μ m region [28].

So far, the basic properties of EDF have been extensively studied numerically and experimentally and many breakthroughs have been followed at explosive rate [29-38]. Thus, EDFA provided new region to optical fiber communication transmission window centered at around 1550nm and research into technologies that allow high bit-rate transmission over long distances.

1-3. Erbium-Doped Fiber in Optical Transmission System

Now the increase of the number of optical signal channels in the C-band wavelength region accelerates the installation of dense wavelength-division multiplexing (DWDM) technique particularly into the trans-oceanic optical transmission system in order to suppress the non-linear effects in fiber [39-41]. The installation of DWDM technique into optical transmission system has the possibility to enhance the degradation of optical pulse due to the nonlinear optical effect [42-44]. Therefore, the chromatic dispersion management scheme in transmission fiber and the new pulse modulation format such as the combination of DPSK (differential phase shift keying) with CSRZ (Carrier Suppressed Return-to-Zero) or RZ (Return-to-Zero) have been keenly proposed for the key optical modulation for the next optical transmission system [45-47]. DWDM optical transmission system also requires a flat gain spectrum of EDFA across the whole usable bandwidth. In general, it is difficult to achieve the gain flatness in DWDM trans-oceanic system in particular because EDFA has the narrow high gain in the C-band wavelength region (1530nm-1570nm) centered at 1550nm. Therefore, to equalize the gain spectrum profile after transmission completely, the combination of EDF and/or

Poole suggested that optical fiber amplifier could be realized with the fibers doped with the rare earth ion [23]. A research group of Southampton University showed that optical fibers doped with the rare earth erbium ion can exhibit laser gain at a wavelength near 1.55 μ m [24-26].

In 1987, the first erbium-doped optical fiber amplifier was made [27].

In 1989, the erbium-doped optical fiber amplifier was pumped by 1480nm InGaAsP semiconductor laser and could obtain 12.5dB in 1.55 μ m region [28].

So far, the basic properties of EDF have been extensively studied numerically and experimentally and many breakthroughs have been followed at explosive rate [29-38]. Thus, EDFA provided new region to optical fiber communication transmission window centered at around 1550nm and research into technologies that allow high bit-rate transmission over long distances.

1-3. Erbium-Doped Fiber in Optical Transmission System

Now the increase of the number of optical signal channels in the C-band wavelength region accelerates the installation of dense wavelength-division multiplexing (DWDM) technique particularly into the trans-oceanic optical transmission system in order to suppress the non-linear effects in fiber [39-41]. The installation of DWDM technique into optical transmission system has the possibility to enhance the degradation of optical pulse due to the nonlinear optical effect [42-44]. Therefore, the chromatic dispersion management scheme in transmission fiber and the new pulse modulation format such as the combination of DPSK (differential phase shift keying) with CSRZ (Carrier Suppressed Return-to-Zero) or RZ (Return-to-Zero) have been keenly proposed for the key optical modulation for the next optical transmission system [45-47]. DWDM optical transmission system also requires a flat gain spectrum of EDFA across the whole usable bandwidth. In general, it is difficult to achieve the gain flatness in DWDM trans-oceanic system in particular because EDFA has the narrow high gain in the C-band wavelength region (1530nm-1570nm) centered at 1550nm. Therefore, to equalize the gain spectrum profile after transmission completely, the combination of EDF and/or

distributed Raman amplification is being proposed for the amplification scheme in the next high bit-rate optical transmission system [47, 48-50].

Now over 40Gb/s (160Gb/s) optical transmission system based on the amplification scheme using EDFA is being already under evaluation using the installed terrestrial commercial fiber system as shown in Fig. 5 [51]. In the near future, it is much anticipated that EDFA will also play major roles in optical amplification scheme in next high bit-rate system. From the design of optical transmission system, two things are mainly needed for EDF as optical amplifier. One is the expanding of emission bandwidth, and the other is high energy efficiency. Expanding the bandwidth of optical amplifier is one of the easiest ways in order to reduce non-linear effect in DWDM optical transmission system because each adjacent channels of optical signal can be located with broad channel spacing. Therefore, the enhancement of the bandwidth of silica-based EDF has been major interest not only in the C-band wavelength region but the L-band (1575nm-1605nm) and the S-band (1450nm -1530nm) wavelength regions. On the other hand, high energy efficiency is strongly needed from the aspect of the realization of cost-efficient optical transmission system, which leads to the decrease of the number of pumping LD and the simplification of the system design.

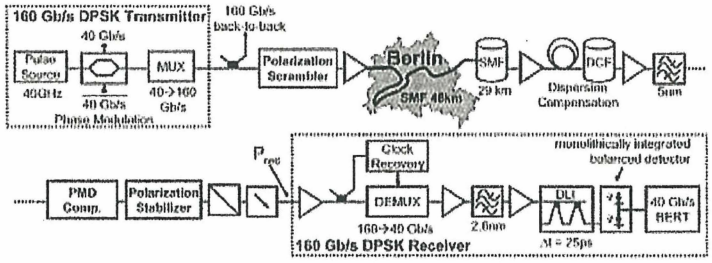

Fig. 5 Experimental setup for 160Gb/s DPSK transmission over installed fiber in Berlin [51].

To realize the optical amplifier in the S-band and L-band regions, silica-based S-band and L-band EDFAs have been proposed [31-33]. The L-band EDFA has reached at practical use and the feasible study on the L-band EDFA to install it into optical transmission system has almost done today. The modification of the gain flatness in the L-band region has been continued to blush up the gain performance with the distributed Raman amplification technique

[49, 50]. On the other hand, the amplification possibilities of the S-band EDFA in optical transmission system have been evaluated in some studies [31, 54-56].

1-4. Various Other Glasses for Erbium Hosts

In addition, various glass systems have been investigated as hosts for Er^{3+} ion in order to realize the optical amplifier that has broad bandwidth and high efficiency so far. To enhance the optical transmission bandwidth of the 1.5 μ m emission of Er^{3+} ion, Er^{3+}-doped tellurite glass has been proposed by NTT research group. Tellurite glass has the good stability, rare-earth ion solubility, a slow corrosion rate, a relative low phonon energy among oxide glass formers and a high refractive index [52]. Therefore, using tellurite glass, Er^{3+} -doped tellurite amplifier and fiber lasers has been studied [53-55].

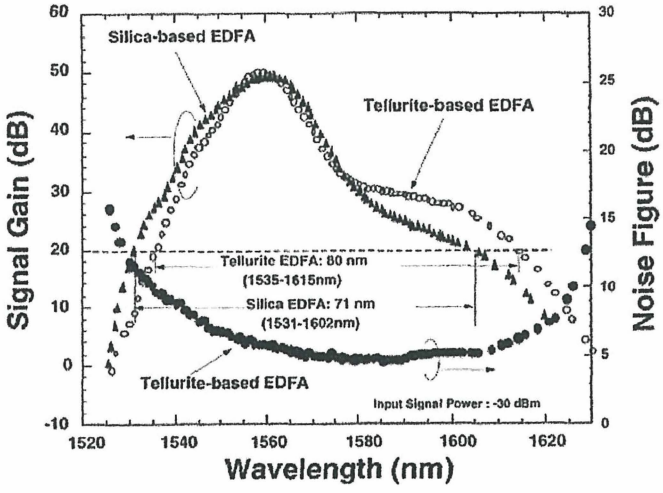

Fig. 6 Gain spectrum of Er^{3+}-doped tellurite glass fiber [56].

For the bandwidth of Er^{3+} doped-tellurite amplifier, it has been reported to hold the 20dB gain about 80nm (1535nm-1615nm) as shown in Fig. 6 [56]. However, tellurite glass does not have the favorable suitability of to the telecom silica fiber which leads to the high splice loss. This unsuitability of tellurite glasses is very major problem to the promotion of the realization of Er^{3+} -doped tellurite amplifier. For the flattened gain performance of optical amplifier, Er^{3+}-doped

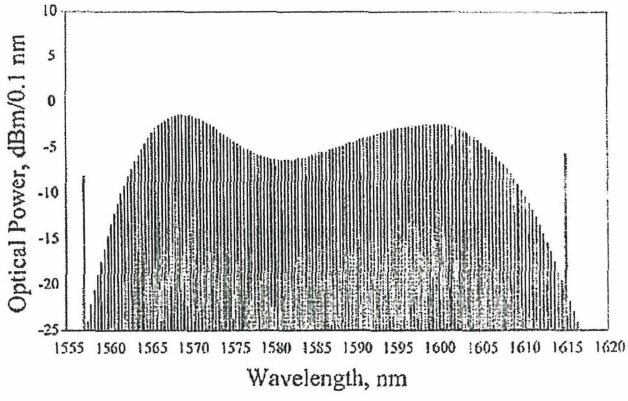

Fig. 7 Optical power spectrum of La-co doped bismuth-based glass fiber [61].

fluoride glass are capable of realizing a flat gain over a broadband width of 1530nm-1560nm [57-59]. Recently, Er^{3+}-doped bismuth-based glass has been also proposed for one of the other promising host glasses for the wideband optical amplifier in the C-band and the L-band wavelength regions. It was reported that considerably high Er^{3+} could be doped in bismuth-based glass without quenching, which can lead to the shortening of fiber length [60]. Based on these advantages, the gain performance of the L-band EDFA based on the 2.5m La-co-doped bismuth-based glass in DWDM system was shown (Fig. 7) [61].

In order to achieve high efficiency, it has been needed to suppress the concentration quenching of the emission of Er^{3+} ion [62, 63]. So far, Er^{3+}-Yb^{3+} ion doped phosphate glass planar amplifiers and Er^{3+}-doped fluoride fiber amplifiers have been constructed and their amplification characteristics studied [55, 64-66]. Phosphate glasses can be doped with high concentrations of Er^{3+} without quenching, making it possible to construct planar amplifiers with a short waveguide length. In addition, Er^{3+}-doped fluorophosphate glass was also investigated in order to achieve the gain flatness and high output power for the optical amplifier in WDM optical transmission system [67-72].

However, compared with silica-based EDFA, no other optical amplifier that shows the more favorable suitability to the optical transmission system has been realized so far. In addition, from the aspect of the optical system design, higher bit-rate TDM over 40Gb/s becomes the latest trend of both the trance-oceanic and terrestrial optical transmission system. And the use of silica-based EDFA with Raman amplifier becomes the major amplification scheme in such optical transmission systems. Therefore, silica-based erbium-doped fibre is considered to remain in the major promising for the optical amplifier in the C-band and new-band wavelength regions in the future. However, there still remain associated problems with EDFA such as the concentration quenching [60-65] and gain spectral hole burning [73-81], which leads to the degradation of performance of optical transmission system. It is possible to extract more potential abilities of erbium-doped silicate glasses and fiber for advanced EDF by

resolving these problems.

1-5. Instructions for Chapters

For such reasons, we have been investigated the gain characteristics and the optical properties of silica-based erbium doped fiber (EDF) in fiber form to improve the optical amplifier performance of silica-based EDF. In the present study, the optical properties and gain characteristics of silica-based EDF were investigated with experimental measurements and numerical calculations in order to extract more potentials and improve the transmission performance of silica-based EDF.

Chapter 2 concerns the optical properties of Al_2O_3-doped Er^{3+}-doped fibers with different Al_2O_3 content for the improvement of the optical amplifier performance. In Chapter 3 and 4, the numerical simulator to predict the optical amplifier performance was built, which could take into account of the Stark energy structure of Er^{3+} ion and the degradation of the population inversion due to the energy transfer between Er^{3+} ions. Using these simulators, the evaluation of the S-band gain characteristics of EDFA and the effects of the concentration quenching of Er^{3+} ions on the degradation of the gain performance were evaluated precisely. Chapter 5 and 6 describe the studies on the physical mechanism of gain spectral hole burning (GSHB) in EDFA. The Er^{3+} ion concentration dependence of the gain spectral hole was firstly investigated. In addition, the relation between the Stark manifold structure of Er^{3+} ion and the hole formation mechanism was discussed based on a proposed hole shape model. The contents of the respective Chapters are as follows.

In Chapter 2, precise spectroscopic absorption measurements of Er^{3+}- doped aluminosilicate fibers with different Al_2O_3 content were performed with the Judd-Ofelt analysis. From the Judd-Ofelt analysis, the Ω_2 parameters of Er^{3+} ions in the fibers were found to be about three times as large as those in alumino-silicate bulk glasses. Due to the enhancement of Ω_2 parameters, the line strength of the hypersensitive transition $^2H_{11/2} \rightarrow {}^4I_{15/2}$ become much stronger in a fiber form than in a bulk glass. This indicates that the distortions of the ligand

field around the Er^{3+} ions are more enhanced in a fiber form. Furthermore the Ω_6 and the Ω_2 parameter increased with increasing Al_2O_3 content up to 20000ppm. This Al_2O_3 content dependence of the Ω_6 parameter was consistent with that of the line strength and the spontaneous emission probabilities of the transition corresponding to the $^4I_{13/2} \rightarrow ^4I_{15/2}$. The change of the coordination number of Al^{3+} ion is discussed in connection with the change of the solid state parameters.

In Chapter 3, numerical and experimental evaluations of the gain characteristics of silica-based erbium-doped fiber (EDF) were performed in the S-band wavelength region (1450nm-1530nm). With the gain spectrum measurements in the 1.5 μ m region from 77K up to 373K, the increase of the gain in the S-band wavelength region was observed with increasing temperature. This change of the gain in the S-band wavelength region was verified by the numerical simulation based on the temperature-dependent McCumber relation considering the thermal distribution over the Stark manifolds of Er^{3+} energy levels. As a result, it was found that the change in the thermal distribution of the population densities of the upper Stark manifolds within the $^4I_{13/2}$ level contributes to the improvement of the gain in the S-band wavelength region. The validity of the temperature-dependent McCumber simulation model based on the two level system from 77K to 373K is also shown.

In Chapter 4, the effect of Er^{3+} ion concentration quenching on the gain characteristics of silica-based erbium doped fiber (EDF) was investigated at 77K and 300K, focusing on the concentration quenching mechanism of Er^{3+} ions. With the saturation gain measurements at 77K, the interaction between Er^{3+} ions were verified to exist, which leads to the degradation of the gain characteristics of EDFA at room temperature. The concentration quenching effect due to this interaction between erbium ions was examined by the Er^{3+} ion concentration-dependent gain simulation model, which was based on the two level system energy model.

As a result, it was estimated that even about 2% paired Er^{3+} ions in silica-based EDF can cause about the 10% degradation of population densities of the $^4I_{13/2}$ level, which leads to about

the 1dB degradation of the gain spectrum in the C-band wavelength region.

The degradation of the population densities of the $^4I_{13/2}$ level in connection with the concentration quenching mechanism is discussed.

In Chapter 5, the effect of Er^{3+} concentration on the gain spectral hole burning in silica-based EDF at 77K was investigated precisely in both C-band and L-band wavelength regions. When a saturation signal of longer wavelength than 1530nm was input into a silica-based EDF, two gain spectral holes were observed at around 1530nm and the wavelength of the saturation signal. The depth of the second hole at around 1530nm was found to become shallower in the silica-based EDF that had higher Er^{3+} content. This Er^{3+} ion concentration dependence of the second hole depth suggests that the contribution of the energy transfer interaction between Er^{3+} ions exists in the Stark levels of the $^4I_{13/2}$ manifold to the relaxation process and plays an important role in the gain spectral hole formation at 77K. This is the first report of the Er^{3+} concentration effect on the gain spectral hole burning in EDF.

In Chapter 6, the signal wavelength dependence of gain spectral hole burning in erbium-doped fiber (EDF) was investigated at 77K. The main hole accompanied with two side holes was clearly burned when the saturation signal was input at 1530nm. A side hole was also observed when the wavelength of the saturation signal was varied.

Two side holes were also observed in other EDFs which had different Er^{3+} ion content. As in the case of the second hole, the same Er^{3+} ion concentration dependence of the side holes was also observed for the two side hole depths. These results indicates that gain spectral hole burning can have more wide-raging impact on the gain shape and the gain fluctuation of EDF than expected so far. In addition, the depth of the second hole did not decrease monotonically and showed the interesting saturating signal wavelength dependence when the wavelength of saturating signal was varied across100nm bandwidth in the C-band and the L-band wavelength regions. The gain spectral hole formation mechanism is discussed in connection with the Stark manifold structure of Er^{3+} ion considering these characteristics of the holes.

References

[1]. P. Myslkinski, J. Chrostowski, J. A. Koningsten, and J. R. Simpson, "High power Q-switched erbium-doped fiber laser," IEEE J. Quantum Electron., vol. 28, no1, pp. 371-377, 1992.

[2]. W. L. Barnes, P. R. Morkel, L. Reelie, and D. N. Payne, "High –quantum efficiency Er^{3+} fiber lasers pumped at 980nm," Opt. Lett., vol. 14, no18, pp1002-1004, 1989.

[3]. D. J. Rchardson, R. I. Laming, D. N. Payne, V. J. Matsas, and M. W. Phillips, "Pulse repetition rates in passive self-starting , femtosecond soliton fiber laser," Electron. Lett., vol 27, no16, pp.1451-1453, 1992.

[4]. V. J. Matsas, D. J. Ridhardson, T. P. Newson, and D. N. Payne," Characterization of a self-starting passively mode-locked fiber ring laser that exploits nonlinear polarization evolution," Opt. Lett., vol. 18, no5, pp. 358-360, 1993.

[5]. V. C. Lauridsen, J. H. Povlsen, and P. Varming, "optimizing erbium-doped DFB fiber laser," Electron. Lett., vol. 35, pp. 300-302, 1999.

[6]. L. Moller, Y. Su, C. Xie, R. Ryf, X. Liu, X,. Wei, and S. Cabot, "All-optical phase construction of ps-pulses from fiber lasers for coherent signaling at ultra-high data Rates(>160Gb/s)," *in the Proceedings of Optical Fiber Communications2004*, OFC'04, PD 20, Los Angels, 2004.

[7]. J. Lee and J. H. Shin, "Optical gain at 1.5 μ m in nanocrystal Si sensitized, Er-doped silica waveguide using top-pumping 470nm LD," *in the Proceedings of Optical Fiber Communications2004*, OFC'04, PD 19, Los Angels, 2004.

[8]. D.M. Baney, and J. Stimple, "WDM EDFA gain characterization with a reduced set of saturating channels", IEEE Photon. Technol. Lett., vol.8, no. 12, pp.1615-1617, 1996.

[9]. H. Masuda, S. Kawai, K. Suzuki, K. Aida, "Wide band and low noise optical amplification using distributed Raman amplifiers and erbium-doped fiber amplifiers", *in the Proceedings of European Conference on Optical Communication 1998,* ECOC'98, vol. 1, pp. 51 -52, 1998.

[10]. M. Jinno, T. Sakamoto, J. Kani, S. Aisawa, K. Oda, M. Fukui, H. Ono and K. Oguchi, "First demonstration of 1580 nm wavelength band WDM transmission for doubling usable bandwidth and suppressing FWM in DSF," Electron. Lett. vol. 33, no. 10, pp.882-883, 1997.

[11]. G. Vareille, F. Pitel, R. Uhel, G. Bassier, J-P. Collet, G. bourret, J-F. Marcerou, "340Gb/s(34 x10 Gb/s, 50GHz spcing DWDM) straight line transmission over 6380km with full system implementation assessment," OFC'99, PD 18, San Diego, 1999.

[12]. M. Nissov, "100Gb/s (10 x 10Gb/s) WDM transmission over 7200km using distributed Raman amplification, "*in the Proceedings of European Conference on Optical Communication 1997,* ECOC'97, PD pp. 9-12, 1997.

[13]. N. S. Bergano, C. R. Davidson, M. A. Mills, P. C. Corbett, S. G. Evangelides, B. Pedersen, R. Menges, J. L. Zyskind, J. W. Sulhoff, A. K. Srivasta, C. Wolf and J. Judlins, "Long-haul transmission using optimum channel modulation :a 160 Gb/s (32 x 5Gb/s) 9300km demonstration," *in the Proceedings of Optical Fiber Communications '97,* OFC'97, PD.16, Dallas, 1997.

[14]. John M. Jacob, Ekaterina A. Golovchenko, Alexei N. Pilipetskii, Gary M. Carter, "10-Gb/s Transmission of NRZ over 10 000 km and Solitons over 13 500 km Error-Free in the Same Dispersion-Managed System," IEEE Photon. Technol. Lett., vol. 9, no. 10, pp. 1412-1414, 1997.

[15]. M. Murakami, T.Matsuda, and T. Inami,"Quatrter Terabit over 9288km WDM transmission experiment using non linear supported RZ pulse in high order fiber dispersion managed line," *in the Proceedings of European Conference on Optical Communication 1998,* ECOC'98, Madrid.

[16]. J-B. Lerot, P. Marmier, C. Laval, and O.Gautheron,"32 x 10Gb/s transmission over 8000km using hybrid Raman-Erbium doped fiber optical amplifiers," *in the Proceedings of Optical Fiber Communications '99,* OFC'99, WJ3-1, San Diego, 1999.

[17]. T. Komukai, T. Yamamoto, T. Sugawa, Y. Miyajima, "1.47 μm band Tm3+ doped fluoride fibre amplifier using a 1.064 μm upconversion pumping scheme," Electronics Letters vol.29, no. 1, pp. 110-112, 1993.

[18]. T. Sakamoto, M. Shimizu, T. Kanamori, Y. Terunuma,Y. Ohishi, M. Yamada, and S. Sudo, "1.4-μm-band gain characteristics of a Tm-Ho-doped ZBLYAN fiber amplifier pumped in the 0.8-μm band," IEEE Photon. Technol. Lett. vol. 7, no9, pp. 983-985, 1995.

[19]. E. Snitzer, "Optical maser action of Nd^{+3} in a barium crown glass," Phys. Rev. Lett. 7, pp. 444–446, 1961.

[20]. E. Snitzer, "Neodymium glass laser", in Proc. 3rd Int. Conf. Quantum Electronics, Paris, France, pp. 999-1019, 1963.

[21]. C. J. Koester and E. Snitzer, "Amplification in a fiber laser", Appl. Opt. 3, pp. 1182-1186, 1964.

[22]. E. Snitzer, "Proposed fiber cavities for optical masers", J. Appl. Phys., vol. 32, pp. 36-39, 1961.

[23]. S. B. Poole, D. N. Payne, and M. E. Fermann, "Fabrication of low loss optical fibres containing rare-earth ions", Electron. Lett. vol. 21, pp. 737-738 ,1985.

[24]. R. J. Mears, L. Reekie, S. B. Poole, and D. N. Payne, "Neodymium-doped silica single-mode fibre laser", Electron. Lett. vol. 21, pp. 738-740, 1985.

[25]. S. B. Poole, D. N. Payne, M. E. Fermann and R. Laming, "Fabrication and Characterization of low-loss optical fibres containing rare-earth ions", J. Lightwave Technol., vol. 4, no. 7, pp. 870-876, 1986.

[26]. R. J. Mears, L. Reekie, S. B. Poole, and D. N. Payne, "Low-threshold tunable CW and Q-switched fibre laser operating at 1.55 μm", Electron. Lett. vol. 22, pp. 159-160, 1986.

[27]. R. J. Mears, L. Reekie, I. M. Jauncey, and D. N. Payne, "Low-noise erbium-doped fibre amplifier operating at 1.54 μm", Electron. Lett., vol. 23, pp. 1026-1028, 1987.

[28]. M. Nakazawa, Y. Kimura, and K. Suzuki, "Efficient Er^{3+}-doped optical fiber amplifier

pumped by a 1.48 mm InGaAsP laser diode," Appl. Phys. Lett., vol. 54, pp. 295-297, 1989.

[29]. K. I. Ueda, H. Sekiguchi, and H. Kan, "1 kW cw output from fiber embedded lasers", in Proc. Conference on Lasers and Electro-Optics, Long Beach, USA, 2002, post-deadline paper CPDC4.

[30]. F. Massicott, R. Wyatt, B.J. Ainslie and S.P. Craig-Ryan, "Efficient, high power, high gain, Er^{3+} dope silica fiber amplifier," Electron. Lett., vol. 26, pp. 1038-1039, 1990.

[31]. E. Ishikawa, M. Nishikawa, Y. Sato, C. Ohshima, Y. Sugaya, and J. Kumasako, "Novel 1500nm-band EDFA with discrete Raman amplifier," *in the Proceedings of European Conference on Optical Communication 2001,* ECOC2001 paper PD.A.1.2, 2001.

[32]. J. F. Massicott, R. Wyatt, and B. J. Ainslie, "Low noise operation of Er3+ doped silica fiber amplifier around 1.6μm," Electron. Lett., vol. 28, pp. 1924-1925, 1992.

[33]. J. F. Massicott, J. R. Armitage, R. Wyatt, B. J. Ainslie, and S. P. Craigryan, "High gain, Broadband, 1.6μm Er3+ doped silica fiber amplifier," Electron. Lett., vol. 26, pp. 1645-1646, 1990.

[34]. H. Ono, M. Yamada, and Y. Ohishi, "Gain-flattened Er^{3+}-doped fiber amplifier for a WDM signal in the 1.57-1.60-μm wavelength region," IEEE Photon. Technol. Lett., vol. 9, pp. 596-598, 1997.

[35]. R. Olhansky, "Noise figure for erbium-doped optical fiber amplifiers," Electron. Lett., vol 24, no. 22, pp. 1363-1364, 1988.

[36]. J. R. Armitage "Three-level fiber laser amplifier: a theoretical model," Applied optics, vol 27, no. 23, pp. 4831–4836, 1988.

[37]. E. Desurvire, J. L. Zyskind, and J. R. Simpson, "Study of spectral dependence of gain saturation and effect of inhomogeneous broadening in erbium-doped aluminosilicate fiber amplifiers," IEEE Photon. Technol. Lett., vol. 2, no. 4, pp. 246-248, 1990.

[38]. C. R. Giles and E. Desurvire, "Modeling erbium-doped fiber amplifiers," IEEE J. Lightwave Technol., vol. 9, pp. 271-283, 1991.

[39]. H. Suzuki, J. Kani, H. Masuda, N. Takachio, K. Iwatuki, Y. Tada and M. Sumida, "25GHz-spaced, 1Tb/s(100x10Gb/s) Super Dense-WDM Transmission in the C-band over a Dispersion Shifted Fiber Cable Employing Distributed Raman Amplification," *in the Proceedings of European Conference on Optical Communication '99,* ECOC'99, PD2-4, pp. 30-31, 1999.

[40]. H. Taga, S. Nakagawa, and K. Goto, "Ultra-dense 80 EDM transmission experiments over 3800km with 0.34bit/s/Hz spectral efficiency," OECC2000, pp. 14-15, 2000.

[41]. M. Nissov, J. X. Cai, M. I. Hayee, A. N. Pilipetskii, S. G. Evangelides Jr., B. Pedersen, N. Ramanujam, C. R. Davidson, C. J. Chen, M. A. Mills, R. Menges, P. C. Corbett, C. Rivers, and N. S. Bergano, "32x20Gb/s Transmission over Trans-Atlantic Distance (6200Km) with 31% Spectral Efficiency," *in the Proceedings of Optical Fiber Conference 2000,* OFC'2000, PD30, Baltimore, 2000.

[42]. D. Marcuse, A. R. Chraplyvy, and R. W. Tkach, "Dependence of cross-phase modulation on channel number in fiber WDM systems," IEEE/OSA J. Lightwave Technol., vol. 12, no. 5, pp. 885-890, 1994.

[43]. D. G. Schadt, "Effect of amplifier spacing on four-wave mixing in multichannel coherent communications," Electron. Lett., vol. 27, no. 20, pp. 1805-1807, 1991.

[44]. G. P. Agrawal, Fiber-Optical Communication System, John Wiley & Sons, Inc., New York, 1997.

[45]. I. Morita and N. Edagawa, "50GHz-spaced 64x42.7Gbit/s transmission over 8200km using ore-filtered CS-RZ DPSK signal and EDFA repeaters," *in the Proceedings of European Conference on Optical Communication 2003,* ECOC'03, Th4.3.1, Rimini, Italy.

[46]. L. Becouarn, G. Vareille, S. Dupont, P. Plantady, and J. F. Marcerou, "42x42.7Gb/s RZ-DPSK transmission over a 4820km long NZDSF deployed line using C-band-only EDFAs," *in the Proceedings of Optical Fiber Communications 2004,* OFC' 04, PD 37, Los Angels, 2004.

[47]. G. Charlet, E. Corbel, J. Lazaro, A. Klekamp, R. Dischler, P. Tran, W. Idler, H. Mardoyan,

A. Konczykowska, F. Jorge, S. Bigo, A. Klekamp, R. Discheler, W. Idler and C. Charlet " WDM Transmission at 6Tbit/s capacity over transatrlantic distance, using 42.7Gb/s Differential Phase-Shift Keying without pulse carver," *in the Proceedings of Optical Fiber Communications' 2004,* OFC'04, PD 36, Los Angels, 2004.

[48]. A. H. Gnauck et al.,"2.5Tb/s (64x42.7Gb/s) transmission over 40x100km NZDSF using RZ-DPSK format and all Raman amplified spans," *in the Proceedings of Optical Fiber Communications 2002,* OFC'02, FC2, Anaheim, 2002.

[49]. C. Rasmussen, T. Fjelede, J. Bennike, F. Liu, S. Dey, B. Mikkelsen, P. Serbe, P. van der Wagt, D. Harris, D. Gapontsev, V. Ivshin, and P. Reeves-Hall," DWDM 40G transmission over trans-Pacific distance (10000km) using CS-DPSK, enhanced FEC and all-Raman amplified 100km Ultra Wave™ fiber spans," *in the Proceedings of Optical Fiber Communications 2003,* OFC'03, PD18, Atlanta, GA, 2003.

[50]. A. H. Gnauck, J. Leuthold, C. Xie, I. Kang, S. Chandrasekhar, P. Bernasconi, C. Doerr, and L. Buhl, J. D. Bull, N. A. F. Jaeger, H. Kato, and A. Guest, "6x42.7Gb/s transmission over ten 200km EDFA-amplified SSMF spans using polarization-alterneting RZ-DPSK, " *in the Proceedings of Optical Fiber Communications2004,* OFC'04, PD 18, Los Angels, 2004.

[51]. S. Kieckbusch, S. Ferber, H. Rosenfeldt, R. Ludwig, C. Boerner, A. Ehrhardt, E. Brinkmeyer, and H. G. Weber, "Adaptive PMD compensation in 160Gb/s DPSK transmission over installed fiber," *in the Proceedings of Optical Fiber Communications 2004,* OFC'04, PD 18, Los Angels, 2004.

[52]. M. Rochette, M. Guy, S. LaRochelle, J. Lauzone and F. Trenpanier, "Gain equalization of EDFA's with Bragg gratings" , IEEE Photonics Technol. Lett., vol. 11, no.5, pp. 536-538, 1999.

[53]. H. Masuda, "Optical SNR enhanced amplification in long-distance recirculating-loop WDM transmission experiment using 1580nm band hybrid amplifier," Electron. Lett., vol. 35, no. 5, pp. 411-412, 1999.

[54]. H. Ono, M. Yamada and M.Shimizu, "S-Band Erbium-Doped Fiber Amplifiers With a

Multistage Configuration-Design,Characterization, and Gain Tilt Compensation," J. Lightwave Technol., vol.21, no.10, pp. 2240-2246, 2003.

[55]. H. Ono, M. Yamada, and M. Shimizu, "S-band erbium-doped silica fiber amplifier with flattened-gain of over 21 dB," Electron. Lett., vol. 33, no. 19, pp. 1084–1086, 2002.

[56]. J. S. Wang, E. M. Vogel and E. Snitzer, "Terullite glass: a new candidate for fiber devices," Opt. Mat., vol. 3, no.8, pp. 187-203, 1994.

[57]. A. Mori, Y. Ohishi, and S. Sudoi, "Erbium-doped tellurite-based fiber laser and amplifier," Electron. Lett., vol. 33, no. 10, pp. 863-865, 1997.

[58]. A. Mori, Y. Ohishi, M. Yamada, M. Yamada, H. Ono, Y. Nishida, K. Oikawa and S. Sudo, "1.5 μm Broadband Amplification by tellurite - based EDFAs", *in the Proceedings of Optical Fiber Communications '97,* OFC'97, PD 1, 1997.

[59]. A. Mori, K. Kobayashi, M. Yamada,T. Kanamori, K. Oikawa, Y. Nishida, and Y. Ohishi, "Low noise broadbandtellurite-based Er -doped fiber amplifiers," Electron. Lett., vol. 34, no. 9, pp.887-888, 1998.

[60]. N. Sugimoto, K. Ochiai, S.Ohara, H. Hayashi, Y. Fukasawa, T. Hirose, and M. Reyes, "Highly efficient and short length Lanthanum codoped Bi_2O_3-based EDF for extended L-band amplification," *in the Proceedings of Optical Amplifiers and their applications 2002,* OAA'02, PD 5, Vancouver, 2002.

[61]. B. O. Guan, H. Y. Tam, S. Y. Liu, P. K. A. Wai, and N. Sugimoto, "Ultrawide-Band La-Codoped Bi_2O_3-Based EDFA L-Band DWDM systems," IEEE Photon. Technol. Lett., vol. 6, pp. 383–385, 1994.

[62]. M. Yamada, A. Mori, K. Kobayashi, H. Ono, T. Kanamori, K. Oikawa, Y. Nishida and Y. Ohishi, "Gain-flattened tellurite-based EDFA with a flat amplification bandwidth of 76 nm," IEEE photon. Technol. Lett., vol. 15, no. 11, pp. 1525-1527, 2003.

[63]. M. Yamada, H. Ono, T. Kanamori, T. Sakamoto, Y. Ohishi and S. Sudo, "A low-noise and gain-flattened amplifier composed of a silica-based and a fluoride-based Er^{3+}-doped fiber

amplifier in a cascade configuration," IEEE Photon. Technol. Lett., vol. 8, no. 5, pp. 620-622, 1996.

[64]. M. Yamada, T. Kanamori, Y. Terunuma, K. Oikawa, M. Shimizu, S. Sudo, and K. Sagawa, "Fluoride-based erbium-doped fiber amplifier with inherently flat gain spectrum", IEEE Photon. Technol. Lett., vol. 8, pp. 882-884, 1996.

[65]. H. Ono, M. Yamada, T. Kanamori, and Y. Ohishi, "Low-Noise and High-Gain 1.58μm Band Er^{3+}-Doped Fibre Amplifiers with Cascade Configurations," Electron. Lett., vol. 33, no. 17, pp. 1477-1479, 1997.

[66]. V. P. Gapontsv, and N. S. Platonov, "Migration-Accelerated Quenching in Glasses Activated by Rare Earth Ions", in Dynamical Processes in Disordered Systems, Material Science Forum, vol. 51, 1990.

[67]. C. Lester, A. Bjarklev, T. Rasmussen, and P. G. Dinsen, "Modling of Yb^{3+} -Sensitised Er^{3+}-Doped Silica Waveguide Amplifiers," J. Lightwave Technol., vol.13, No.5, pp. 740-743, 1995.

[68]. D. Barbier, M. Rattay, F. Saint Andre, A. Kevorkian, J. Delavaux, E. Murphy, "Amplifying Four Wavelengths Combiner Based On Erbium-Ytterbium Doped Planar Integrated Optical Modules", *in the Proceedings of 22nd European Conference on Optical Communication*, ECOC'96, Oslo, 1996.

[69]. Nilsson, P. Scheer, and B.Jaskorzynska, "Modeling and optimization of short Y b -sensitized Er-doped fiberamplifiers," IEEE Photon. Technol. Lett., vol. 6, pp. 383–385, 1994.

[70]. Di Pasquale, and F. Federighi, "Improved gain characteristics in high-concentration Er^{3+}/Yb^{3+} codoped glass waveguide amplifiers," IEEE J. Quantum Electron. vol. 30, no. 9, pp. 2127–2131, 1994.

[71]. Y. C. Yan, A.J. Faber, H. de Waal, P.G. Kik and A. Polman, "Erbium-doped phosphate glass waveguide on silicon with 4.1 dB/cm gain at 1.535 μm," Appl. Phys. Lett. vol. 71, no. 20, pp. 2922-2924, 1997.

[72]. H. Ono, K. Nakagawa, M. Yamada and S. Sudo "Er^{3+}-doped fluorophosphate glass fiber amplifier for WDM systems," Electron. Lett.,vol. 32, no. 17, pp. 1586-1587, 1996.

[73]. E. Desurvire, J. L. Zyskind, and J. R. Simpson, "Study of spectral dependence of gain saturation and effect of inhomogeneous broadening in erbium-doped aluminosilicate fiber amplifiers," IEEE Photon. Technol. Lett.vol. 2, no4, pp246-248, 1990.

[74]. E. Rudkevich, D. M. Baney, J. Stimple, D. Derickson and G. Wang, "Nonresonant spectral-hole burning in erbium-doped fiber amplifier," IEEE Photon. Technol. Lett., vol. 11, no. 5, pp. 542-544, 1999.

[75]. N. S. Bergano, C. R. Davidson, M. A. Mills, P. C. Corbett, S, G, Ecangelides, B. Pederson,R. Menges, J. L. Zyskind, J. W. Sulhoff, A. K. Srivastava, C. Wolf, and J. Judkins, *in Proceedings of Optical Fiber Conference,* OFC'97, PD16, Dallas, 1997.

[76]. M. Nishihara, Y. Sugaya, and E. Ishikawa, "Characterization and new numerical model of spectral hole burning in broadband erbium-doped fiber amplifier," *in Proceedings of Optical Amplifiers and Their Applications*, OAA'03, Tud3, 2003.

[77]. M. Bolshtyansky, "Spectral hole burning in erbium-doped fiber amplifiers," IEEE Photon. Technol. Lett., vol. 21, no4, pp. 1032-1038, 2003.

[78]. J. W. Sulhoff, A. K. Srivastava, C. Wolf, Y. Sun, and J. L. Zyskind, "Spectral-hole burning in erbium-doped silica and fluoride fibers," IEEE Photon. Technol. Lett., vol. 9, no12, pp. 1578-1579, 1997.

[79]. I. Joindot and F. Dupre, "Spectral hole burning in silica-based and in fluoride-based optical fibre amplifiers," Electron. Lett., vol. 33, no. 14, pp. 1239-1240, 1997.

[80]. L. Bigot, A. Jurdyc, B. Jacquier, L. Gasca, and D. Bayart, "Resonant fluorescence line narrowing measurements in erbium-doped glasses for optical amplifiers," Phys. Rev. B vol. 66, pp. 1- 6, 2002.

[81]. F. I. Kharti, D. G. Duff, M. Vaa and A. L. Simons,"Spectral hole burning effects on partially loaded, 19 nm bandwidth, 6246 km long EDFA lightwave transmission system,"

Electron. Lett., 36, no. 8, pp. 739-740, 2000.

Chapter 2

Evidence of enhanced hypersensitive transition in erbium-doped fibers with different Al_2O_3 content

2-1. Introduction

Silica-based erbium-doped fiber amplifier (EDFA) has been an indispensable key device in the telecommunication system based on wavelength division multiplexing (WDM). Almost all installed 1.5 μ m optical telecommunication system has used EDFA. This widespread of the usage of EDF in optical transmission system as optical amplifier is explicable based on two technical points. One is the favorable suitability of EDF to the telecom silica fiber that has the most low loss region in 1.5 μ m wavelength region. The other is that erbium-doped fiber has the 1.5 μ m induced emission from the $^4I_{13/2}$ level of erbium ion and can amplify the light signal in C-band (from 1530nm to 1570nm), which corresponds to low loss wavelength region of the telecom silica fibre. Due to the rapid increase of information traffic, there is urgent demand for optical amplifiers with a wide and flat gain spectrum. Many studies about non-silicate based

rare earth-doped optical amplifier for new bands (S-band:1450nm–1530nm, L-band:1570nm–1630nm) have been performed in order to expand transmission bandwidth [1],[2]. Thulium-doped fiber (TDF) is one of the most well known new promising fiber glass for the S-band optical amplifier and utilizes stimulated emission between the $^3H_4$ and the $^3F_4$ energy level [3, 4]. However, silica-based Er^{3+}-doped fiber is still considered to be a promising candidate not only for the C-band optical amplifier but for the new-bands optical amplifiers such as the S-band L-band amplifier because of its high reliability and favorable properties to the silica-based telecom fiber in the optical transmission system.

Today, many efforts to modify the properties of silica-based Er-doped fiber (EDF) are being made to make it a new band amplifier [5], extracting more potential abilities of Er^{3+}-doped silica-based glasses for the advanced EDF. So far, spectroscopy of erbium-doped bulk glasses has been well studied in order to improve the properties of EDF [6]. Various glass systems have been investigated as Er^{3+} ion hosts in order to realize the optical amplifier that has broad band width and high efficiency so far. However, as far as we know, few spectroscopic studies based on the Judd-Ofelt analysis on Er^{3+} ions have been carried out in fiber forms.

Therefore, this study focuses on the precise spectroscopy based on the Judd-Ofelt analysis of alumino-silicate EDF with different Al_2O_3 content in order to investigate the change of the ligand field structure around the Er^{3+} ions by adding Al_2O_3. The basic optical properties of EDF with different Al_2O_3 content were investigated mainly with optical absorption measurements and analyzed precisely by the Judd-Ofelt theory using fiber samples. As a result, the difference between the optical properties of the Er^{3+} emission in a bulk glass and a fiber form was found for the first time as far as we know. The effect of the Al_2O_3 content on the change of the ligand field in alumino-silicate EDFs is discussed based on the coordination number of Al^{3+} ion in alumino-silicate EDFs..

2-2. Experimental

2-2-1. Absorption measurements of EDF.

Four EDF samples with different Al_2O_3 content were used for investigating the compositional dependence of optical properties of EDF. The concentrations of Er_2O_3 and Al_2O_3 of four EDF samples are shown in Table 2-1. The refractive index of EDF samples at 1310nm was measured using a reflectometer, (Ando, AQ7413). Absorption spectra of EDF in 1.5 μ m region were measured with three tunable laser sources, (Santec, TSL210) in the range of 1420nm-1640nm and an optical spectrum analyzer, OSA, (Anritsu, MS9780A). The signal input power was -30dBm in order not to saturate fiber loss. In absorption measurement in 1.5 μ m region, fiber lengths of four EDFs were 1m.

The TSL and OSA were controlled with a personal computer using GPIB. Loss was determined by detecting the peak power of signal output power and subtracting a signal output power from a signal input. In order to carry out the Judd-Ofelt analysis, absorption measurements in the wavelength region from 400nm to 1650nm were performed using a white light source (Ando, AQ4303B), fiber optic spectrometer (Ocean optics, USB2000) and the OSA.

2-2-2. Emission measurements and cross section analysis based on the McCumber theory

Spontaneous emission of EDF sample (Al_2O_3:20000ppm) was measured with monochromator, (Nikon G250) and photo-detector, (Electro Optical Systems). Experimental emission cross section was calculated using obtained emission spectrum. In addition, theoretical emission cross section was also calculated using the measured absorption cross section σ_a of EDF sample (Al_2O_3:20000ppm) through McCumber relation as follows:

$$\sigma_e(\nu) = \sigma_a \exp[(E_0 - h\nu)/\kappa T] \cdot \frac{1 + \sum_{j=2}^{8} 7\exp(-\Delta E_{1j}/kT)}{1 + \sum_{J-2}^{7} 6\exp(-\Delta E_{2j}/kT)} \quad (1)$$

where E_0 is the separation energy between the lowest component of each manifold and assumed to be 6535cm^{-1} (λ =1530nm). ΔE_{1j} and ΔE_{2j} is the difference in energy between the jth and the lowest component of $^4I_{13/5}$ and $^4I_{15/2}$ level. Here, we supposed that adjacent components in the same manifold are separated by the same energy δE_1 and δE_2. Comparison of the experimental cross section with theoretical one was performed in next Results session.

Table 2-1 Basic parameters for alumino-silicate EDF samples.

sample	Er_2O_3 (ppm)	Al_2O_3 (ppm)	ρ_{Er2O3} ($/\times 10^{18}cm^3$)	$n_{1.3\mu m}$ (-)	. λ_{mean}(nm) (1.5 μ m region)
EDF1	780	5000	5.21	1.476	1523.8
EDF2	880	10000	5.53	1.475	1525.3
EDF3	630	20000	4.10	1.474	1524.6
EDF4	800	40000	5.44	1.481	1523.9

2-3. Results and Discussions

2-3-1. Al_2O_3 dependence of absorption cross section.

The solid state parameters and optical parameters for Al_2O_3-doped silicate EDF samples shown in Table 2-1 were used in the calculations for the cross section analysis and the Judd-Ofelt analysis.

Fig. 2-1(a) shows the absorption cross section σ_a calculated from the loss spectra. σ_a showed the Al_2O_3 dependence and increased about double with the increase of Al_2O_3 up to 20000ppm. Fig. 2-1(b) shows the comparison of the experimental emission cross section for Al_2O_3-doped EDF (Al_2O_3:20000ppm) with theoretical one. The theoretical emission cross section was calculated from the absorption cross section using McCumber relation mentioned above. The shape of the theoretical cross section shows fairly good agreement with that of experimental one in longer wave length region than 1530nm.

Fig. 2-2 shows the line strength, $S_{JJ'}$ corresponding to the 1.5 μm transition and the spontaneous probability, $A_{JJ'}$ of the $^4I_{13/2}$-$^4I_{15/2}$ transition and the measured lifetime of $^4I_{13/2}$, τ_f. According to the Judd–Ofelt theory, the line strength $S_{JJ'}$ is related to the integrated absorption cross section of 1.5 μm transition in Fig. 2-1 (b) using the equation as follows,

$$S_{jj'} = \frac{3hc(2J+1)}{8\pi^3 e^2 \lambda_{mean} \rho} n \left[\frac{9}{(n^2+2)^2}\right] \int_{band} k(\lambda) d\lambda, \qquad (2)$$

where $k(\lambda)$ is the absorption coefficient at λ, λ_{mean} is the mean wavelength of absorption band, ρ is the concentration of Er^{3+} ions per unit volume, h is the Planck's constant, c is the speed of light, e is the elementary charge and n is the refractive index. The refractive indices of the core of EDFs were about 1.47 and showed little Al_2O_3 content dependence. J is the total angular moment of the initial state, which is the $^4I_{15/2}$, and J' is that of the final state $^4I_{13/2}$ for the 1.5 μm

transition. The spontaneous emission probabilities $A_{JJ'}$ is proportional to the line strength $S_{JJ'}$ probabilities $A_{JJ'}$ using local field correction factor $(n^2+2)^2/9$ through the relation,

$$A_{jj'} = \frac{64\pi^2 e^2}{3h(2J+1)\lambda_{mean}^3} n\left[\frac{(n^2+2)^2}{9}\right] S_{jj'}. \quad (3)$$

As shown in Fig. 2-2, both the $S_{JJ'}$ and A_{JJ} increased with increase of Al_2O_3 content up to 20000ppm and decreased over 20000ppm of Al_2O_3. The increase of $S_{JJ'}$ and $A_{JJ'}$ is considered to be caused by the increase of electric-dipole component of $S_{JJ'}$ because magnetic-dipole component of $S_{JJ'}$ is independent of the change of ligand field. On the other hand, τ_f showed little Al_2O_3 dependence and was about 10(ms), which is typical value for lifetime of $^4I_{13/2}$ level of Er^{3+}.

Fig. 2-3 shows the nonradiative decay rate W_{NR} and quantum efficiency QE. Using τ_f and $A_{JJ'}$, W_{NR} and QE are expressed as,

$$W_{NR} = \tau_f^{-1} - \sum_{J'} A_{JJ'}. \quad (4)$$

$$QE = \frac{\sum_{J'} A_{JJ'}}{W_{NR} + \sum_{J'} A_{JJ'}} \quad (5)$$

According to the Miyakawa-Dexter theory [7], multi-phonon decay rate is described by the equation,

$$W_{NR} = W_0 \exp(-\alpha \Delta E/\hbar\omega), \quad (6)$$

$$\alpha = \ln[\{N/g(n+1)\}-1]. \quad (7)$$

Here, ΔE is the energy gap to the next lower level, $\hbar\omega$ is the phonon energy which contributes to the multiphonon decay process, n is the number of phonons excited at the

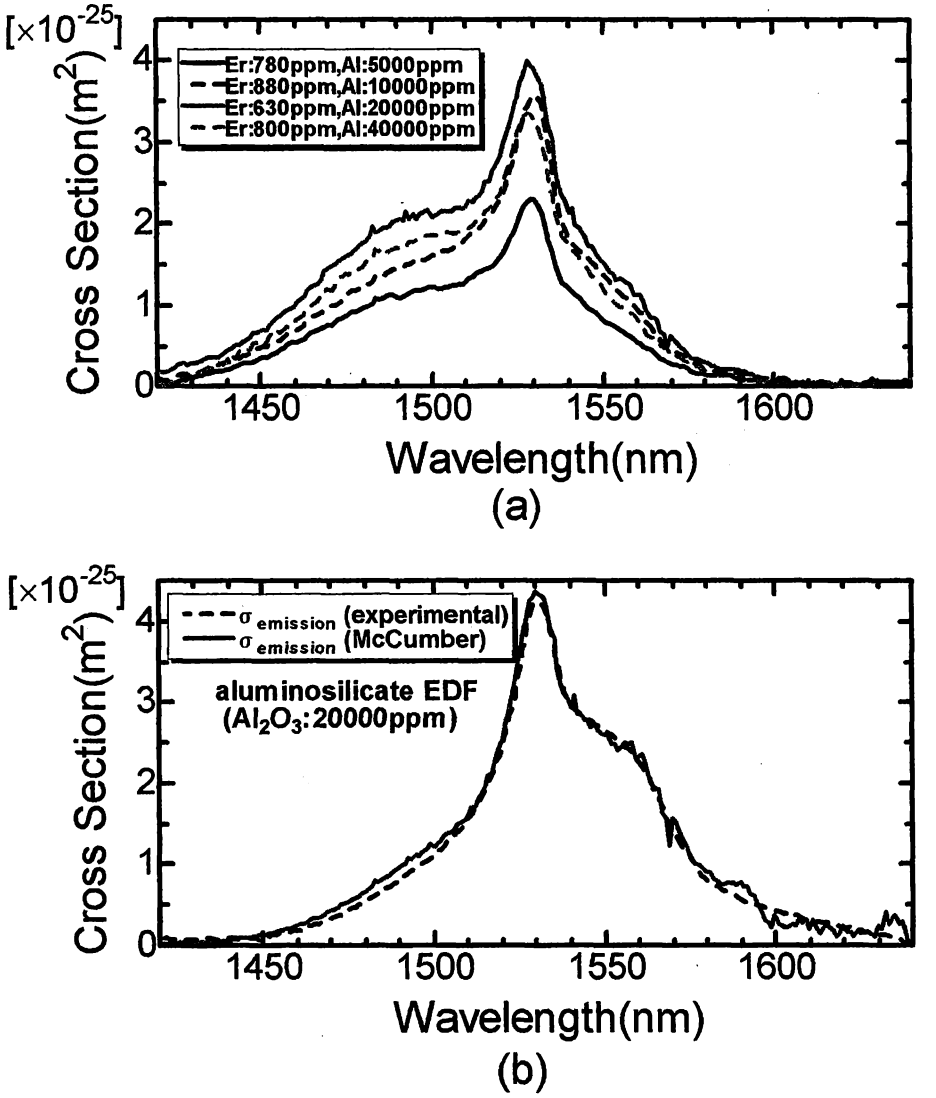

Figure 2-1 (a). Absorption cross section spectra for Al_2O_3-doped EDF in 1.5 μ m region. (b). Comparison of the experimental emission spectra for Al_2O_3-doped EDF(Al_2O_3:20000ppm) with theoretical one based on McCumber theory.

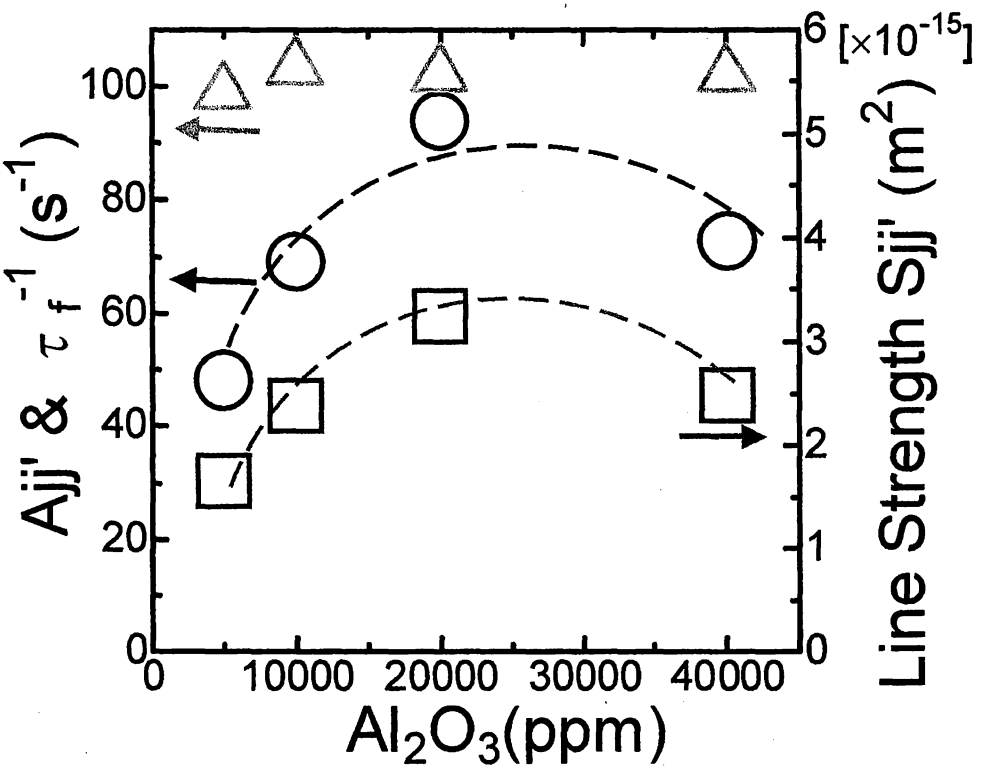

Figure 2-2 Al_2O_3 dependence of the line strength Sjj', the spontaneous emission probability Ajj' and the relaxation time τ_{meas} of EDF samples.

temperature of the system and N is the number of phonons emitted in nonradiative transition process, namely,

$$N = \Delta E / \hbar\omega . \qquad (8)$$

g is the electron- lattice coupling constant. Since the phonon energy of Al-O bond ($800cm^{-1}$) is lower than that of Si-O bond ($1000cm^{-1}$), the difference of this phonon energies may be one of the cause of the decrease of the multi-phonon decay rate, W_{NR} with an increase of the coordination of Al-O bonding around the Er^{3+} ion sites. However, this difference of phonon energies is not considered to be dominant origin of the nonradiative decay because the difference of the multi-phonon decay rate due to the difference of phonon energies is relatively small. Therefore, this significant increase of the nonradiative energy transfer decay rate seems to be enhanced by the other nonratiative energy transfer process, which is caused by the existence of some defects or OH in EDF samples.

As shown in Fig. 2-3, W_{NR} decreased with an increase of Al_2O_3 up to 20000ppm. This shows good agreement with the expectation based on the (5), (6). However, the behavior of W_{NR} over 20000ppm of Al_2O_3 region is not fully explained at present.

2-3-2. Absorption spectrum in 400nm -1650nm

In order to investigate the Al_2O_3 content dependence of the Ω_t (t=2,4,6) parameters, each absorption band was measured and analyzed, which corresponds to the optical transition between 4f-multiplets of Er^{3+} ions using the Judd-Ofelt theory.

Fig. 2-4 shows the comparison of the absorption spectrum of EDF (Al_2O_3 content: 20000ppm) with that of an alumino-silicate bulk glass. We can see the four absorption bands corresponding to the transitions from the $^4I_{15/2}$ to the $^4F_{9/2}$, $^4S_{3/2}$, $^2H_{11/2}$ and $^4F_{7/2}$. Five absorption bands including, these four bands, were used to analyze Ω_t (t=2,4,6) parameters.

The absorption spectrum of the $^2H_{11/2}$ was found to become remarkably larger in the EDF than those in alumino-silicate and borate bulk glasses.

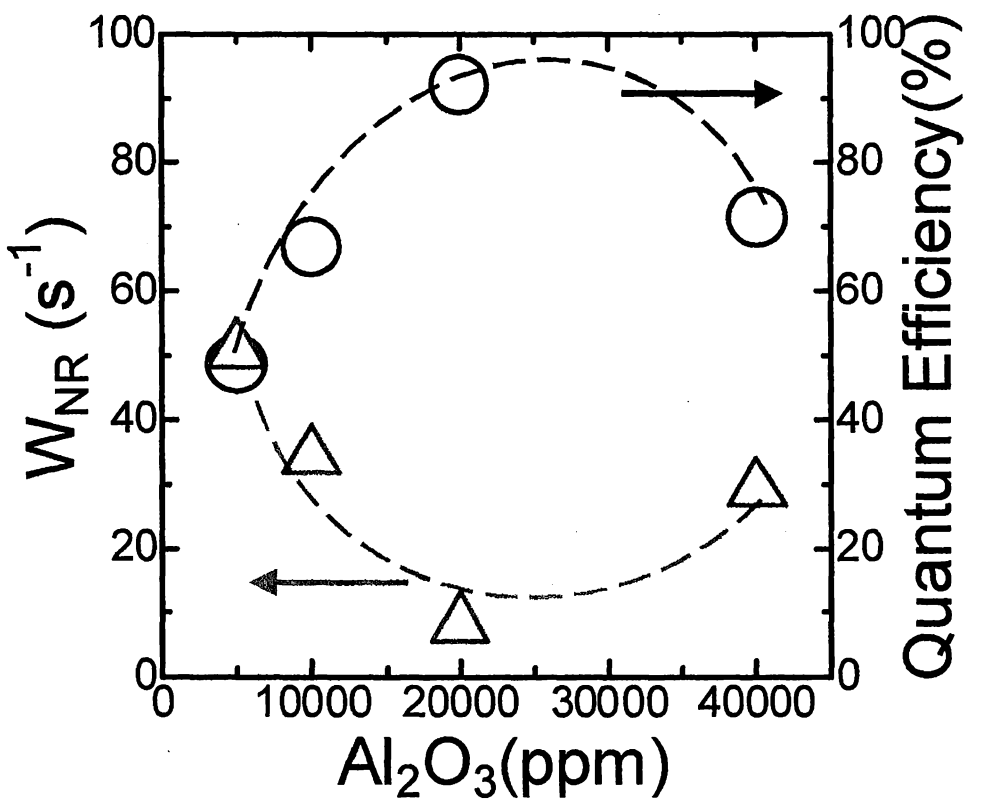

Figure 2-3 Al_2O_3 dependence of the nonraditive decay rate W_{NR} and the quantum efficiency QE of EDF samples.

The enhancement of the absorption peak of the $^2H_{11/2}$ was also observed in other erbium doped fibers.

2-3-3. Judd-Ofelt analysis and Ω_t parameters.

a) Al_2O_3 dependence of Ω_6 parameters.

Fig. 2-5 shows the Al_2O_3 content dependence of the Judd-Ofelt intensity parameters Ω_2, Ω_4 and Ω_6 calculated from the line strength of absorption spectra in the range of 400nm-1100nm. The measured line strength could be matched with the best fit Ω_t results to 10 – 15% (rms) accuracy for all the alumino-silicate EDFs examined.

As shown in Fig. 2-5, the Ω_6 parameter was found to increase with an increase of the Al_2O_3 content up to 20000ppm. According to the Judd-Ofelt theory, $S_{JJ'}$ can be defined with the Ω_t parameter as follows,

$$S^{ed}[S,L,J;S',L',J'] = \sum_{t=2,4,6}\Omega_t \times |< 4f^N S,L,J \,|\, U^{(t)} \,|\, 4f^N S',L',J' >|^2, \quad (9)$$

where $< 4f^N S,L,J \,|\, U^{(t)} \,|\, 4f^N S',L',J' >$ denotes the reduced matrix element.

The coefficients Ω_2, Ω_4 and Ω_6 contain the effects of odd symmetry crystal field terms.

In particular, the $S_{JJ'}$ of electric dipole components of the 1.5 μm transition with Al_2O_3 content is given by [8],

$$S^{ed}[^4I_{13/2};^4I_{15/2}] = 0.019\Omega_2 + 0.118\Omega_4 + 1.462\Omega_6 . \quad (10)$$

While S_{ed} is a function of glass structure and composition using Ω_t (t=2, 4, 6) parameter, S_{md} is independent of the ligand fields and is characteristic to the transition determined by the quantum numbers. For the transition between the states which meet the transition selective rules $\Delta S = \Delta L = 0$, $\Delta J = 0, \pm 1$, there exists the contribution of magnetic dipole transition [9, 10]. Therefore the increase of total line strength $S_{JJ'}$ of 1.5 μm transition with the increase of Al_2O_3 shown in Fig. 2-2 can be largely dominated and explained well by the increase of the Ω_6 intensity parameter shown in Fig. 2-5.

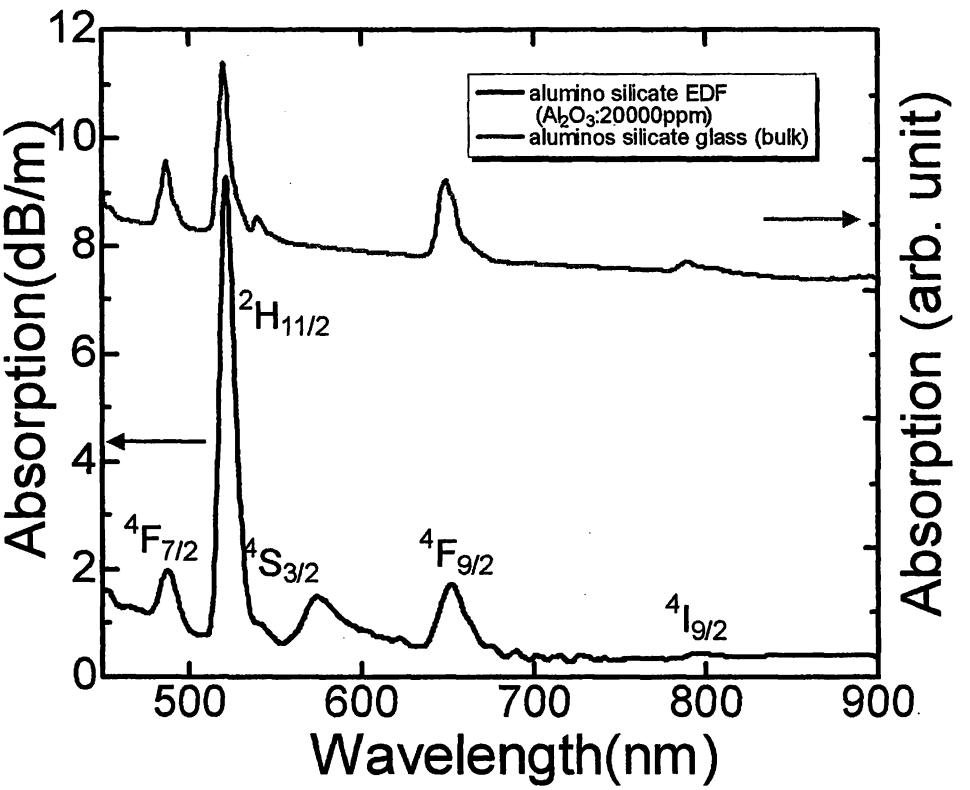

Figure 2-4 Comparison of absorption spectra for Al_2O_3-doped EDF with an alumino-silicate bulk glass in 400nm -900nm wavelength region

The value of the Ω_6 particularly tends to be affected by the basicity of glass and is known empirically to become larger as the basicity decreases [11]. Therefore the increase of Ω_6 parameter indicates that the increase of Al_2O_3 weaken covalent character of Er-O as a results the formation of Si-O-Al. Generally, it is known that the coordination number of Al^{3+} ion becomes smaller in the host glasses with higher basicity and the production of four-coordinated Al^{3+} ion is enhanced compared to the formation of six–coordinated Al^{3+} ion [12].

Moreover the optical basicity of four-coordinated Al^{3+} ion in the network of SiO_4 is known to be smaller than that of six-coordinated Al^{3+} ion (microscopic λ of Si-O-Al is 0.59 for four-coordinated Al^{3+} ion and 0.65 for six-coordinated Al^{3+} ion) [13]. Therefore Er^{3+} ions have the possibility to be surrounded by more four-coordinated Al^{3+} ions rather than six-coordinated Al^{3+} ion with increase of Al_2O_3 content. The decrease of the basicity around Er^{3+} sites up to 20000ppm of Al_2O_3 content can be considered in particular as the result of the increase in the number of the four-coordinated Al^{3+} ion surrounds Er^{3+} site.

b) Al_2O_3 dependence of Ω_2 parameters

As shown in Fig. 2-5, the value of Ω_2 parameter in fibers takes about three times large value as those in alumino-silicate and borate bulk glasses [14] ($\Omega_{2:\,(Al\text{-}Si)\,glass}$=4.6, $\Omega_{2:\,(Bo)\,glass}$=3.21), which corresponds to the experimental results of a strong absorption band of the $^2H_{11/2}$ as shown in Fig. 2-4.

The relation between the Ω_t parameter and the electric-dipole line strength component of $^2H_{11/2}$ is given by,

$$S^{ed}[^2H_{11/2};^4I_{15/2}] = 0.7056\Omega_2 + 0.4109\Omega_4 + 0.0870\Omega_6. \quad (11)$$

This relation shows that the electric-dipole line strength of the $^2H_{11/2}$ – $^4I_{15/2}$ is largely dominated by the value of the Ω_2 parameter. Therefore the experimental results of a strong absorption band of the $^2H_{11/2}$ can be explained well by this equation. In case of Er^{3+}, the electric-

dipole line strength of the $^4G_{11/2} - {}^4I_{15/2}$ is also expected to show very strong absorption in fibers because the reduced matrix element $<\|U^{(2)}\|>$ of the $^4G_{11/2} - {}^4I_{15/2}$ takes dominantly large value similar to that of $^2H_{11/2} - {}^4I_{15/2}$.

$$S^{ed}[^4G_{11/2};{}^4I_{15/2}] = 0.9178\Omega_2 + 0.5271\Omega_4 + 0.1197\Omega_6. \quad (12)$$

Both the $^4G_{11/2} - {}^4I_{15/2}$ and the $^2H_{11/2} - {}^4I_{15/2}$ are called the hypersensitive transitions that are dominated and enhanced by the large Ω_2 parameter in the fibers. It is known that the value of the Ω_2 is raised drastically by lowering the symmetry of the rare earth ligand field [15]. According to the Judd-Ofelt theory, the Ω_2 dominates critically the hypersensitive transition that was reported to be largely affected by the polarized distortion of the ligand field [16,17]. Therefore the Er^{3+} sites in fibers are considered to have larger polarization or asymmetric distortion than in bulk glasses. Moreover, the Ω_2 also increased with the increase of the Al_2O_3 content. Considering the Al_2O_3 dependence of Ω_6 parameter, this result indicates that the substitution of six-coordinated Al^{3+} ion for four-coordinated Al^{3+} ion with the increase of Al_2O_3 may occur. Therefore high Al_2O_3-doping is likely to enhance the distortion of the ligand field of Er^{3+} site caused by the existence of four and six-coordinated Al^{3+} ion.

2-4. Conclusion

The $S_{JJ'}$ and the $A_{JJ'}$ of the Er:1.5μm transition increased with increase of Al_2O_3 content in EDF. The Ω_6 parameter increased with increase of Al_2O_3 content, which can be well explained by the compositional dependence of the $S_{JJ'}$ of the Er:1.5μm transition. These results indicate that a decrease of local basicity occurs by adding Al_2O_3. The Ω_2 parameter in fiber form was found to be about three times as large as those in alumino-silicate bulk glasses and also increased with increase of Al_2O_3 content. This shows that the polarization or asymmetric distortion at erbium ion site is more likely to be enhanced in the fiber form than in the bulk glass.

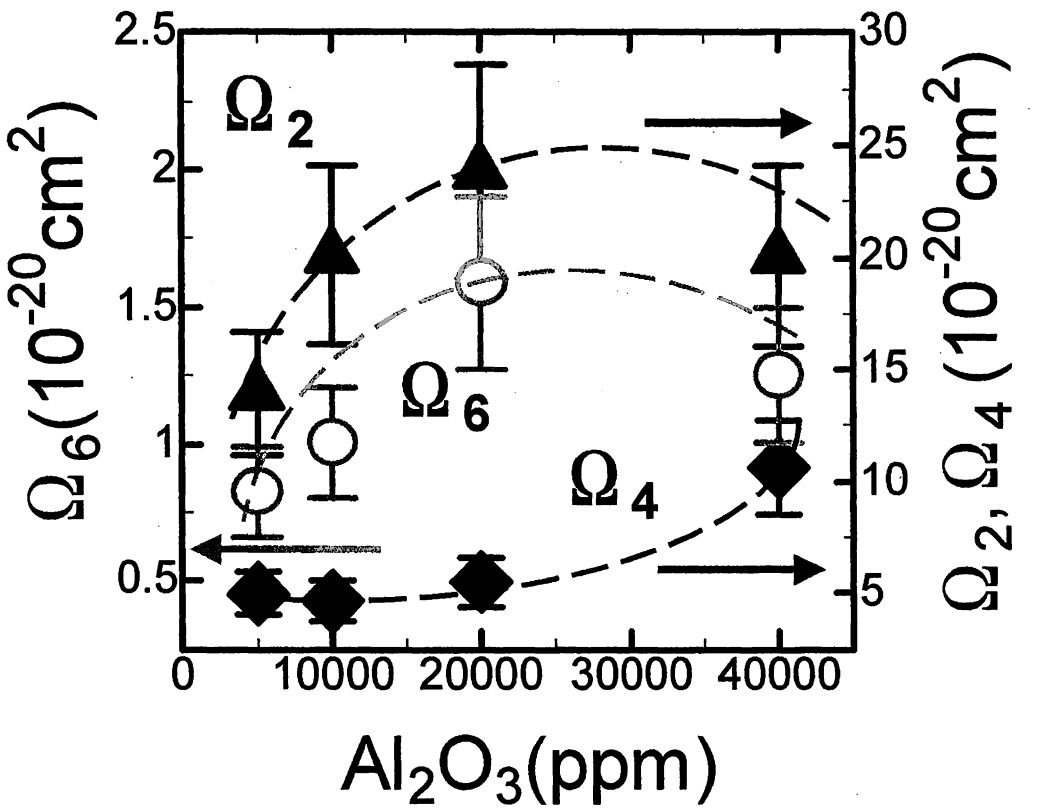

Figure 2-5 Al_2O_3 content dependences of the Judd-Ofelt intensity parameter Ω_2, Ω_4 and Ω_6.

The decrease of local basicity and symmetry of the Er^{3+} ligand field in alumino-silicate EDF are attributed to the increase of four-coordinated Al^{3+} ion.

References

[1] Y. Ohishi, A. Mori, M. Yamada, H. Ono, Y. Nishida, and K. Oikawa, "Gain characteristics of tellurite-based erbium-doped fiber amplifiersfor 1.5-mm broadband amplification," *Opt. Lett.*, vol. 23, pp. 274-276, 1998.

[2] S. Aozana, T. Kanamori, K. Hoshino, and M. Shimizu, "Gain-shifted thulium-doped fibre amplifiers employing novel high concentration doping technique," *Electron. Lett.* vol. 36, pp. 418-419, 2000.

[3] E. Ishikawa, M. Nishihara, Y. Sato, C. Ohshima, Y. Sugaya, and J. Kumasako, "Novel 1500nm-band EDFA with discrete Raman amplifier," in *Proc. ECOC*, 2001, paper PD.A.1.2.

[4] E. Snoeks, P. G. Kik, and A. Polman, "Concentration quenching in erbium implanted alkali silicate glasses," *Opt. Mat.* vol. 5, pp. 159-167, 1996.

[5] D. E. McCumber, "Theory of Phonon-Terminated Optical Masers," *Phys. Rev.* vol. 134, pp. A299- A306, 1964.

[6] M. J. Weber, "Probabilities for Radiative and Nonradiative Decay of Er^{3+} in LaF_3," *Phys. Rev.* vol. 157, pp. 262- 272, 1967.

[7] B. R. Judd, "Optical Absorption Intensities in Rare-Earth Ions," *Phys. Rev.* vol. 127, pp. 750-761, 1962.

[8] G. S. Ofelt, "Intensities of Crystal Spectra of Rare-Earth Ions," *J. Chem. Phy.* vol. 37 , pp. 511-520, 1962.

[9] S. Tanabe, T. Hanada, "Local structure and 1.5μm quantum efficiency of erbium doped glasses for optical amplifiers," *J. Non-Cryst. Solids.*, vol. 196, pp.101-105, 1996.

[10] H. Kawazoe, "Coordination number and chemical shift in $K\alpha_{12}$ emission of Mg^{2+} in oxide glasses," *J. Non-Cryst. Solids.*, vol. 42, pp. 281-285, 1980.

[11] J. A. Duffy and M. D. Ingram, "An interpretation of glass chemistry in terms of the optical basicity concept," *J. Non-Cryst. Solids.*, vol. 21, pp. 373-410, 1976.

[12] S. Tanabe, T. Ohyagi, S. Todoroki, T. Hanada, and N. Soga, "Relation between the Ω_6 intensity parameter of Er^{3+} ions and the ^{151}Eu isomer shift in oxide glasses," *J.Appl. Phys.* vol. 73, pp. 8451-8454, 1993.

[13] C. K. Jφrgensen and B. R. Judd, "Hypersensitive pseudoquadrupole transitions in lanthanides," *Mol. Phys.* vol. 8, pp. 281-290, 1964.

[14] M. Eyal, R. Reisfeld, A. Schiller, C. Jacobini, and C. K. Jφrgensen, "Energy transfer between manganese(II) and thulium(III) in transition-metal fluoride glasses," Chem. Phys. Lett. vol. 140, pp.595-602, 1987.

[15] R. D. Peacock, "The intensities of lanthanide f-f transitions," in Structure and Bonding (Springer, Berlin, 1975), vol. 22, pp. 83-121.

Chapter 3

Numerical and experimental evaluation of S-band gain characteristics of erbium-doped fiber

3-1. Introduction

In the last decade, the transmission capacity of trans-oceanic and terrestrial optical transmission system has been explosively increased using wavelength-division-multiplex (WDM) and time division multiplex (TDM) transmission technique. Now, broadband telecommunication system come into widely use now. Based on these facts, there has been required the erbium-doped fiber amplifier (EDFA) that have wide and flat gain characteristics, which has high reliability and favorable properties for the optical transmission system in the C-band wavelength region (1530nm-1570nm). Since the Er^{3+} ion has the emission transition corresponding to the $^4I_{13/2} \rightarrow {}^4I_{15/2}$ of Er^{3+} ion and can amplify stably the light signal in the C-band region, which corresponds to the low loss wavelength region of optical transmission silica fiber, EDFA has been well established and reached a stage of practical use in the C-band

wavelength region. Today, extracting more potential abilities from silica-based EDF has been a practically important subject in the development of EDFA.

So far, many attempts to modify the properties of silica-based EDF are being made for the application to the L-band amplifier (1580nm-1630nm) [1-4]. E. Ishikawa demonstrated the application of EDFA to the S-band (1450nm-1530nm) amplifier. This study was made using many ASE-suppression filters to suppress generated ASE around 1530nm and demonstrate the feasibility of the transmission system with the S-band EDFA [5]. However, few detailed studies on the origin of the S-band gain characteristics have been reported experimentally and theoretically. The purpose of this study is to clarify and predict the S-band gain characteristics of EDF theoretically and qualitatively for the precise amplifier design in the S-band wavelength region. The temperature dependence of the S-band gain spectra of EDF was investigated by the absorption measurements in 1.5 μ m wavelength region and was predicted by the numerical simulation based on the cross section analysis using the McCumber theory. The origin of the S-band gain characteristics is discussed regarding the population density of the Stark manifolds within the $^4I_{13/2}$ and $^4I_{15/2}$ level.

3-2. Experimental

3-2-1. Absorption measurements

A silica-based EDF sample with a core glass composition of $75.8SiO_2$-$22.6GeO_2$-$1.4Al_2O_3$-$0.01Er_2O_3$, was used. Er^{3+} ion concentration is 4.10×10^{18}(/cm^3). The refractive index of EDF sample was measured with a reflectometer (Ando, AQ7413). The refractive index measured at 1.3 μ m is 1.474.

3-2-2. Absorption measurements

Absorption spectra of EDF sample were measured with three tunable laser sources, TLS (Santec, TSL210) and an optical spectrum analyzer, OSA (Anritsu, MS9780A) in order to investigate the change of the absorption cross sections at 77K, 293K, 303K, 333K and 373K in the wavelength region 1420-1640nm. Liquid nitrogen was used for 77K and a constant-temperature bath was used to keep high temperature. The TLS and OSA were controlled by a personal computer. The signal input power was –30dBm in order not to saturate the $^4I_{13/2}$ level by the strong excitation of probe signal.

3-2-3. Spontaneous emission measurements

In order to compare experimental cross sections with theoretical ones obtained through the McCumber theory, the spontaneous emission spectrum of an EDF sample was measured at 77K and 293K. A transparent glass dewar was used in order to detect the spontaneous emission from the EDF sample. The EDF sample was pumped by a 979nm laser diode (FITEL).
An InGaAs photodiode (Electro-Optical-System) was used as a detector in the wavelength region 1400-1700nm with monochromator (Nikon, G250) controlled by a personal computer

3-2-4. Gain characteristics measurements

The temperature dependence of the S-band gain characteristics of EDF was also investigated at 77K, 293K and 373K experimentally and verified analytically using the numerical simulation model based on the two level system of Er^{3+} ion using the McCumber theory. Signal input power was –30dBm. The length of the EDF sample was 10m. The EDF sample was forwardly pumped with a 979nm LD. Pumping power was 150mW.

3-3. Theory and Numerical model

3-3-1. Gain coefficient analysis based on the McCumber theory

According to the McCumber theory [6], the absorption cross section σ_a is relevant to the emission cross section σ_e through this relation,

$$\sigma_e(\nu) = \sigma_a \exp[(\varepsilon - h\nu)/kT], \qquad (1)$$

where ε is the temperature-dependent excitation energy. A physical interpretation of ε is the net free energy, may be considered to be the effective energy that required to excite one Er^{3+} ion from the $^4I_{15/2}$ level to the $^4I_{13/2}$ level at temperature T. $\exp[(\varepsilon - h\nu)/\kappa T]$ is determined by homogeneous broadening process.

In order to take into account the degeneracy in the $^4I_{13/2}$ and $^4I_{15/2}$ level of Er^{3+} ions, the simple Stark splitting model for the energy structure of Er^{3+} ion was assumed as shown in Fig. 3-1. Therefore, (1) can be rewritten as follows,

$$\sigma_e(\nu) = \sigma_a \exp[(E_0 - h\nu)/kT] \cdot \frac{1 + \sum_{j=2}^{8} 7\exp(-\Delta E_{1j}/kT)}{1 + \sum_{j=2}^{7} 6\exp(-\Delta E_{2j}/kT)}, \qquad (2)$$

where E_0 is the separation energy between the lowest components of each manifold, which is assumed to be 6535cm^{-1} (λ =1530nm). ΔE_{1j} and ΔE_{2j} is the difference in energy between the jth and the lowest components of the $^4I_{13/2}$ and the $^4I_{15/2}$ level. Here, we supposed that the adjacent components in the same manifold are separated by the same energy δE_1 and δE_2. Because the homogeneous linewidth for the 1.5 μ m transition in the erbium-doped aluminosilicate glass was found to vary as $50(T/293)^{1.73}$ (cm^{-1}) by spectral gain hole burning techniques [7], the separation energy δE_i (i=1,2) in Fig. 3-1 is assumed to be 50cm^{-1} at room temperature. E_{2j} is the difference in energy between the jth and the lowest components of the $^4I_{13/2}$ and the $^4I_{15/2}$ level.

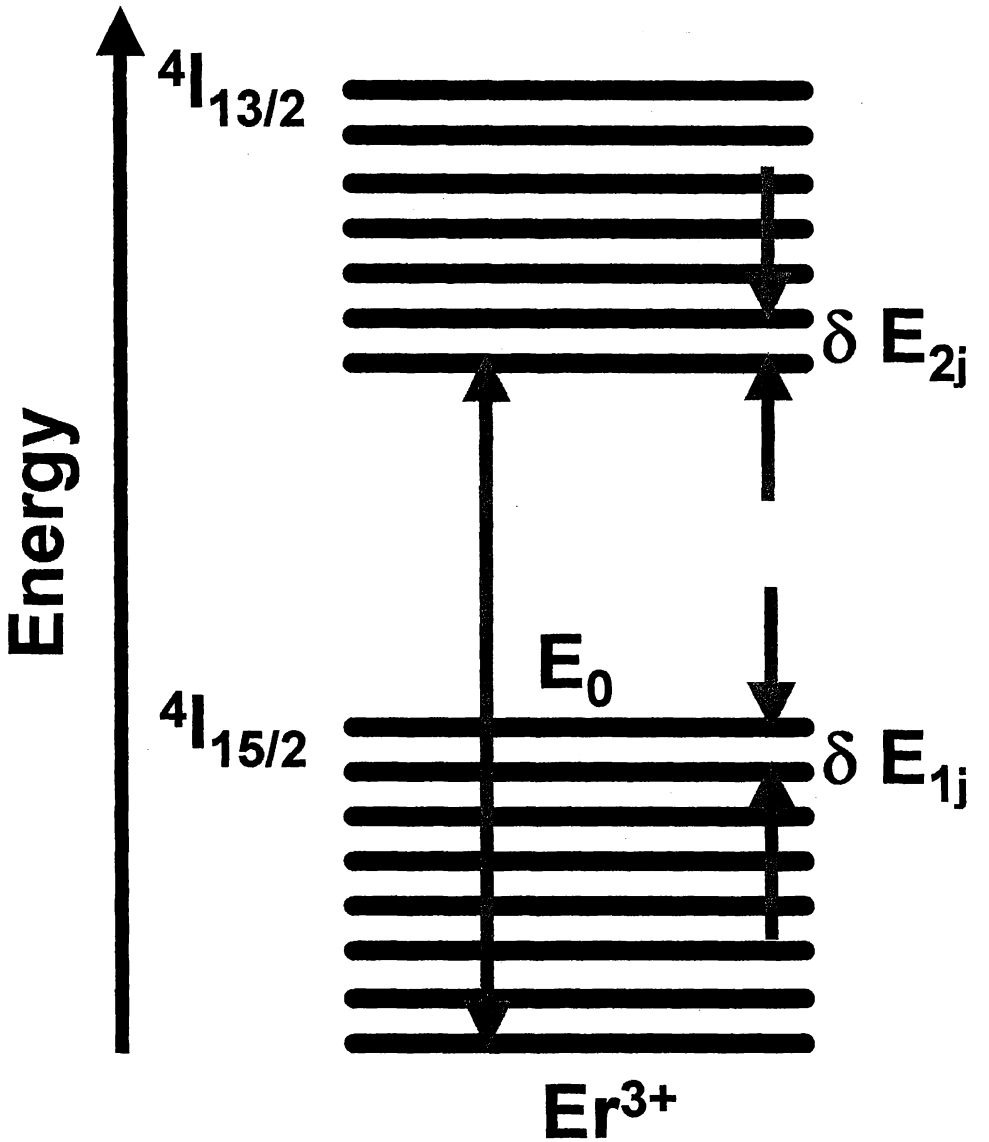

Figure 3-1 Energy diagram for each Stark manifold within the $^4I_{13/2}$ and $^4I_{15/2}$ level of Er^{3+} ion.

Here, we supposed that the adjacent components in the same manifold are separated by the same energy δE_1 and δE_2. Because the homogeneous linewidth for the 1.5 μ m transition in the erbium-doped aluminosilicate glass was found to vary as $50(T/293)^{1.73}$ (cm^{-1}) by spectral gain hole burning techniques [7], the separation energy δE_i (i=1,2) in Fig. 3-1 is assumed to be $50cm^{-1}$. If the 1.5 μ m transition system for Er^{3+} ion is expressed by the two level system that consists of the $^4I_{13/2}$ and the $^4I_{15/2}$ level, the gain coefficient γ (dB/m) is given by,

$$\gamma(\nu) = N_2(\sigma_e(\nu) + \sigma_a(\nu)) - N_{total}\sigma_a(\nu). \qquad (3)$$

N_{total} means the total population in the system and N_2 means the population of the $^4I_{13/2}$ level. It is clear that the differential of γ with respect to N_2, $d\gamma/dN_2$ is equivalent to the total cross section $\sigma_a + \sigma_e$. Differentiating equation (3) with respect to N_2 with the McCumber relation (2), we get

$$\frac{d\gamma(\nu)}{dN_2(T)} = [1 + \frac{1 + \sum_{j=2}^{8} 7\exp(-\Delta E_{1j}/kT)}{1 + \sum_{j=2}^{7} 6\exp(-\Delta E_{2j}/kT)}\exp[(\varepsilon - h\nu)/\kappa T]]\sigma_a(\nu). \qquad (4)$$

This indicates that the temperature dependence of $d\gamma/dN_2$ is fully dominated by the McCumber relation for the two level system. In addition, the absorption cross section σ_a can be the most basic parameter for the gain characteristics of EDF because it directly shows the relationship between the gain coefficient and the population density of the $^4I_{13/2}$ level.

3-3-2. Numerical Simulation model for gain characteristics

In order to verify whether the temperature variation of the gain characteristics in the S-band region could be reproduced or not by numerical way, the simulation based on the Giles model [8] was implemented. The two level system that consists of the first excited state $^4I_{13/2}$ and the ground state $^4I_{15/2}$ was adopted to describe the 1.5 μ m transition of Er^{3+} ion. The time evolution of N_2 and N_1, which are the total population densities of the $^4I_{13/2}$ and the $^4I_{15/2}$ level,

respectively, are described by the population rate equation and by the population conservation law:

$$N_{total} = N_1 + N_2, \quad (5)$$

$$\frac{dN_2}{dt} = -\frac{dN_1}{dt} = -(A_{21} + W_{21})N_2 + (W_{12} + R)N_1, \quad (6)$$

$$W_{21(12)} = \int \frac{\sigma_{as(es)}(\nu)P_s(\nu)}{h\nu\pi b^2} d\nu, \quad (7)$$

$$R = \int \frac{\sigma_{ap}(\nu)P_p(\nu)}{h\nu\pi b^2} d\nu, \quad (8)$$

where A_{21} is the spontaneous emission rate, W_{12} and W_{21} are the stimulated emission and absorption rates of the signal, R is the stimulated pump rate, $h\nu$ is the photon energy, b is the radius of the uniformly erbium-doped region, P_s and P_p are the signal and pump power, σ_{as}, σ_{es} and σ_{ap} are the absorption and emission cross section for the signal and pump, respectively. The contributions of the quenching and the excited state absorption cross section σ_{ESA} are not taken into consideration for this simple simulation procedure. The evolutions of pump, signal and bidirectional ASE powers, P_p, P_s and $P_{\pm ASE}$, along the fibers are given by,

$$\frac{dP_p(z)}{dz} = -\sigma_{pa}N_1P_p(z), \quad (9)$$

$$\frac{dP_s(z)}{dz} = (\sigma_{se}N_2 - \sigma_{sa}N_1)Ps(z), \quad (10)$$

$$\frac{dP_{ASE}(z)}{dz} = \pm(\sigma_{se}N_2 - \sigma_{sa}N_1)P_{ASE}(z) \pm mh\nu\Delta\nu\sigma_{se}N_2. \quad (11)$$

h is Plank's constant, m is the number of guided modes, normally 2, propagating at the signal wavelength and $\Delta\nu$ is the ASE bandwidth. For the ASE bandwidth, $\Delta\lambda$, which corresponds to $\Delta\nu$=0.2nm, was chosen uniformly for all wavelength. Fiber parameters used in the simulation are shown in Table 3-1. Fig. 3-2 shows the comparison of the experimental gain in 1.5 μm region with the theoretically simulated one.

3-4. Results and Discussions

3-4-1. Temperature dependence of Loss and absorption cross section

Fig. 3-3 (a) shows the loss spectra of EDF sample at 77K, 293K and 373K in the wavelength region from 1420nm to 1640nm. Fig. 3-3 (b) shows the absorption cross sections σ_a calculated from the loss spectra at 77K, 293K and 373K, respectively.

The σ_a shows the temperature dependence in the temperature region from 77K to 293K. But, in the range from 293K to 373K, the σ a does not show any change in the spectral shape.

3-4-2. Temperature dependence of emission cross section

Fig. 3-4(a) and 3-4(b) show the comparisons of the experimental σ_e with the theoretical σ_e obtained at 77K and 293K, respectively, through the temperature-dependent the McCumber relation. Fig. 3-4(a) and 3-4(b) show good agreements between the experimental and the theoretical σ_e. This indicates that the temperature-dependent the McCumber relation can predict well the shape of the spontaneous emission using the absorption cross section σ_a in terms of temperature. The deviation of theoretical σ_e from experimental one at 77K in longer wavelength region than 1600nm is caused by the enhancement of noise level of the experimental σ_a, which is brought by the factor $\exp[(\varepsilon - h\nu)/kT]$.

3-4-3. Evaluation of temperature dependence of emission cross section using the McCumber relation

In order to investigate the thermal characteristics of the gain in the S-band region, the absorption and the emission cross sections were examined experimentally and numerically at temperatures above 293K. Fig. 3-5(a) shows the temperature dependences of the cross section $\sigma_a(T)$ obtained by the absorption measurements at 293K, 333Kand 373K.

TABLE 3.1 Simulation parameters for silica-based EDF

E_0 (nm)	1530
$\delta E_1(cm^{-1})$	50
$\delta E_2(cm^{-1})$	50
Total number of Er^{3+} ($/m^3$)	3.746×10^{24}
Number of Er^{3+} in $^4I_{15/2}$ (293(K))	3.746×10^{24}
Number of Er^{3+} in $^4I_{13/2}$ (293(K))	4.51×10^{9}
b(μ m)	4.7
Meta-Stable Time(ms)	10
ASE Bandwidth(nm)	0.2
EDF Length(m)	10
Pump Wavelength(nm)	980
Absorption $\sigma_p(cm^2)$	7.93×10^{-22}
Pump Power(mW)	150
Signal Wavelength(nm)	1420-1640
Absorption $\sigma_s(cm^2)$	$\sim 3.02 \times 10^{-21}$
Signal power(dBm)	-30

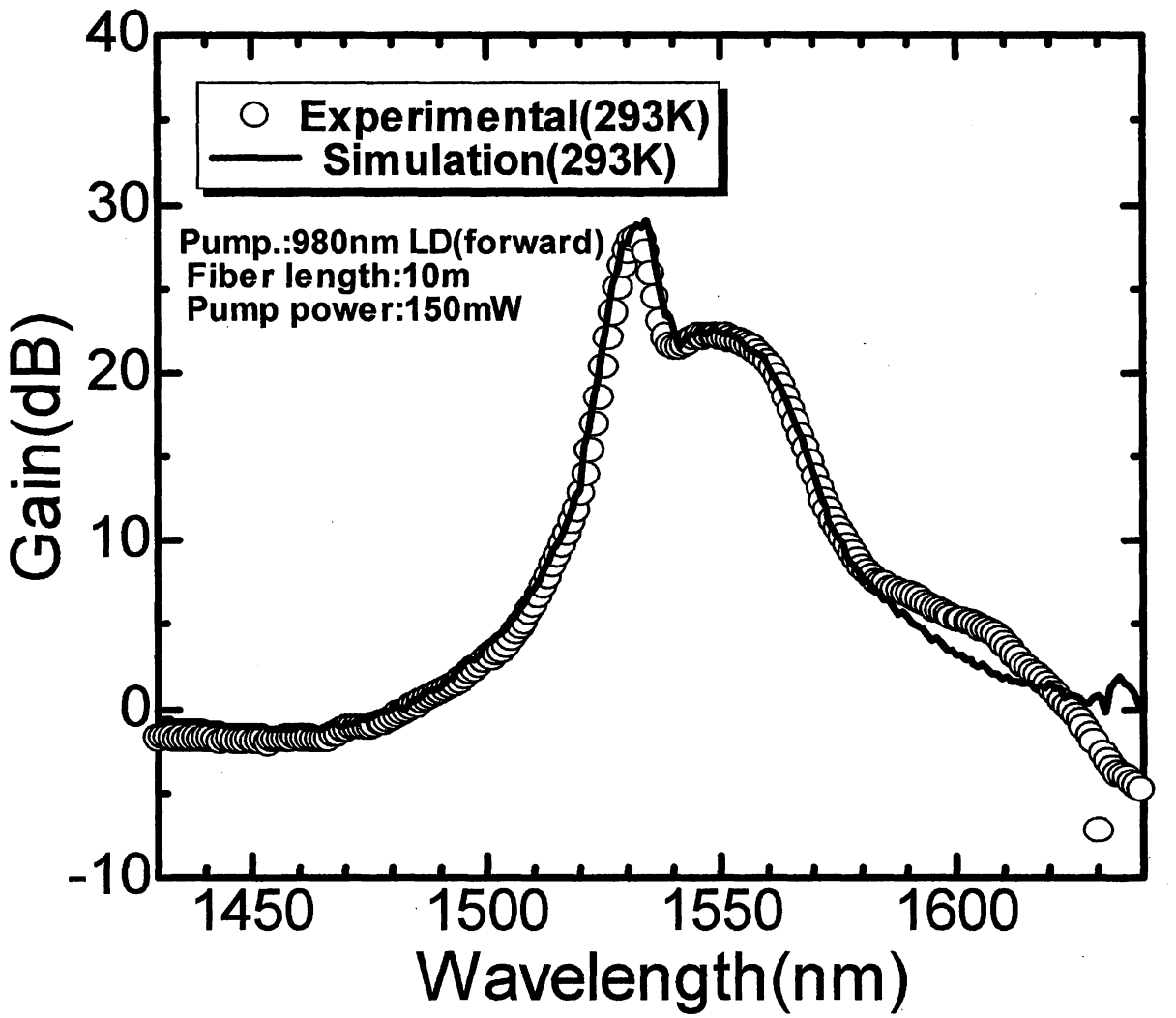

Figure 3-2 Comparison of the experimental gain in 1.5 μ m region with the theoretically simulated one.

As shown in Fig. 3-5(a), the $\sigma_a(T)$ does not show any temperature dependences up to 373K, indicating that the line strength in 1.5 μ m does not change up to 373K. This also suggests that there does not occur any significant changes of the glass structure and basicity up to 373K because the line strength in 1.5 μ m reflects the intensity parameter Ω_t (τ=2, 4, 6).[9, 10] Hence, the temperature dependence of the emission cross section $\sigma_e(T)$ was examined based on the temperature-dependent McCumber relation, assuming that the $\sigma_a(T)$ is constant. The accuracy of the McCumber theory in this temperature region have been reported to be kept fairly well for Er^{3+} ions [11] in aluminosilicate glass, considering the temperature variation of homogeneous linewidth as T^{α}, with $1.6<\alpha<2$ [12-14]. Fig. 3-5(b) shows the temperature dependence of the $\sigma_e(T)$ predicted numerically. As shown in Fig. 3-5(b), the emission cross section in the wavelength region shorter than 1530nm increased with increasing temperature while the emission cross section in the wavelength region than 1530nm decreases.

Therefore, the S-band gain can be expected to increase as temperature increases whereas the gain in longer wavelength region longer than 1530nm decreases. These spontaneous emissions at temperatures above 293K obtained numerically were used in the numerical prediction of the temperature dependence of the S-band gain characteristics to compare with experimental results in Next session.

3-4-4. Temperature dependence of gain characteristics in the S-band wavelength region

Fig. 3-6 (a) and 3-6(b) show the experimental gain profiles in the wavelength region from 1420nm to 1640nm, obtained at 77K, 293K and 373K, and those numerically calculated from the emission and absorption cross sections at 293K, 333K, 373K and 573K. Simulation parameters of EDF are the same ones as in Table 3-1. Then the temperature-dependent McCumber model, which took into account the temperature dependence of the spontaneous emission, was used in numerical simulation for gain spectrum of EDF.

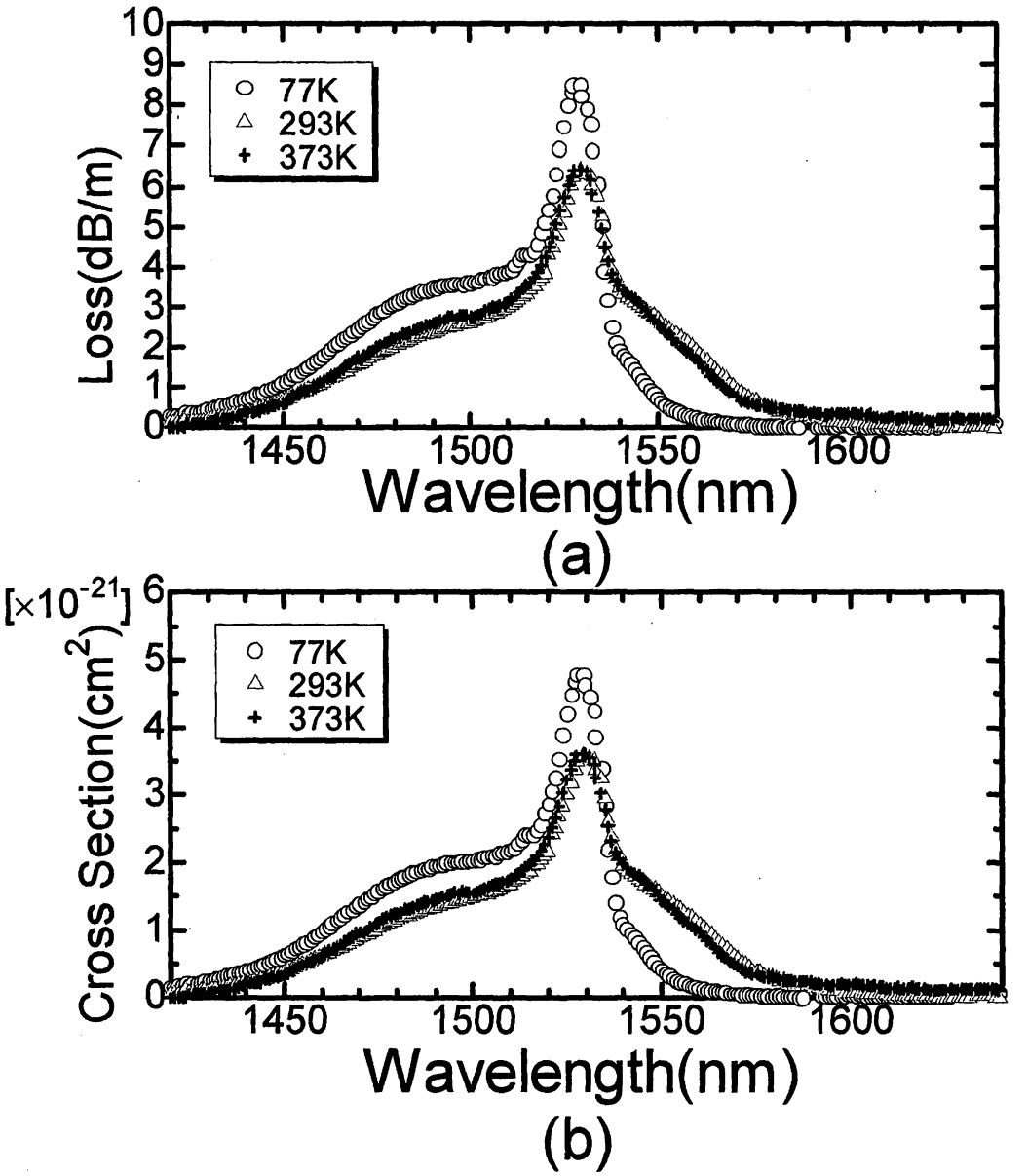

Figure 3-3 (a) Loss spectra of EDF sample at 77K, 293K and 373K in the wavelength region from 1420nm to 1640nm.

(b) Absorption cross section σ_a calculated from the loss spectra at 77K, 293K and 373K, respectively.

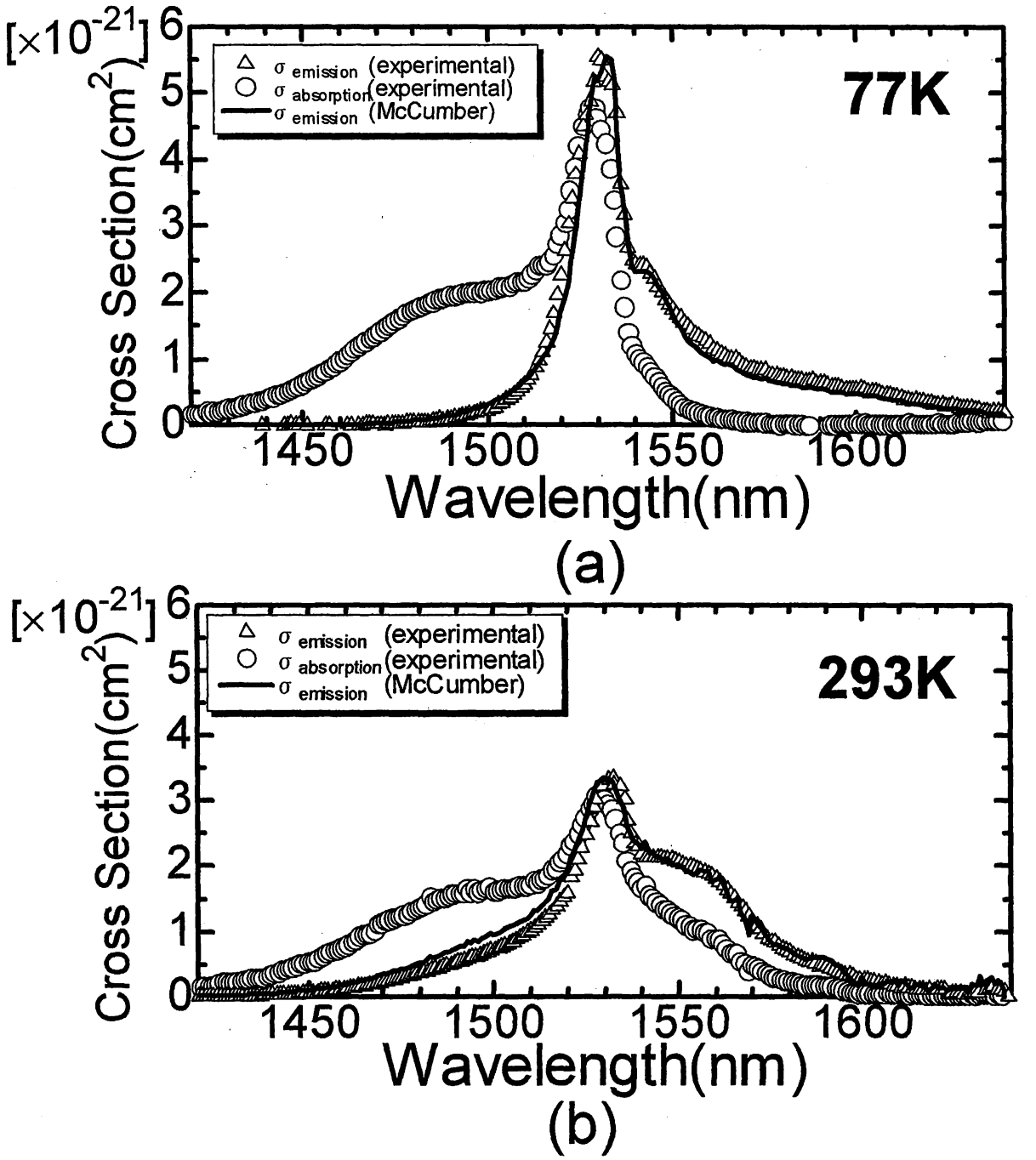

Figure 3-4 (a) Comparison of the experimental σ e at 77K with the theoretical σ_e.

(b) Comparison of the experimental σ e at 293K with the theoretical σ_e.

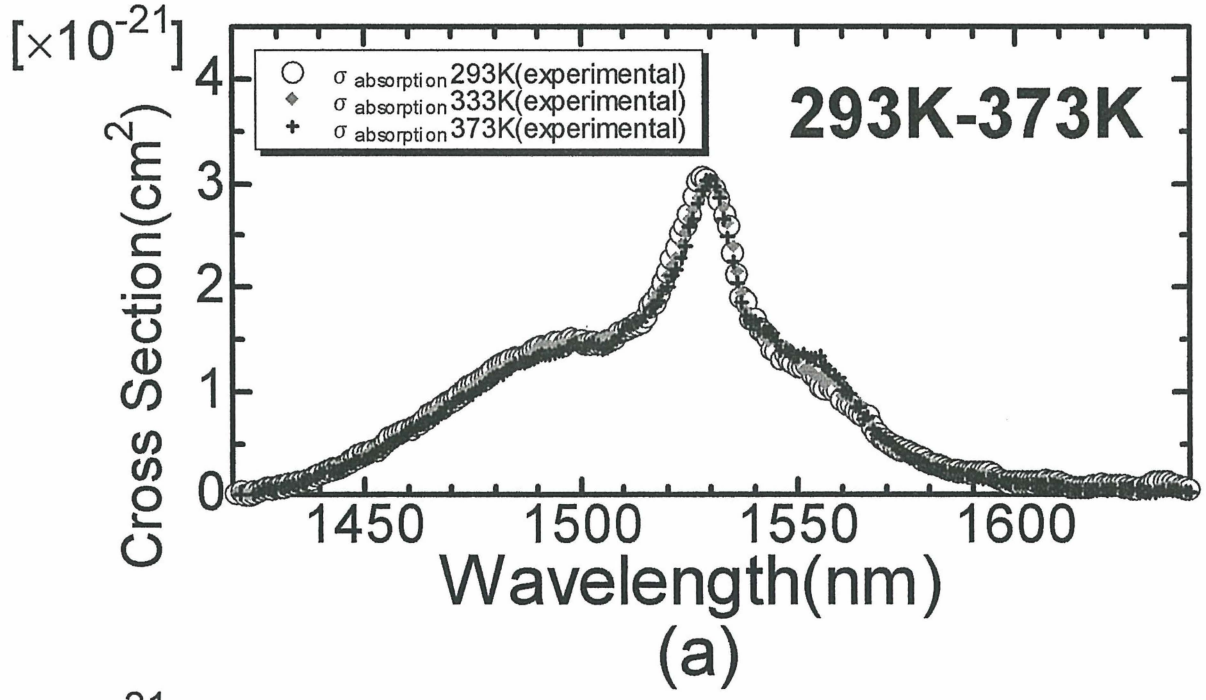

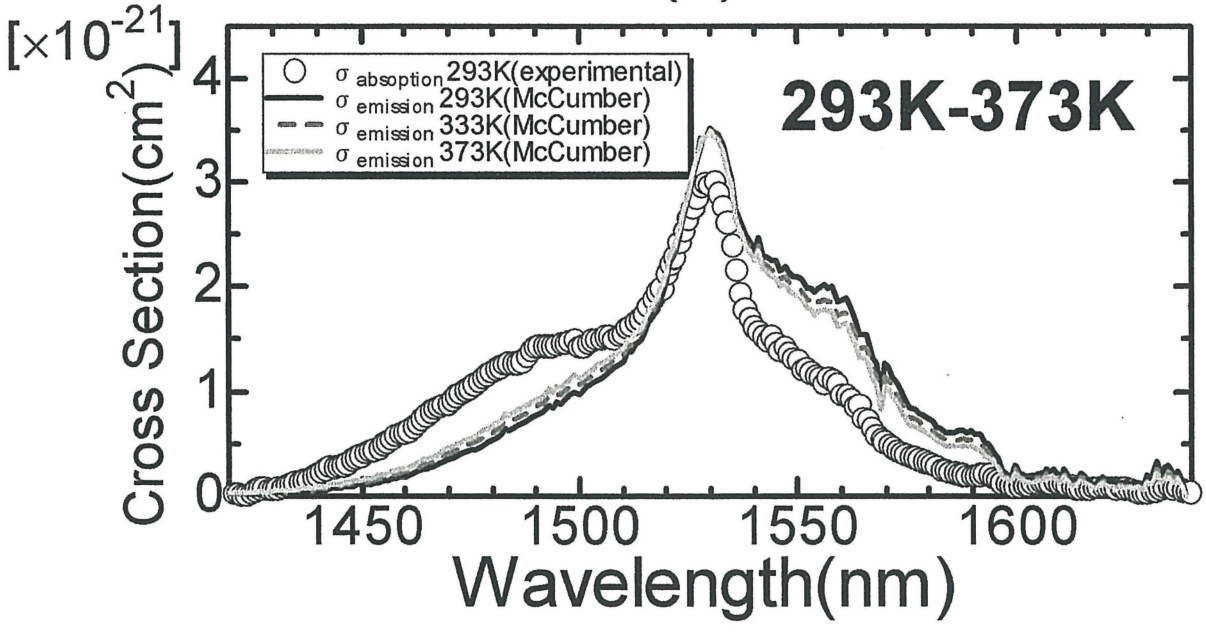

Figure 3-5 (a)Temperature dependences of the cross section $\sigma_a(T)$ at 293K, 333K and 373K.

(b)Temperature dependence of $\sigma_e(T)$ calculated based on McCumber relation.

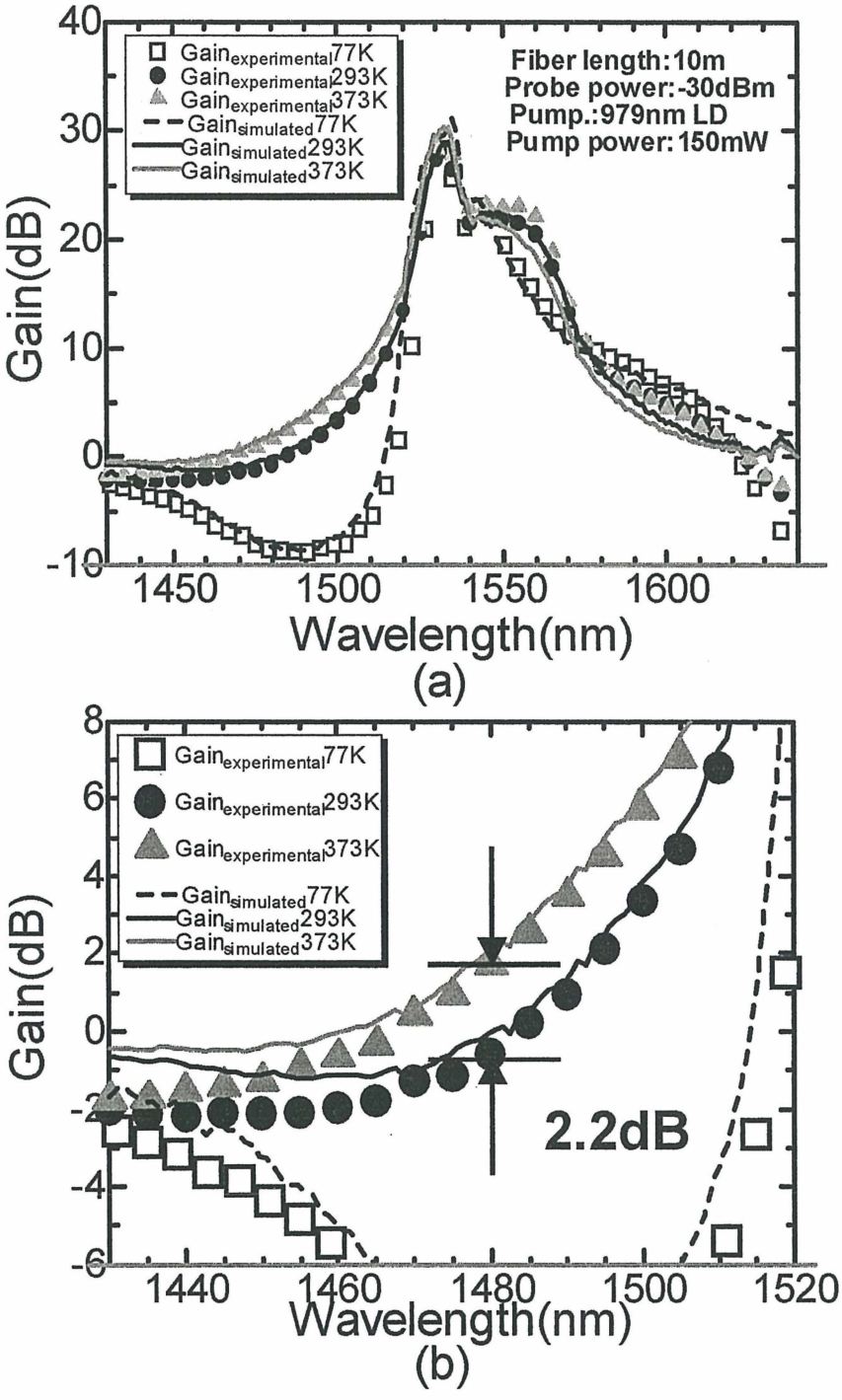

Figure 3-6 (a) Comparison of experimental gain profiles with simulated ones in the wavelength region from 1420nm to 1640nm, at 77K, 293K and 373K.

(b) Close-up of Figure 3-6(a).

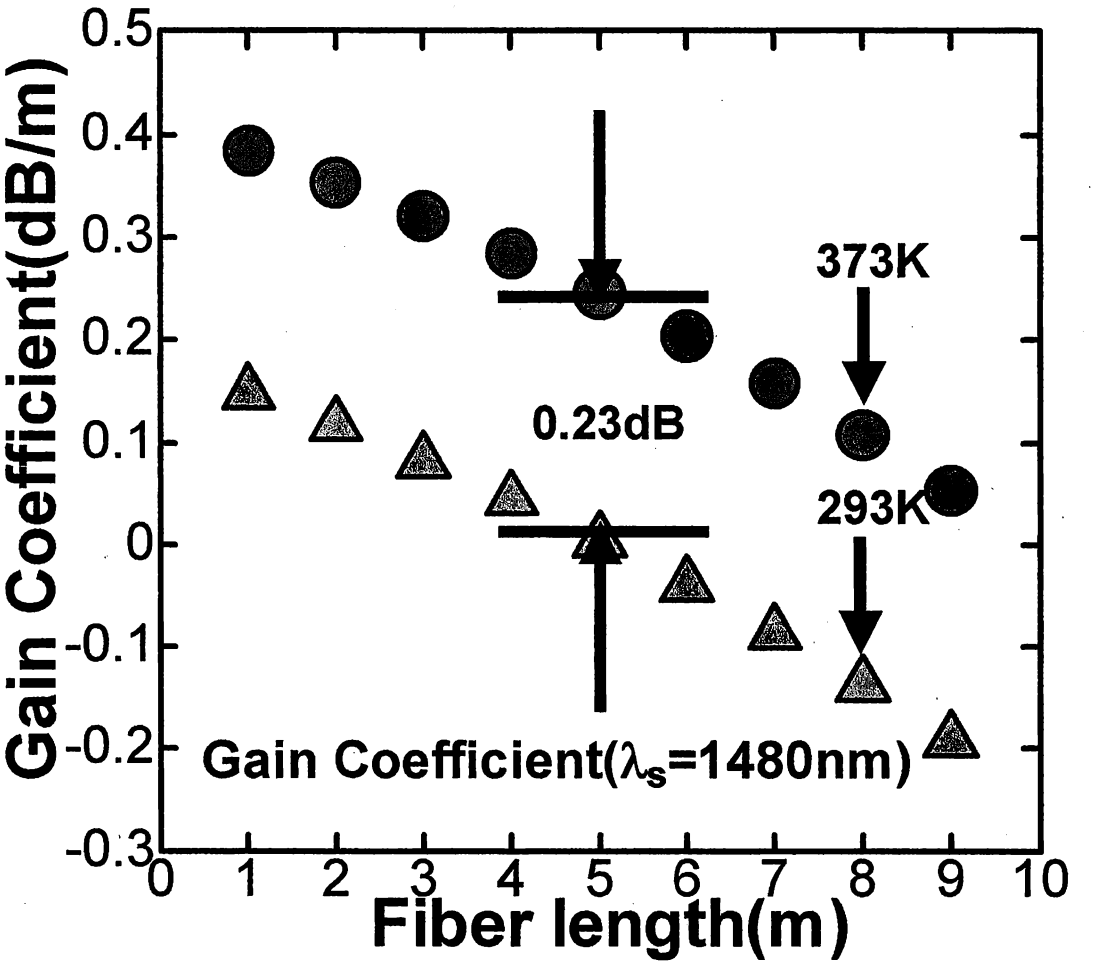

Figure 3-7 Gain Coefficients along the EDF simulated at 293K and 373K (λ_s=1480nm).

As shown in Fig. 3-6(b), the numerical and experimental gains in the S-band region (1430nm-1580nm) increase with increasing temperature. The increasing rate of the gain in the S-band region with increasing temperature was well explained by numerical model. This temperature dependence of the S-band gain can be explained well and introduced by the temperature term in the McCumber relation though the numerical gain value is slightly different from experimental ones in the S-band wavelength region. Compared with the gain at room temperature, the gain at 373K shows about 2dB increase in the S-band wavelength region. On the other hand, the degradation of the gain in the longer wavelength region than 1530nm, which was predicted by the spontaneous emission cross section analysis numerically, did not occur experimentally with increasing temperature.

3-4-5. Temperature dependence of Noise Figure and population density in the S-band wavelength region

Fig. 3-7(a) shows the wavelength dependences of the noise figure (NF). Fig. 3-7(b) shows the ratios of the factor $N_a(\lambda_i)/N_b(\lambda_i)$ at 77K and 373K to that at 293K. NF and $N_a(\lambda_i)/N_b(\lambda_i)$ were calculated from the ASE power and the gain obtained by the gain measurements. Here, $N_a(\lambda_i)$ and $N_b(\lambda_i)$ describe the population densities within the $^4I_{13/2}$ and $^4I_{15/2}$ level, which contribute to the emission whose wavelength is λ_i. $N_a(\lambda_i)$ and $N_b(\lambda_i)$ satisfy these population conservation laws as follows:

$$\sum_{\lambda_i} N_a(\lambda_i) = N_2 \qquad (12)$$

$$\sum_{\lambda_i} N_b(\lambda_i) = N_1 \qquad (13)$$

N_2 and N_1 show the total population densities of the $^4I_{13/2}$ and $^4I_{15/2}$ level, respectively. As shown in Fig. 3-7(a), NF in the S-band wavelength region decreases as temperature increases from 77K to 373K. This indicates that the population densities in the upper Stark manifolds within the $^4I_{13/2}$ level increase due to the thermal excitation of Er^{3+} ions, which leads to the

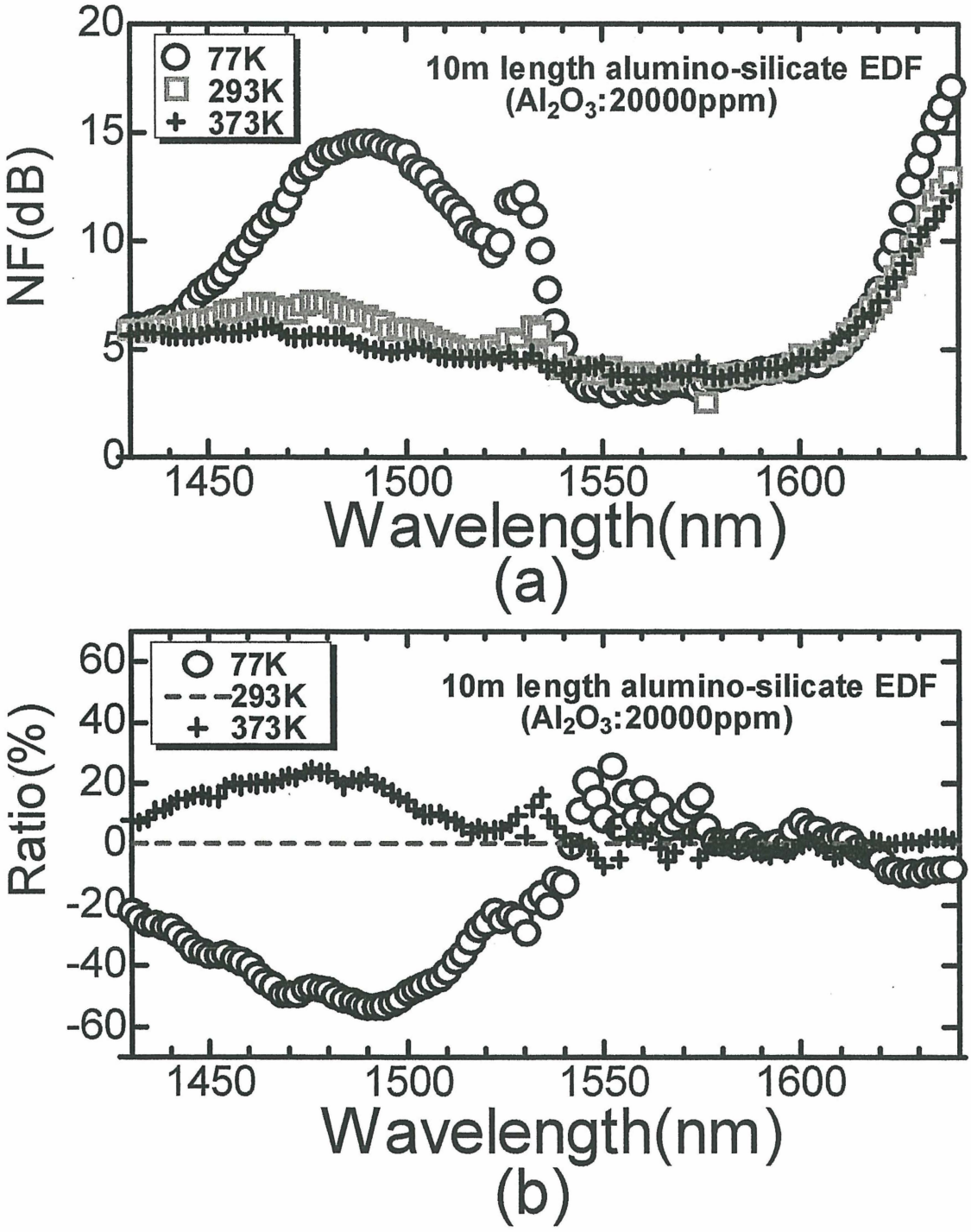

Figure 3-8 (a) Wavelength dependence of NF at 77K, 293K and 373K.

(b) Ratio of the factor $N_a(\lambda_i)/N_b(\lambda_i)$ at 77K and 373K to that at 293K.

improvement in the emission and gain character in the S-band region mentioned above. Actually, $N_a(\lambda_i)/N_b(\lambda_i)$ in creases in the S-band region with increasing temperature as shown in Fig. 3-7(b). About 20% increase of $N_a(\lambda_i)/N_b(\lambda_i)$ in the S-band region were observed at 373K compared with that at room temperature. Therefore, about 2dB increase in the S-band gain is considered to be as a result of the 20% increase of $N_a(\lambda_i)/N_b(\lambda_i)$.

This can be explained by the increase of the population densities in the upper Stalk manifolds of the $^4I_{13/2}$ level and the decrease of population densities in the lower Stark manifolds of the $^4I_{15/2}$ level. On the other hand, NF in the longer wavelength region than 1530nm shows little temperature dependence compared with that in the S-band region. The slight improvement in NF in the C-band region observed at 77K. This indicates that the increase of the population densities in the lower Stark manifolds within the $^4I_{13/2}$ and $^4I_{15/2}$ level, which contribute to the emission in the C-band region. In addition, $N_a(\lambda_i)/N_b(\lambda_i)$ in the L-band region (1580nm-1640nm) shows little change with increasing temperature from 77K to 373K. This is consistent with the character that the gain degradation does not occur experimentally in the L-band wavelength region as shown in Fig. 3-7(a). This L-band gain character cannot be fully explained by the temperature-dependent McCumber model. The violation of two level system for the Er^{3+} ion energy structure caused by the contribution of some other energy levels to the gain spectrum is possibly an explanation for the thermal gain character in the C-band and the L-band wavelength regions. Compared with the S-band wavelength region, the temperature-dependent McCumber simulation model based on the two level system for Er^{3+} ion energy structure needs more consideration when it is applied to the thermal gain characteristics in the C -band and the L-band regions.

3-5. Conclusion

Numerical and experimental evaluation of the gain characteristics of a silica-based EDF was performed. The temperature dependence of these gain properties was investigated numerically and experimentally. As a result, about 2dB increase of the S-band gain was observed as temperature increased up to 373K for a 10m-lengh silica-based EDFA. It was verified that the temperature-dependent McCumber simulation model could explain well the gain character in the S-band wavelength region numerically. Therefore, this result indicates that the change of the population density in the Stark manifolds of the $^4I_{13/2}$ and $^4I_{15/2}$ brought about 0.2dB/m improvement in gain coefficient. On the other hand, the gain spectrum in the C-band and the L-band wavelength regions showed different temperature dependence from that of the temperature-dependent McCumber simulation model.

References

[1]. J. F. Massicott, J. R. Armitage, R. Wyatt, B. J. Ainsile and S. P. Craig-Ryan, "High gain, Broadband, 1.6μm Er^{3+} doped silica fiber amplifier," Electron. Lett., vol. 26, pp. 1645-1646, 1990.

[2]. J. F. Massicott, R. Wyatt and B. J. Ainsile, "Low noise operation of Er^{3+} doped silica fiber amplifier around 1.6μm,"Electron. Lett. vol. 28, pp. 1924-1925, 1992.

[3]. M. Rochette, M. Guy, S. LaRochelle, J. Lauzone and F. Trenpanier, "Gain equalization of EDFA's with Bragg gratings," IEEE Photonics Technol. Lett., vol. 11, pp. 536-538, 1999.

[4]. I. Riant, L. Gasca, P. Sansonetti, G. Bouret and J. Chesnoy, "Gain equalization with optimized slanted Bragg grating on adapted fiber for multichannel long-haul submarine transmission," *in the Proceedings of Optical Fiber Communications1999*, OFC99, ThJ6-1, pp. 147-149, 1999.

[5] E. Ishikawa, M. Nishihara, Y. Sato, C. Ohshima, Y. Sugaya, and J. Kumasako, "Novel 1500nm-band EDFA with discrete Raman amplifier," *in the Proceedings of European Conference on Optical Communication 2001,* ECOC2001 PD.A.1.2, 2001.

[6]. D. E. McCumber, "Theory of Phonon-Terminated Optical Masers," *Phys. Rev.* vol. 134, pp. A299-A306, 1964.

[7]. E. Desurvire, J. L. Zyskind, and J. R. Simpson, "Study of spectral dependence of gain saturation and effect of inhomogeneous broadening in erbium-doped aluminosilicate fiber amplifiers," IEEE Photon. Technol. Lett.,vol. 2, No4, pp. 246-248, 1990.

[8]. C. R. Giles and E. Desurvire, "Modeling erbium-doped fiber amplifiers," IEEE J. Lightwave Technol., vol. 9, pp. 271-283, 1991.

[9]. R. D. Peacock, "The intensities of lanthanide f-f transitions," in Structure and Bonding (Springer, Berlin, 1975), Vol. 22, pp. 83-121.

[10] S. Tanabe, T. Hanada, "Local structure and 1.5 μm quantum efficiency of erbium doped glasses for optical amplifiers," *J. Non-Cryst. Solids.*, vol. 196, pp.101-105, 1996.

[11]. R. S. Quimby, "Range of validity of McCumber theory in relating absorption and emission cross sections," J. Appl. Phys., vol. 92, pp. 180-187, 2002.

[12]. J. Hegarty and W. M. Yen, "Optical Homogeneous Linewidths of Pr^{+} in BeF_2 and GeO_2 Glasses," Phys. Rev. Lett., vol. 43, pp. 1126-1130, 1979.

[13]. G. Lei, J.E.Anderson, M. I. Buchward, B. C. Edwards, and R. I. Epstein, "Determination of spectral linewidths by Voigt profiles in Yb^{3+}-doped fluorozirconate glasses," Phys. Rev. B, vol. 57, pp. 7673-7678, 1998.

[14] L. Bigot, A. Jurdyc, B. Jacquier, L. Gasca, and D. Bayart, "Resonant fluorescence line narrowing measurements in erbium-doped glasses for optical amplifiers," Phys. Rev. B 66, pp. 1-9, 2002.

Chapter 4

Evaluation of quenching effect on gain characteristics in erbium-doped fiber using numerical simulation

4-1. Introduction

Highly erbium-doped glass material has been needed for the high output power devices due to the increase of the number of signals in optical transmission system. On the other hand, one of the serious limiting factors to the performance of the Er^{3+}-doped fiber amplifier (EDFA) is the effect of the concentration quenching of the emission from Er^{3+} ions on the gain. A significant degradation of gain from 18.3 dB to 6.9dB has been reported for the gain characteristics of EDFA, which includes $6.4 \times 10^{25}(/m^3)$ ions [1]. In addition, the concentration quenching effect can be also serious problems for the Er^{3+} doped waveguide amplifier (EDWA) and Er^{3+}-doped fiber laser (EDFL) [2,3].

Today the optical amplification performance of highly erbium doped glass materials becomes more attracting issue in optical product area. The energy-transfer mechanism

between rare earth ions mainly dominated by the electric dipole interaction was modelled by Miyakawa-Dexter theory using the relaxation time of emission and the critical distance between erbium ions. The concentration quenching effect of the 1.5 μ m emission of Er^{3+} is usually caused by the energy-transfers between homogeneously distributed Er^{3+} ions and locally clustered Er^{3+} ions in the host glass. In the case of electric dipole interaction between rare earth ions, the energy transfer probability on the separation between Er^{3+} ions has been well known to be inversely proportional to the sixth power of average distance between Er^{3+} ions (critical distance)[4,5]. Usually, the contribution of the energy-transfers between homogeneously distributed Er^{3+} ions to the degradation of the optical amplification performance of EDFA is called the homogeneous upconversion process (HUC) which is considered to be inevitable phenomenon and occur between the erbium ions separated by about 2.2nm.

In addition to the homogeneous interactions HUC between erbium ions mentioned above, it has been suggested that, in highly Er^{3+}-doped region, Er^{3+} ions tend to cluster in pairs and that a rapid cross-relaxation process takes place between the doubly excited Er^3 ion pairs to the $^4I_{13/2}$ level what we call pair induced quenching process (PIQ). The distance of clustered ions is considered to be comparable to erbium ion diameter of about 0.2nm. In this process, one of the two ions transfers its energy to the other ion and is then nonraditively transferred to the ground state $^4I_{15/2}$ while the other ion is upconverted to the $^4I_{9/2}$ level, where it mostly relaxes rapidly to the metastable level $^4I_{13/2}$. Thus, doubly excited state decays very quickly and can be disregarded in the metastable state. Usually, two states of Er^{3+} ion pairs to be populated are taken into consideration: Either none or one of the ions in the pair can be in its excited state $^4I_{13/2}$. Former is called acceptor, and latter is donor. Generally, the upconversion rate in erbium ion pairs is more rapid than the homogeneous one since the interaction rate is strongly dependent on the distance[6].

The investigation into this PIQ process is considered to become more important as the amount of erbium ions in EDFA become higher. Therefore, in this paper, we focused our

interests on the effect of PIQ on the gain performance of the highly Er^{3+}-doped EDF. The degradation of the power conversion efficiency, the population density of the $^4I_{13/2}$ and the gain performance of EDFA were investigated precisely by both the numerical and experimental evaluations using silica-based EDF with different Er^{3+} ion concentration. In addition, the correlation between the degradation of the population densities of the $^4I_{13/2}$ level is discussed in connection with the concentration quenching mechanism in silica-based highly erbium-doped fiber.

4-2. Numerical Simulation model for the gain characteristics of EDF

In order to analyze the gain characteristics, the simulation based on the Giles model [7] was implemented for the single and paired Er^{3+} ions. In this simulation procedure, the contributions of the excited state absorption cross section σ_{ESA} are not taken into consideration.

For the total Er^{3+} ion concentration, N_t, the paired ion concentration was introduced to as $N_p=mkN_t$, where k is the relative number of clusters and mk is the fraction of clusters. The concentration of single ions is $N_s=(1-mkt)N_t$. Firstly, the two level system that consists of the first excited state $^4I_{13/2}$ and the ground state $^4I_{15/2}$ was adopted in order to describe the 1.5 μ m transition of Er^{3+} ions. The total inversion is given by,

$$N_2 = N_{s2} + N_{p2} \quad (1)$$

$$N_1 = N_{s1} + N_{p1} \quad (2)$$

where N_2 and N_1 are the total population densities of the $^4I_{13/2}$ and the $^4I_{15/2}$ level for the single Er^{3+} ions, respectively. N_{si} and N_{pi}(i=1,2) are the total population densities of the single and paired ions, respectively, in the $^4I_{13/2}$ and the $^4I_{15/2}$ level. C is the cooperative upconversion coefficient which is defined exactly by using the density of erbium ions ρ_{Er} and the critical distance R_0 between erbium ions and the lifetime of emission τ as follows[8-12]:

$$C_{CU} = \frac{16\pi}{9}\frac{R_0^6}{\tau}\rho_{Er} \quad (3)$$

The time evolution of N_{s2} and N_{s1} are described by the population rate equation considering the homogeneous up conversion effect and by the population conservation law:

$$Ns = Ns_1 + Ns_2, \quad (4)$$

$$\frac{dNs_2}{dt} = -\frac{dNs_1}{dt} = -(A_{21} + W_{21})Ns_2 + (W_{12} + R)Ns_1 - C_{cu}Ns_2^2, \quad (5)$$

$$W_{21(12)} = \int \frac{\sigma_{as(es)}(\nu)P_s(\nu)}{h\nu\pi b^2}d\nu, \quad (6)$$

$$R = \int \frac{\sigma_{ap}(\nu)P_p(\nu)}{h\nu\pi b^2}d\nu, \quad (7)$$

where A_{21} is the spontaneous emission rate, W_{12} and W_{21} are the stimulated emission and absorption rates of the signal, R is the stimulated pump rate, $h\nu$ is the photon energy, b is the radius of the uniformly Er^{3+}-doped region, P_s and P_p are the signal and pump power, σ_{as}, σ_{es} and σ_{ap} are the absorption and emission cross section for the signal and pump, respectively. The A_{21}, W_{12}, W_{21}, σ_{as}, σ_{es} and σ_{ap} are assumed to be the same for the single and paired Er^{3+} ions. In addition, the following steady solution for the paired ions were used,

$$N_{p2} = N_p - N_{p1} = N_p \frac{R + W_{12}}{A_{21} + m(R + W_{12}) + W_{21}}. \quad (8)$$

The evolutions of pump, signal and bidirectional ASE powers, P_p, P_s and $P_{\pm ASE}$, along the fibers are given by,

$$\frac{dP_p(z)}{dz} = -\sigma_{pa}N_1P_p(z), \quad (9)$$

$$\frac{dP_s(z)}{dz} = (\sigma_{se}N_2 - \sigma_{sa}N_1)Ps(z), \quad (10)$$

$$\frac{dP_{ASE}(z)}{dz} = \pm(\sigma_{se}N_2 - \sigma_{sa}N_1)P_{ASE}(z) \pm mh\nu\Delta\nu\sigma_{se}N_2. \quad (11)$$

h is the Plank constant, m is the number of guided modes, normally 2(the number of the

polarization mode of signal), propagating at the signal wavelength and $\Delta \nu$ is the ASE bandwidth. For the ASE bandwidth, $\Delta \nu$,which corresponds to the resolution of OSA, $\Delta \lambda$ =0.2nm, was chosen uniformly for all wavelength. Using the obtained population densities by the propagation and rate equations, the gain coefficient γ (dB/m) is given by,

$$\gamma(\nu,z) = N_2(z)(\sigma_e(\nu) + \sigma_a(\nu)) - N_{total}\sigma_a(\nu). \qquad (12)$$

The total gain of EDF in linear scale is obtained by accumulating the gain coefficient γ along the fiber as follows:

$$Gain(\nu,z) = \exp[\int(N_2(z)(\sigma_e(\nu) + \sigma_a(\nu)) - N_{total}\sigma_a(\nu))dz]. \quad (13)$$

This indicates that the decrease in the population density of the $^4I_{13/2}$ level directly leads to the degradation of the gain. Therefore, the gain characteristics of the EDF samples with different Er^{3+} concentration, which have the same cross section, were evaluated in order to investigate the effect of Er^{3+} ion concentration on the degradation of the population densities.

4-3.Experimental

4-3-1. EDF samples

Four silica-based EDF samples with different Er^{3+} ion concentration were used.

The Er^{3+} ions concentrations of samples were 180ppm, 280ppm, 1600ppm, and 2600ppm. Optical parameters for each EDF are shown in Table 4-1.

The fiber length of each EDF was determined to include the same number of the total Er^{3+} ion. The refractive indices of EDF samples were measured with a reflectometer (Ando, AQ7413). The refractive indices of EDF samples at 1.3 μ m are around 1.47.

Table 4-1. Parameters for silica-based EDF samples.

Sample	Er^{3+} ion (ppm.wt)	Fiber Length (m)	$n_{1.3\mu m}$ (-)
EDF I	180	23.2	1.476
EDF II	280	15.7	1.470
EDFIII	1600	2.9	1.470
EDFIV	2600	1.5	1.470

4-3-2. Absorption spectra measurements

Absorption spectra of EDF samples were measured with three tunable laser sources (Santec, TSL210) and an optical spectrum analyzer (OSA) (Anritsu, MS9780A) at room temperature in the wavelength region 1420-1640nm. The TLS and OSA were controlled by a personal computer. Signal input power was –30dBm in order not to saturate the $^4I_{13/2}$ level by the strong excitation of probe signal. The obtained absorption cross sections of four EDF samples were used to simulate the gain characteristics in the wavelength region 1420-1640nm to compare with the experimental results.

4-3-3. Absorption spectra measurements

Absorption spectra of EDF samples were measured with three tunable laser sources (Santec, TSL210) and an optical spectrum analyzer (OSA) (Anritsu, MS9780A) at room temperature in the wavelength region 1420-1640nm. The TLS and OSA were controlled by a personal computer. Signal input power was –30dBm in order not to saturate the $^4I_{13/2}$ level by the strong excitation of probe signal. The obtained absorption cross sections of four EDF samples were used to simulate the gain characteristics in the wavelength region 1420-1640nm to compare with the experimental results.

4-3-4. Quantum Efficiency and Power Conversion Efficiency

The spontaneous emission probabilities $A_{JJ'}$ is proportional to the absorption cross section σ_a as follows:

$$A_{JJ'} = \frac{8\pi c n^2 (2J+1)}{\lambda_{mean}^4 (2J'+1)} \int \sigma_a(\lambda) d\lambda . \qquad (14)$$

where λ_{mean} is the mean wavelength of absorption band, c is the speed of light and n is the refractive index. The refractive indices of the core of EDF were about 1.47 and showed little EDF sample dependence. J is the total angular moment of the initial state, which is the $^4I_{15/2}$, and J' is that of the final state $^4I_{13/2}$ for the 1.5 μ m transition.

Using measured decay time of emission τ_f and $A_{JJ'}$, W_{NR} and QE are expressed as,

$$W_{NR} = \tau_f^{-1} - \sum_{J'} A_{JJ'} . \qquad (15)$$

$$QE = \frac{\sum_{J'} A_{JJ'}}{W_{NR} + \sum_{J'} A_{JJ'}} \qquad (16)$$

Power conversion efficiency (PCE) is one of the indices that evaluate the EDF performance as optical amplifier. PCE of EDF samples were evaluated at the signal wavelength 1550nm pumped by 979nm LD.

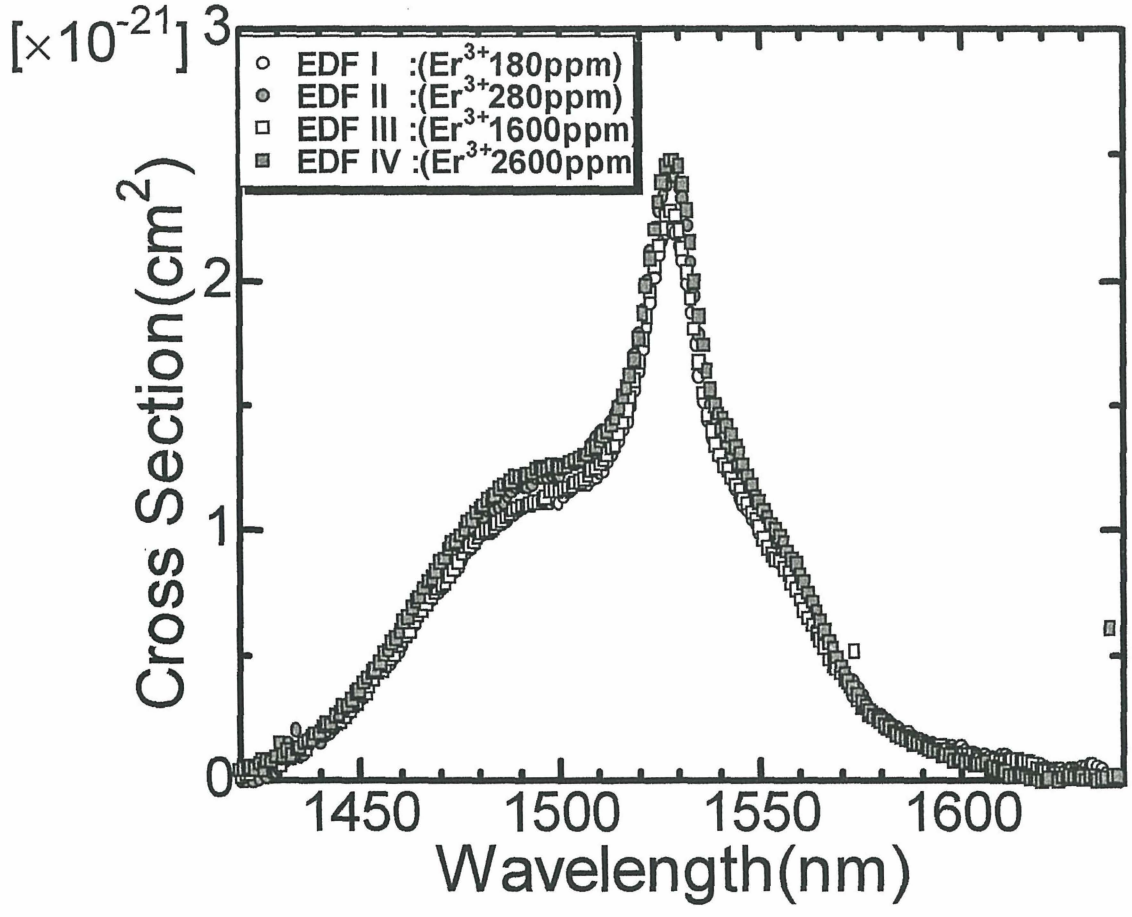

Figure 4-1 Cross sections of four EDF samples.

PCE is defined as follows:

$$PCE = \frac{P_{Sig.out} - P_{Sig.in} - P_{ASE}}{P_{LD}}, \quad (17)$$

where $P_{sig.\ in}$, $P_{sig.\ in}$, P_{ASE} and P_{LD} mean signal input power, signal output power, ASE output power and pump LD power, respectively. PCE shows what extent the input LD power is converted to the signal power. Theoretical maximum limit of PCE of LD is simply estimated by,

$$PCE_{Max.} = \frac{\lambda_{pump.}}{\lambda_{signal}}. \quad (18)$$

4-3-5. Gain saturation measurements

Gain saturation measurements of silica-based EDF were performed at 77K and 300K. For the gain saturation measurements at 77K, EDF sample was cooled directly by liquid nitrogen in a dewar. Two EDF pairs, which have the same absorption cross section, were used in order to compare the degradation of the population inversion ratio.

Probe signal wavelength is 1530nm. Input signal power was varied from –40dBm to about 5dBm using a variable ATT (Santec). In the gain saturation measurements, EDF samples were forwardly pumped by a 979nm LD (FITEL). Pump power was varied from 10mW to 30mW.

4-3-6. Gain spectra measurements

The gain characteristics of EDF were measured at room temperature in the wavelength region 1420-1640nm to evaluate the gain degradation caused by the Er^{3+} concentration quenching. Signal input power was –30dBm. The EDF sample was forwardly pumped with a 979nm LD. Pumping power was varied from 10mW to 50mW.

4-4. Results and Discussion

4-4-1. Absorption cross sections

Fig. 4-1 shows the absorption cross sections of four EDF samples.

Pairs of (EDFI & EDFIII) and (EDFII & EDFIV) have almost the same absorption cross sections, respectively. Peak absorption at about 1530nm is 38dB. Then, total number of erbium ions in each EDF sample is estimated to be about 2.11×10^{25}.

The degradation of the population density of the $^4I_{13/2}$ level can be estimated by the comparison of the gain characteristics of the EDF sample pair which has the same absorption cross section.

4-4-2. Relaxation time t_f, spontaneous emission probability Ajj' and nonradiative decay rate W_{NR}

Fig. 4-2 shows Er^{3+}ion concentration dependence of the inverse of relaxation time τ_f^{-1}, the spontaneous emission probability Ajj' and the nonradiative decay rate W_{NR}. τ_f^{-1} increases with increasing Er^{3+}ion concentration. The value of τ_f^{-1} varied from 101(s^{-1}) to 118(s^{-1}). This increase of τ_f^{-1} indicates the degradation of the population inversion ratio of the $^4I_{13/2}$ level caused by the interaction between Er^{3+} ions. On the other hand, nonradiative decay rate W_{NR} increases with increasing Er^{3+}ion concentration.

4-4-3. Quantum Efficiency and Power Conversion Efficiency

Fig. 4-3 shows the erbium ion concentration dependence of QE and PCE. As shown in Fig. 4-3, QE and PCE of EDF decreases with increasing erbium ion content.

About 26% decrease of QE occurs with increase of erbium ion content. There is significant nonradiative relaxation, resulting in a QE of between 65-90 %. However, the multiphonon relaxation rate in silicate glasses for such a large energy gap is negligible ($<< 1\ s^{-1}$).

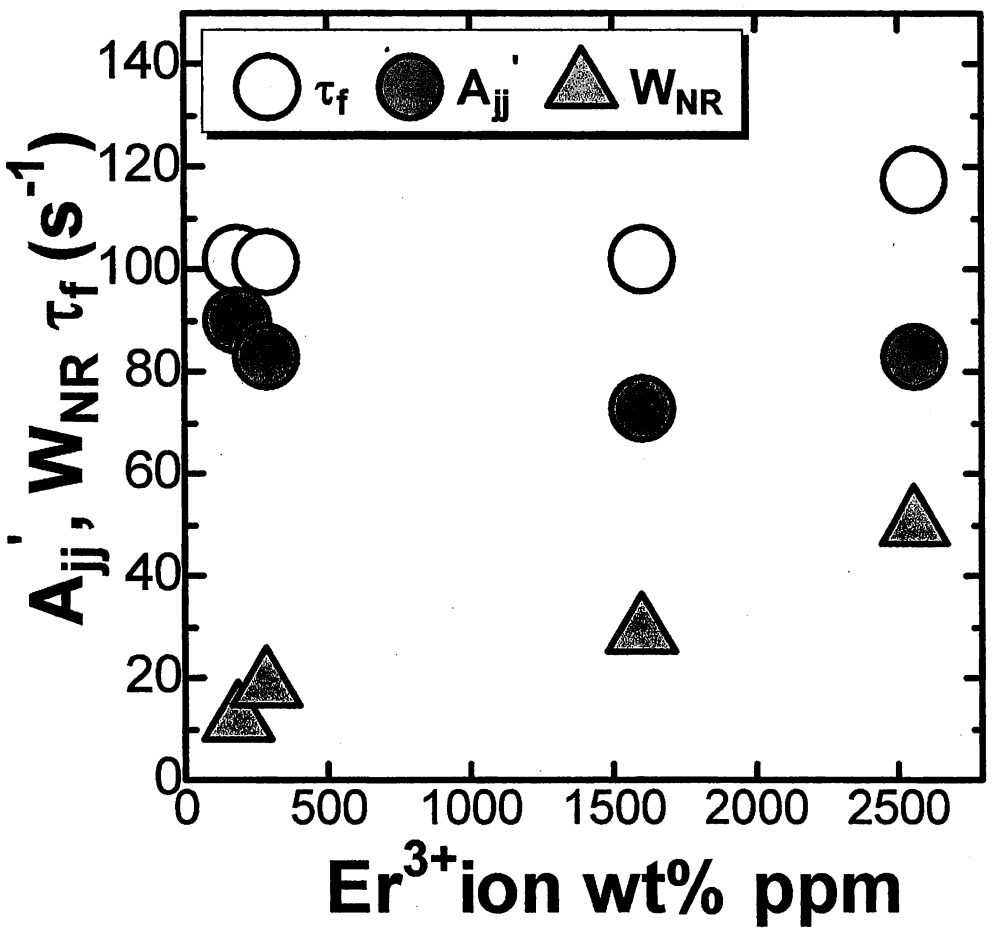

Figure 4-2 Er^{3+} ion concentration dependence of the spontaneous probability Ajj', the nonraditive decay rate W_{NR} and the decay rate t_f^{-1} of the $^4I_{13/2}$ level of Er^{3+} ion.

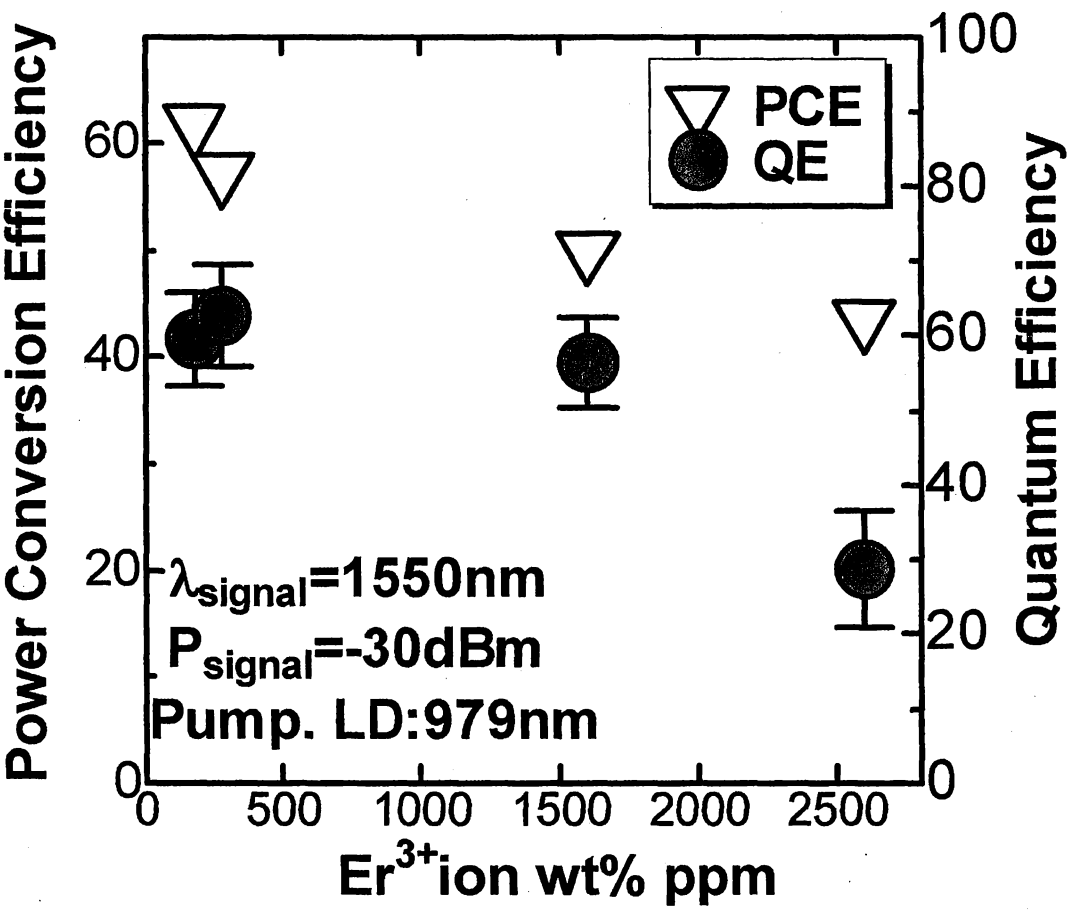

Figure 4-3 Er^{3+} ion concentration dependence of Power conversion efficiency PCE and Quantum efficiency QE.

The difference between the Al-O bond and the Si-O bond is irrelevant , because in either case, the nonradiative rate is much less (orders of magnitude) than the radiative decay rate. Therefore, the QE of the $^4I_{13/2}$ seems to be affected by other types of nonradiative processes. For example, there may be energy transfer to defects or impurities such as OH in the glass. This situation is more likely when the Er^{3+} ion concentration becomes higher.

On the other hand, about 20% degradation of PCE occurs in EDF IV(Er^{3+};2600pm) compared with PCE of EDF I (Er^{3+};180ppm),. PCEs for our EDF samples, EDF I and EDFII were about 45%, which is lower about 18% than theoretical maximum PCE. For 980nm LD pumping scheme, about 56% has been reported as highest PCE so far[13]. Taking into account that the total erbium concentration is the same for four EDF samples, this decrease in PCE is considered to be due to the quenching effect induced by the interaction between erbium ions. Above higher erbium doped region than 1500ppm, PCE decreases rapidly.

4-4-4. Gain saturation measurements

In the gain saturation measurements at room temperature, the difference between the gain saturation characteristics was observed for four EDF samples. Fig. 4-4(a) and 4-4(b) shows the gain saturation characteristics of the EDF sample pairs (EDFI & EDFIII) and (EDFII & EDFIV), respectively. These samples were forwardly pumped at three pumping power (10mW, 15mW and 30mW). About 1 dB degradation of the gain saturation was observed for the EDF sample EDFIII:1600ppm. This degradation between the saturation gains of two EDF samples was also found at 77K (solid lines). Therefore, this degradation of the gain saturation of EDFIII is considered to be caused by the Er^{3+}-Er^{3+} ion interactions because the interaction between Er^{3+} ions have littile temperature dependence and is supposed to be maintained even at 77K. In addition, more apparent degradation of the gain saturation (about 4dB) was observed in the EDF sample EDFIV:2600ppm. For two pairs of EDF samples, the degradation of the gain saturation became most significant at 15mW of pumping power.

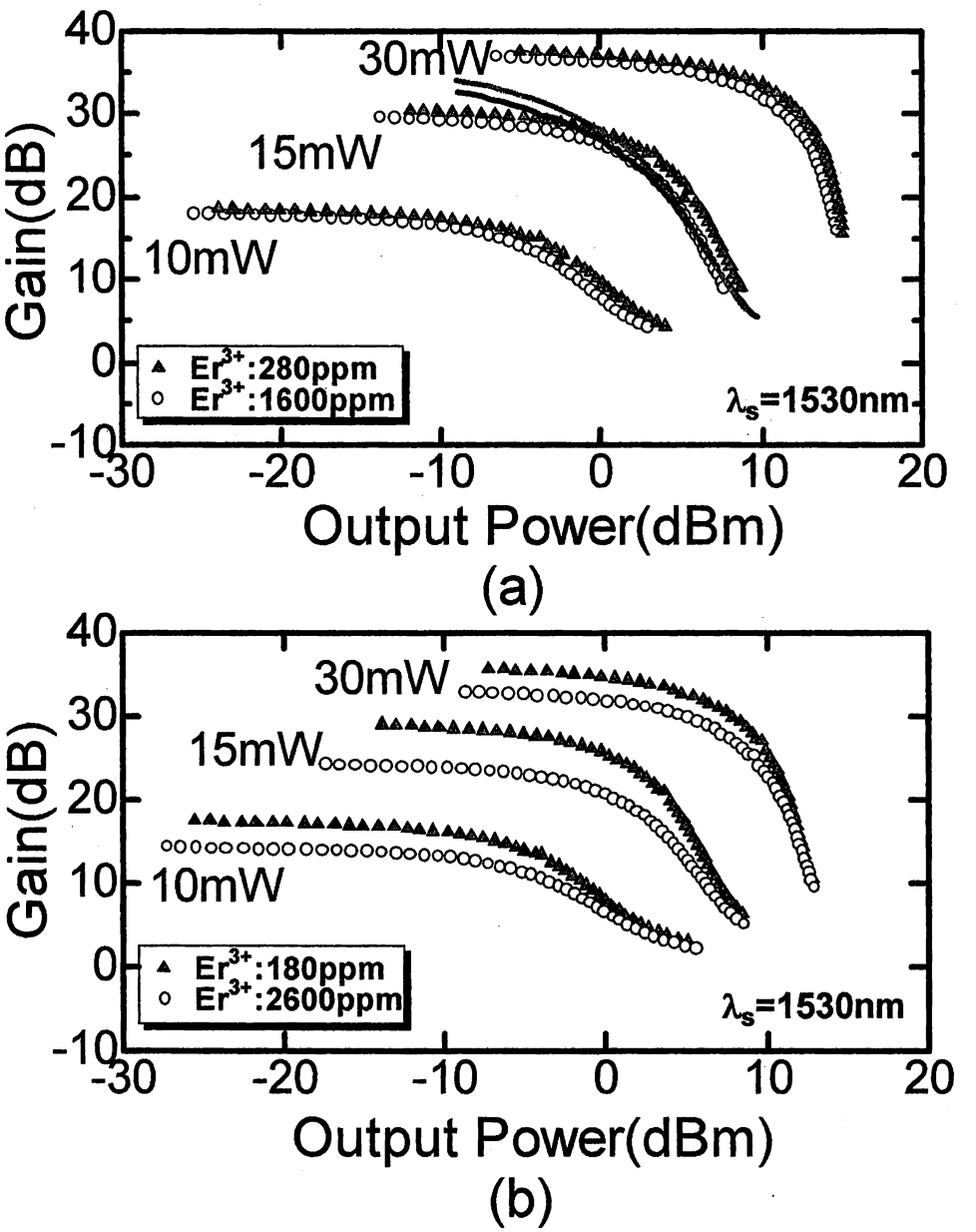

Figure 4-4 Power dependences of gain saturations.

(a):EDFI(280ppm),EDFIII(1600ppm), (b):EDFII(180ppm), EDFIV(2600ppm)

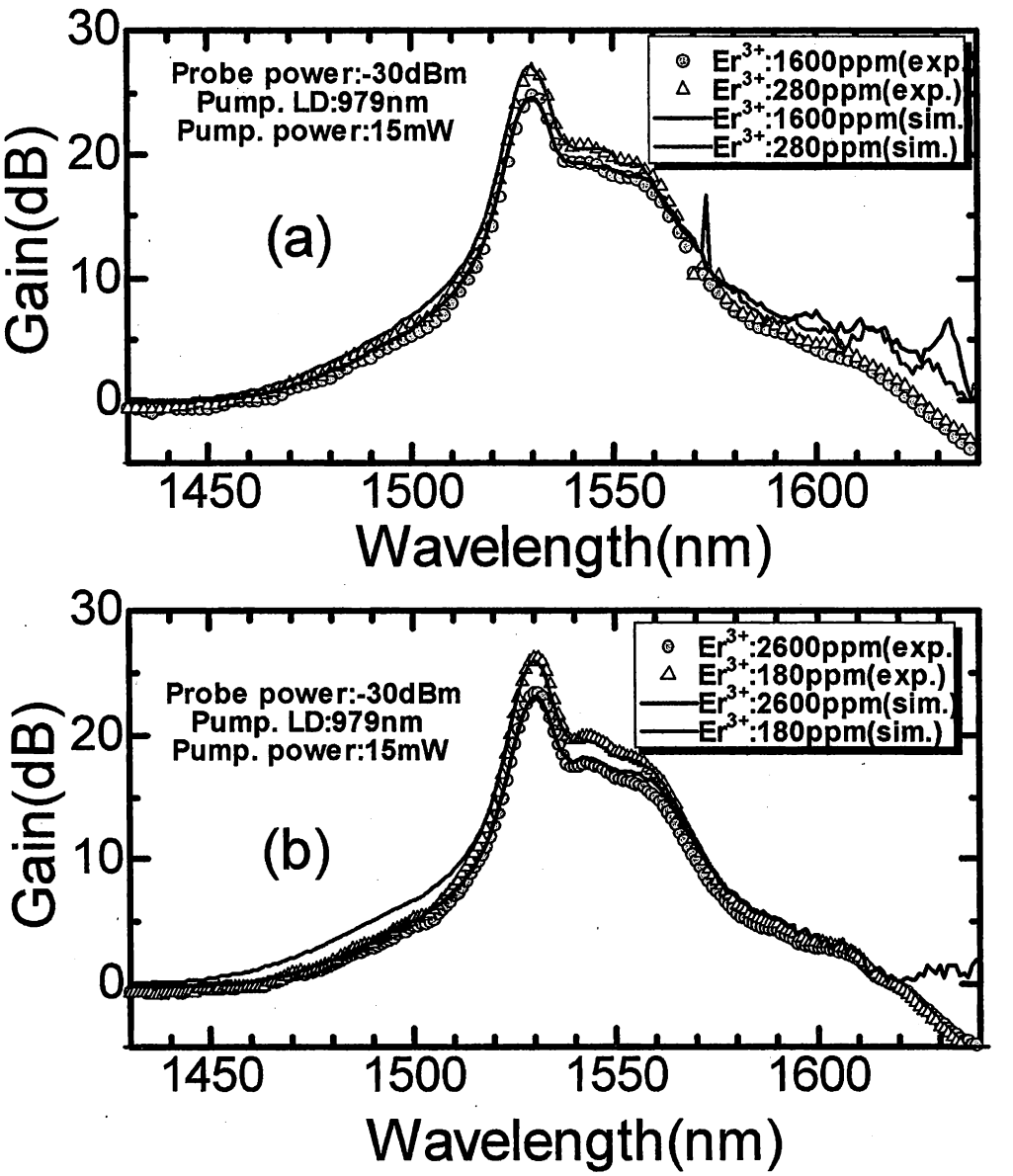

Figure 4-5 Comparison between the experimental and numerical gain.

(a):EDFI(280ppm),EDFIII(1600ppm), (b):EDFII(180ppm), EDFIV(2600ppm)

4-4-5. Gain spectra evaluations

Fig. 4-5(a) and 4-5(b) show the gain characteristics of the EDF sample pairs (EDFI & EDFIII) and (EDFII & EDFIV), respectively. The samples were pumped at 15mW of pumping power because the most apparent gain degradation was expected from the obtained gain saturation results. Dots and solid lines show the experimental and numerical results, respectively. About 1dB and 4dB degradations of the gain characteristics was observed for the EDF sample pairs (EDFI & EDFIII) and (EDFII & EDFIV), respectively. The difference between the experimental and simulated gain spectra in the L-band wavelength region is considered to be caused possibly by the $^4I_{13/2} - {}^4I_{9/2}$ excited-state absorption (ESA) because the ESA cross section is not taken into account in the simulation model. In addition, the effect of concentration quenching originated from the Er^{3+}-Er^{3+} ion interactions was examined using the experimentally obtained gain characteristics by the Er^{3+} concentration dependent simulation model considering homogeneous upconversion quenching and pair induced quenching effects mentioned above. The ratio of the paired ions in the sample EDF I (Er^{3+}:180ppm) was assumed to be 0% because the saturated loss of the fiber was verified to be 0dB in the high input signal power region. As a result of the numerical analysis, the ratio of the paired ions to the total ions increases with increasing Er^{3+} ion concentration. For the sample EDF III (Er^{3+}:1600ppm), about 2% of total Er^{3+} ions were estimated to be paired. In addition, about 0.4% and 5 % of total Er^{3+} ions were estimated to be paired in the sample EDF II (Er^{3+}:280ppm) and EDF IV (Er^{3+}:1600ppm), respectively. Fig. 4-6(a) and 4-6(b) show the signal input power dependence of the simulated normalized population densities of the $^4I_{13/2}$ and the $^4I_{15/2}$ level considering the degradation caused by the Er^{3+}-Er^{3+} ion interaction. Except the signal input power, the simulation parameters were the same in the gain characteristic simulation. The obtained population densities in the gain characteristics evaluation correspond to those at –30dBm of input signal power shown in Fig. 4-6(a). The degradation of the normalized

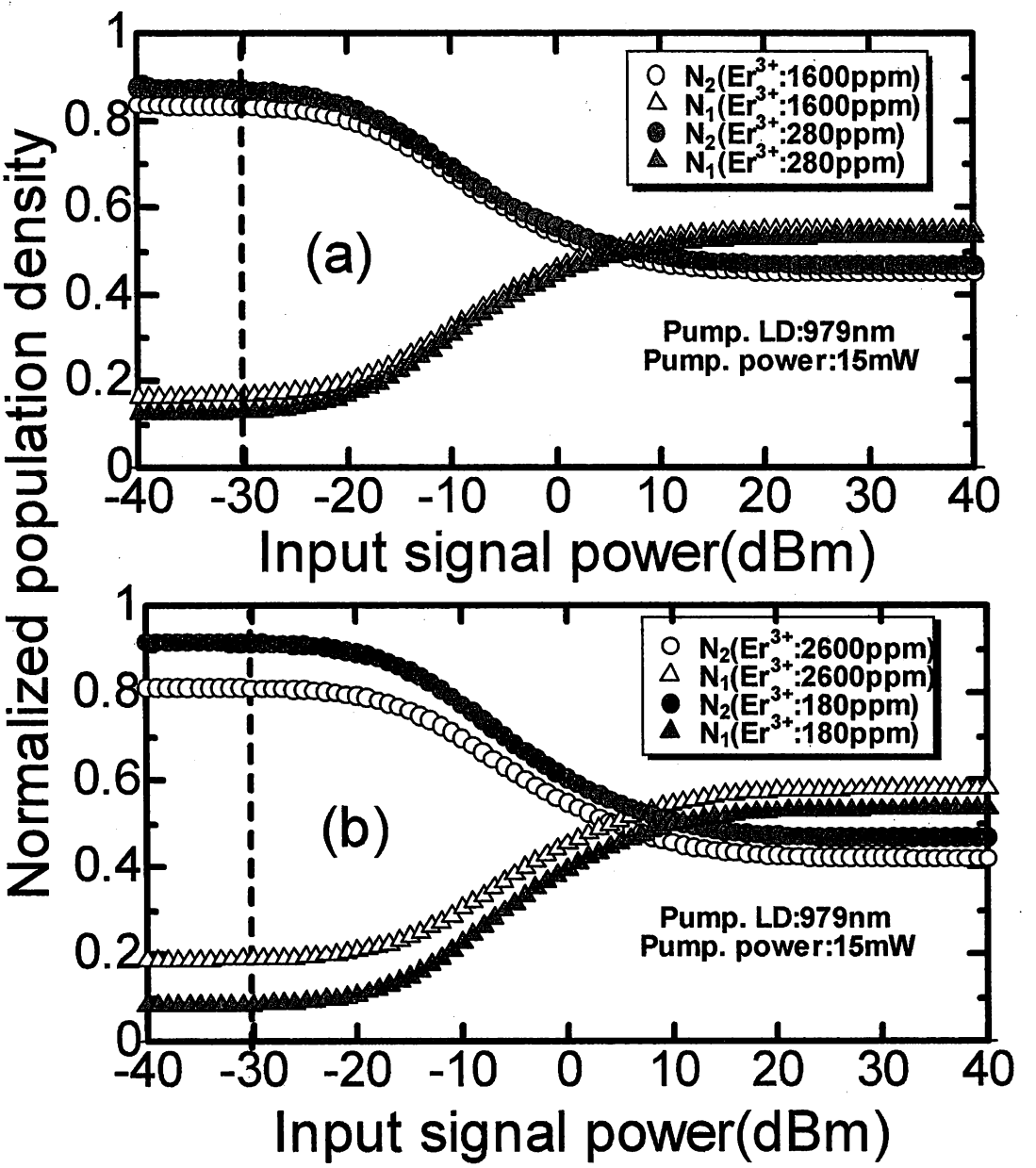

Figure 4-6 Input power dependence of the normalized population densities.

(a):EDFI(280ppm),EDFIII(1600ppm), (b):EDFII(180ppm), EDFIV(2600ppm)

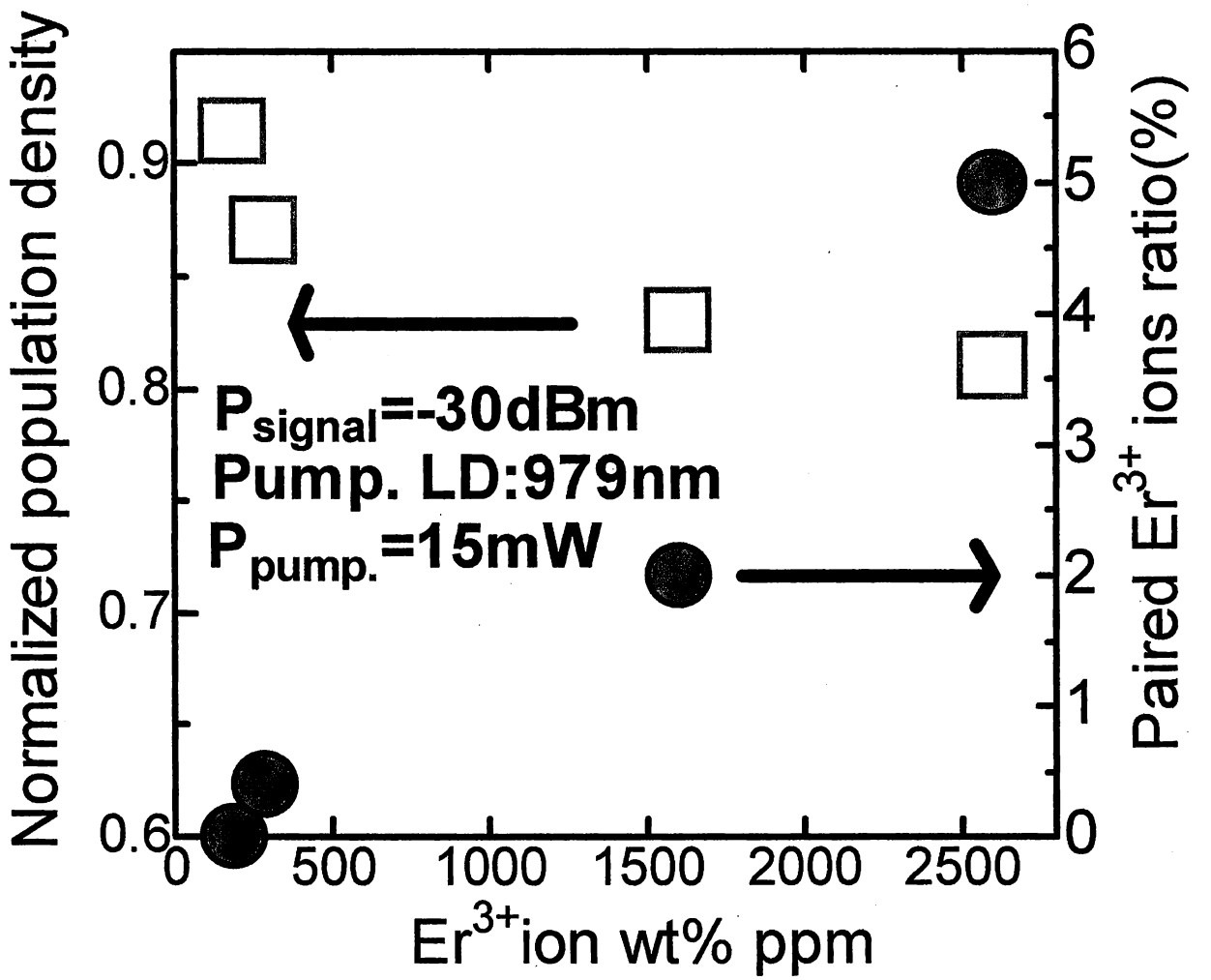

Figure 4-7 Er^{3+} ion concentration dependence of Normalized population density and Paired Er^{3+} ions ratio in EDF sample.

population densities is found to be more significant in the EDF sample that has higher Er^{3+} ion concentration. In addition, the degradation of the population densities in the highly erbium–doped EDF samples was found to occur more significantly in small signal power region rather than in large signal power region.

Fig. 4-5 shows the Er^{3+} ion concentration dependence of the paired Er^{3+} ions ratio and the normalized population density of the $^4I_{13/2}$ level. The normalized population density of the $^4I_{13/2}$ level shows the more significant degradation in the Er^{3+} ion concentration region below 280ppm. In the concentration region above 280ppm, the normalized population density seems to decrease at a constant rate with increasing Er^{3+} ion concentration. In addition, the ratio of the paired ions to the total ions increases with increasing Er^{3+} ion concentration. The degradation of the population density of the $^4I_{13/2}$ level obtained by the gain characteristics analysis is considered to be caused by the short range Er^{3+}-Er^{3+} ion interactions PIQ because the total Er^{3+} ion number in each EDF sample is the same in all four EDF samples. In addition, the degradation of PCE shown in Fig. 4-2 is possibly caused by the PIQ effect because PCE and the ratio of paired ions has negative correlation in terms of the erbium concentration

4-5. Conclusion

The effect of Er^{3+} concentration quenching on the gain characteristics and optical properties of silica-based EDF was investigated by the experimental measurements and the numerical evaluation of gains.

The effect of Er^{3+} concentration quenching can bring the decrease of PCE and QE with increasing Er^{3+} concentration. The decrease of PCE and QE were about 26% and 20%, respectively. The decrease of QE is caused by the increase of the non radiative decay rate with increasing Er^{3+} ion concentration. This increase of the nonradiative decay rate can be affected by nonradiative energy transfer to defects or impurities such as OH in the glass because this

situation is more likely when the Er^{3+} ion concentration becomes higher.

In addition, from the numerical analysis on the gain characteristics of EDF samples which have different Er^{3+} ion concentrations and same absorption cross sections, the number of the paired ion was verified to increase with increasing Er^{3+} ion concentration. On the other hand, the degradation of the population density of the $^4I_{13/2}$ is estimated to be enhanced with increasing Er^{3+} ion. Therefore, the population density of the $^4I_{13/2}$ state is assumed to be degraded mainly by the increasing the number of paired Er^{3+} ions. Also, as a relation between the gain degradation and the number of paired Er^{3+} ions, it is estimated that even about 2% paired Er^{3+} ions in silica-based EDF possibly cause about 1dB degradation of the gain spectrum.

References

[1]. M. Shimizu, M.Yamada, M. Horiguchi, and E. Sugita, "Concetration effect on optical amplication characteristics of Er-doped silica single mode fibers," IEEE Photon. Technol. Lett., vol. 2, pp. 43-45, 1990.

[2]. J. Schmulovich, A. Wong, Y. H. Wong, P. C. Becker, A. J. Bruce, and R. Adar, "Er^{3+} glass waveguide amplifier at 1.5 μ m on silicon," Electron. Lett., vol. 28, pp. 1181- 1182, 1992.

[3]. A. Bellemare, M. Karasek, C. Riviere, F. Babin, G. He, V. Roy, and G. W. Schinn, "A broadly tunable Erbium-doped fiber ring laser: experimentation and modeling," IEEE J. Sel. Top. Quantum Electron., vol. 7, pp. 22-29 ,2001.

[4] R. Reisfeild, C. K. Jφrgensen, "Lasers and Excited States of Rare Earths," Springer-Veralag, 1977.

[5] D. L. Dexter, "A theory of sensitized luminescence in solids," J. Chem. Phys., vol. 21, pp. 836-850, 1953.

[6] P. Myslinski, J. Fraser, and J. Chrotowski, "Nanosecond kinetics of upconversion process in EDF and its effect on EDFA performance," *in Proceedings of Optical Amplifiers and Their Applications*, OAA 1995, Th3, 1995

[7]. C. R. Giles and E. Desurvire, "Modeling erbium-doped fiber amplifiers," IEEE J. Lightwave Technol., vol.9, pp. 271-283, 1991.

[8]. V. P. Gapontsv, and N. S. Platonov, "Migration-Accelerated Quenching in Glasses Activated by Rare Earth Ions", in Dynamical Processes in Disordered Systems, Material Science Forum, vol. 51, 1990.

[9]. J. L. Pholipsen and A. Bjarklev, "Monte Carlo Simulations of Homogeneous Upconversion in Erbium-Doped Silica Glasses," IEEE J. Quantum Electron., vol. 33, pp. 845-854, 1997.

[10]. H. Hempstead, J. E. Roman, C. Ye, J. S. Wilkinson, P. Camy, P. Laborade, and C. Lerminiaux, "Anomalously High uniform Upconversion in an Erbium-Doped Waveguide Amplifier," *in Proceedings of 7th Eur. Conf. Integrated Optic* , ECIO '95, TuC4, 1995.

[11]. M. Federighi, and F. Di Pasquale,,"The Effect of Pair induced Energy Transfer on the Performance of Silica Waveguide Amplifiers with High Er^{3+}/Yb^{3+} Concentration ," IEEE Photon. Technol. Lett., vol. 7, pp. 303-305, 1995.

[12]. J. Nilsson, P. Scheer, and B. Jascorzynska, "Modeling and Optimizarion of Short Yb^{3+} -Sensitized Er^{3+}-Doped Fiber Amplifiers" IEEE Photon. Technol. Lett., vol. 6, no. 3, pp. 383-385, 1994.

[13]. B. Pedersen, M. L. Dakss, B. A. Thompson, W. J. Miniscalco, T. Wei, and L. J. Andrews, "Experimental and theoretical analysis of efficient erbium-doped fiber power amplifier," IEEE Photonics. Technol. Lett., vol. 3, pp. 1085-1087, 1991.

Chapter 5

Study on the dynamics of gain spectral hole in silica-based erbium-doped fiber at 77K

5-1. Introduction

Gain spectral hole burning (GSHB) in the Er^{3+} doped fibre amplifier (EDFA) has been a serious problem to be solved for long haul optical transmission systems for over a decade [1]. GSHB is the phenomenon that causes the gain deviation or hole in spectral region when a strong signal is input into EDFA. It has been known that an additional hole (second hole) can be burned at around 1530nm independent of the wavelength of a saturating signal, where a main hole is burned [2]. So far, the second hole depth of GSHB observed at around 1530nm in an EDF has been reported to be about 1dB at room temperature when a strong saturation signal was input into EDF [3]. The physical mechanism of the holes in the gain spectra is complicated and the formation process of the second hole has not been clarified yet. On the other hand, the transmission distance of today's long haul optical system becomes much longer than ever, which includes over 150 EDFAs. Based on these facts, the more precise prediction

of the gain spectral shape after transmission is becoming much more important. However, it is difficult to predict the gain spectral shape after transmission because of the accumulation of the gain spectral characteristics of EDFAs. GSHB has been one of the major problem, which makes it difficult to predict the amplified gain spectra in the C-band wavelength region (1530nm-1565nm) [4-6]. Predicting GSHB accurately is eagerly required to manage the optical gain in optical transmission design. Therefore, many numerical and experimental measurements have been performed to clarify and model the mechanism of GSHB [7-9]. However, no complete physical interpretation of GSHB has been formulated yet. In order to approach the basic physical mechanism of GSHB from different angle, we investigated the Er^{3+} content dependence of the hole shape and depth of GSHB in silica-based EDFA at 77K.

In this study, we performed GSHB measurements of four silica-based EDF at 77K in order to observe the second hole depth and the shape more clearly. As a result, we observed the Er^{3+} concentration dependence of the second hole depth of GSHB at 77K. We will discuss the effect of the energy transfer between Er^{3+} ions on the hole formation mechanism.

5-2. Experimental

5-2-1. Characteristics of EDF samples

Four silica-based EDF samples with different Er_2O_3 content were used as the gain medium for EDFA. The Er^{3+} ion concentrations of samples were 130ppm, 280ppm, 700ppm, and 1600ppm. Optical parameters for each EDF are shown in Table 5-1.

The fiber length of each EDF was decided to include same total number of Er^{3+} ions in EDF, which leads to the equivalent attenuation spectra for all the EDF samples. The absorption spectra of EDF in the wavelength region from 1420nm to 1640nm are shown in Fig. 5-1.

Table 5-1. Parameters for silica-based EDF samples.

Sample	Er^{3+} ion (ppm.wt)	Fiber Length (m)	$n_{1.3\mu m}$ (-)
EDF I	130	30.0	1.469
EDF II	280	15.7	1.470
EDF III	700	4.8	1.468
EDF IV	1600	2.9	1.470

5-2-2. GSHB measurement scheme at 77K

Fig. 5-2 shows the experimental setup of GSHB measurement at 77K. Each EDF was cooled directly by liquid nitrogen in a dewar. The saturating signal and probe or a gain-locking signal were coupled by two 3dB couplers. The wavelength region of probe signals used in these measurements was from 1520nm to 1600nm. Three tunable laser sources were used for the probe and signal light source, (Santec, TSL210). The coupled signals were injected finally into the polarization scrambler to cancel the effect of polarization hole burning. The gain spectrum was measured by an optical spectrum analyser, OSA (Anritsu, MS9780A).

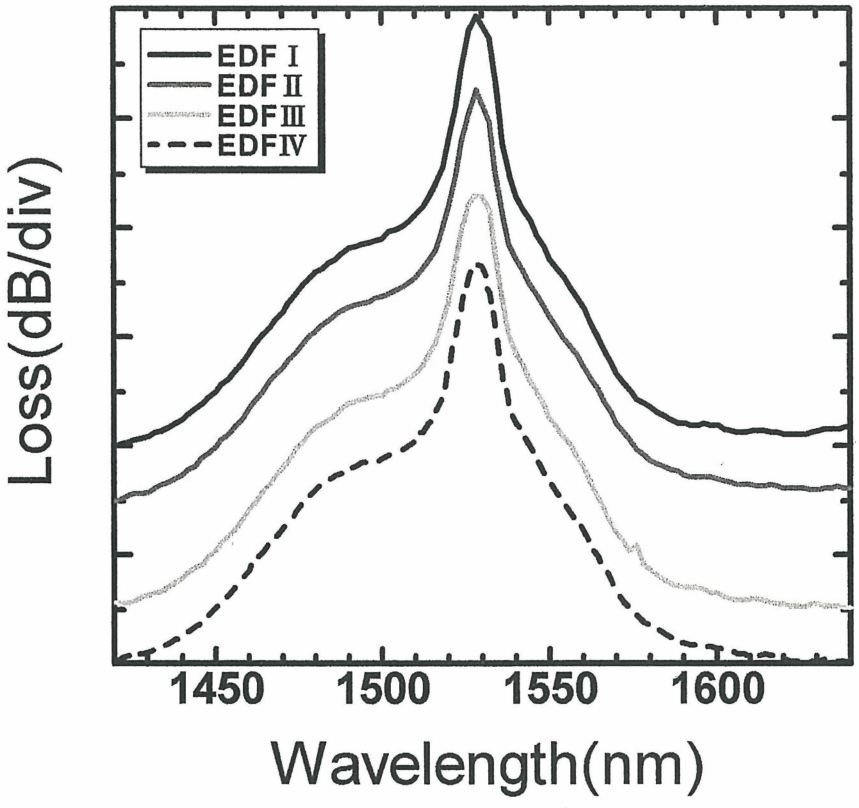

Figure 5-1 The absorption spectra of EDF in the wavelength region from 1420nm to 1640nm.

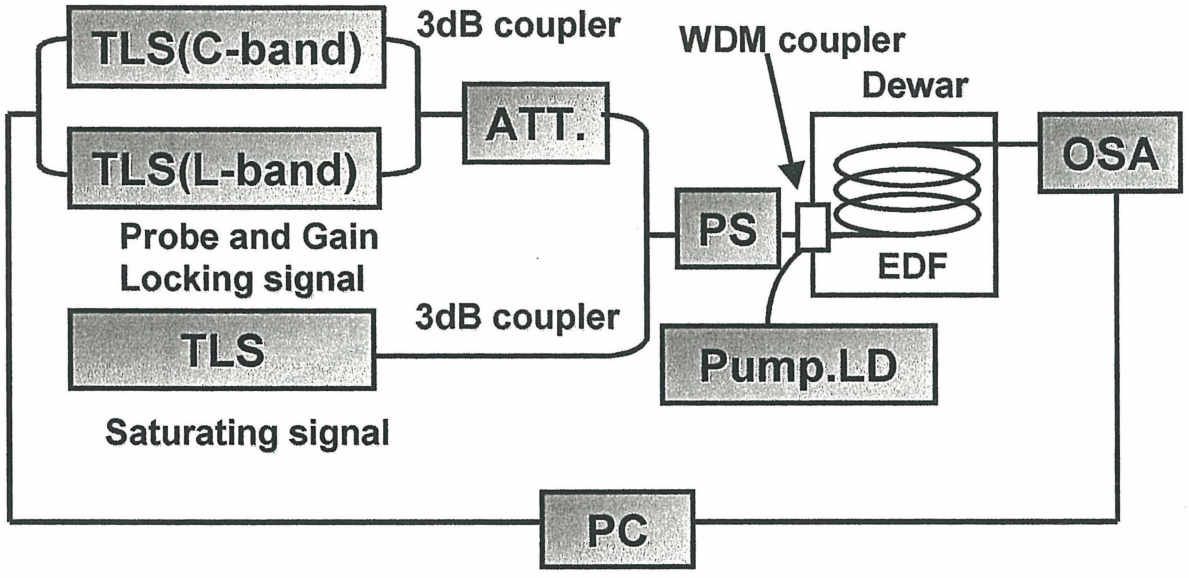

Figure 5-2 Experimental setup of GSHB measurement at 77K.

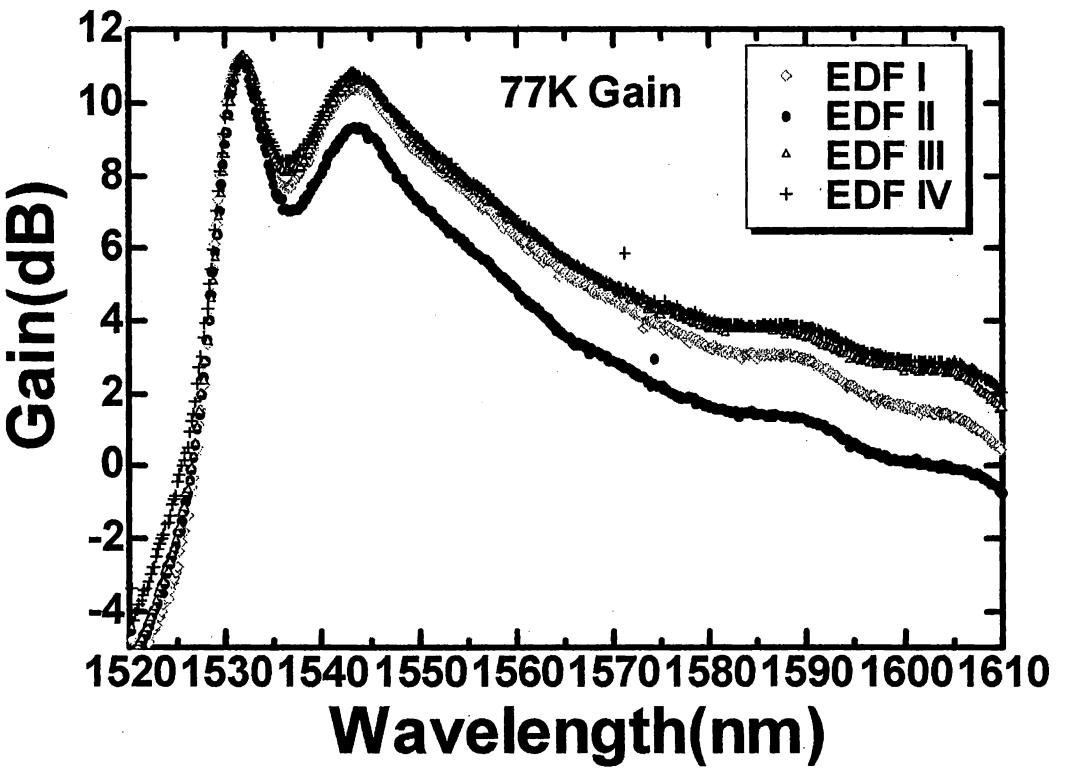

Figure 5-3 Gain spectra of four EDF samples at 77K.

Each EDF was forwardly pumped by a 979nm laser diode (LD) (FITEL) and the pump power of LD was set in order to maintain a constant gain at the gain locking signal when the saturation signal was input into EDF. The gain locking signal wavelength was 1560nm. The wavelength 1580nm signal was temporary used as gain locking signal when the saturation signal was 1560.5nm. The power of the gain locking signal was -30dBm. The probe signal wavelength was scanned from 1520nm to 1620nm at a power of -30dBm. To examine the saturating wavelength dependence of the second hole and main hole width, the wavelength of saturating signal was varied from 1530nm to 1610nm. To investigate the saturating power dependence of the second hole, GSHB was measured at the saturating power of -5.3dBm and 0dBm. The GSHB spectrum was calculated by subtracting a gain spectrum without the saturating signal from that with the saturating signal. The gain spectrum without saturation signal had the same gain 11.1dB at 1531.8nm, which corresponds to the second hole wavelength, to keep the same population inversion ratio of each fiber in order to compare the degradation of population inversion ratio caused by GSHB. Fig. 5-3 shows the gain spectra of four EDF samples at 77K

5-3. Results

5-3-1. Wavelength dependence of the second hole character

Fig. 5-4 shows GSHB spectra with various saturating signal wavelengths of at 77K for EDF I (Er^{3+}:130ppm). The saturation signal power was 0dBm. As expected, a very sharper and deeper second hole at around 1530nm and a main hole were observed compared with those at room temperature. At 77K, the center wavelength of the second hole was independent of the saturating signal wavelength while the center wavelength of the main hole varied with the saturating signal wavelength. This characteristics of the second hole has been also reported at room temperature in the C-band wavelength region. [4]

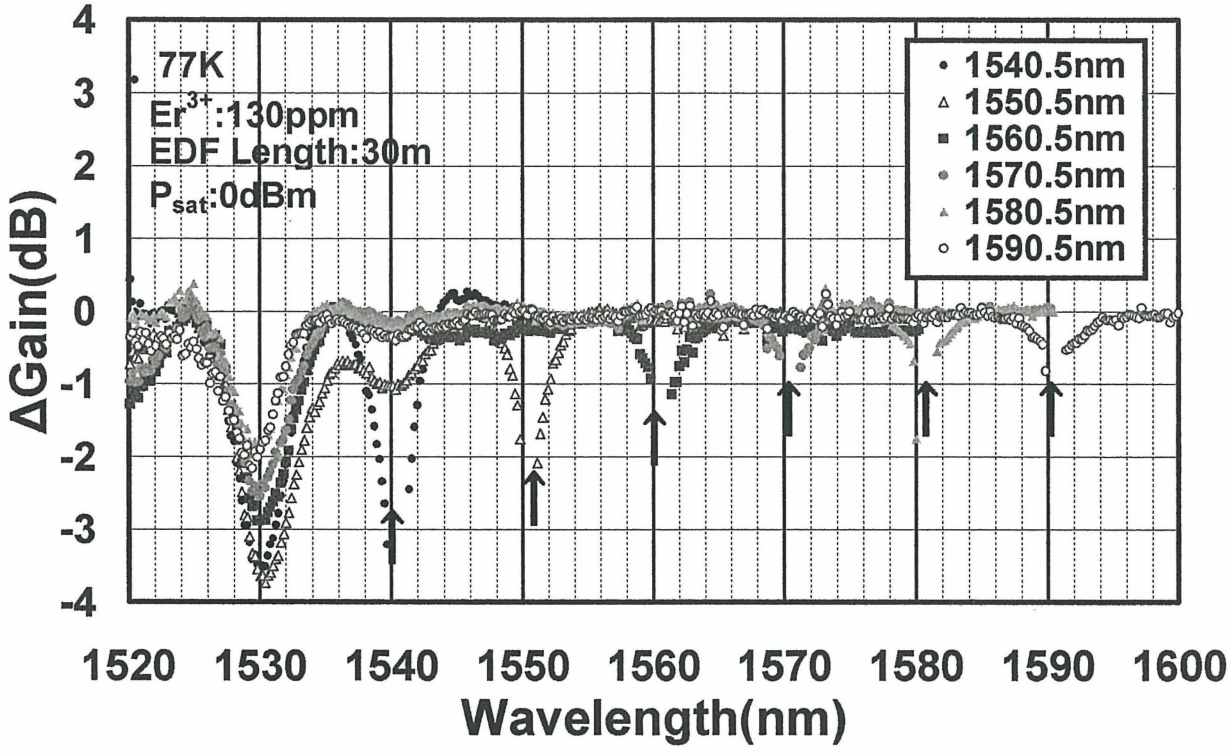

Figure 5-4 GSHB spectra with various saturating signal wavelengths of at 77K for EDF I (Er^{3+}:130ppm).

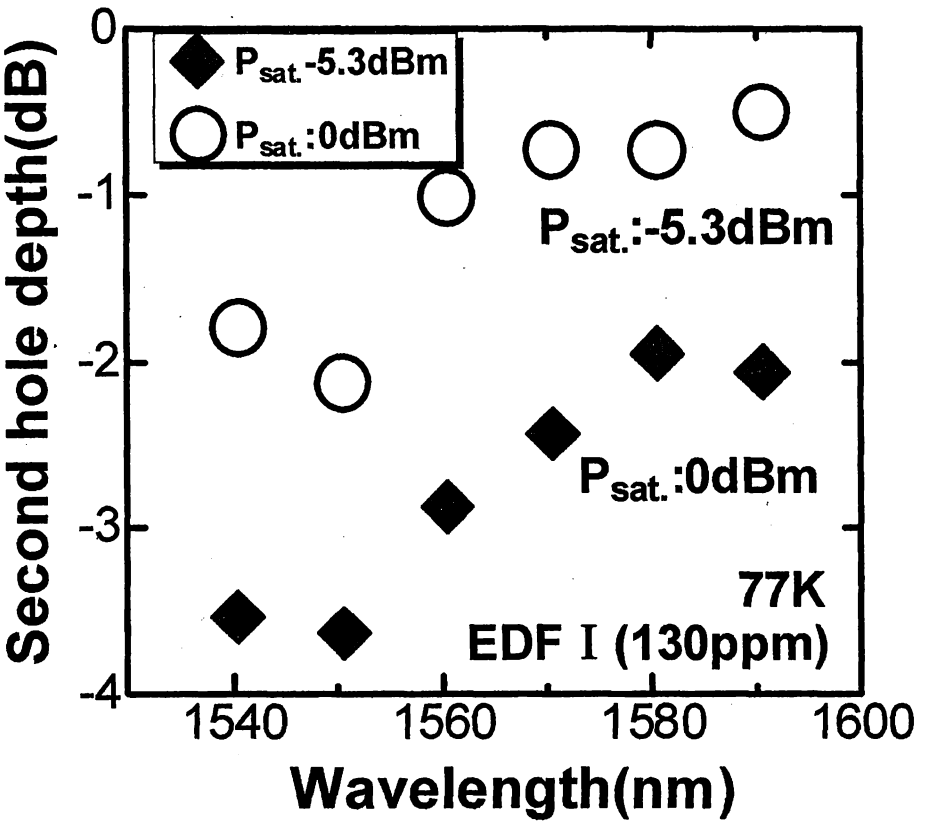

Figure 5-5 Relationship between the second hole depth and the saturating signal wavelength for the cases where the saturating signal power is 0dBm and -5.3dBm.

As the saturating signal wavelength became longer, the second hole depth was found to be decreased at 77K. Fig. 5-5 shows the relationship between the second hole depth and the saturating signal wavelength for the cases where the saturating signal power is 0dBm and -5.3dBm. As shown in Fig. 5-5, the second hole depth at the saturating signal power of –5.3dBm monotonically decreased as the wavelength of saturation signal became longer. On the other hand, the wavelength dependence of the second hole depth at the saturating signal power of 0dBm seems to show the maximum peak at around

1580nm as the saturation signal wavelength became longer. The origin of the peak at around 1580nm of the second hole depth is not clear at present and need more consideration.

5-3-2. Wavelength dependences of the main and second holes

Fig. 5-6 shows the relationships between the main and second hole widths and the saturating signal wavelength for the case where the saturating signal power is 0dBm. The values of the main and second hole widths were obtained by Gaussian fitting. As a result, the main hole width at 1530nm was estimated to be $\Delta\lambda_{Main}$=2.25nm. The main hole width $\Delta\lambda_{Main}$ at 1.53 μ m has been reported to be about 2.4nm at 77K for the silica-based EDF and follow $T^{1.73}$ law in the 20-77K temperature range [1]. This shows good agreement with our result. On the other hand, the second hole width $\Delta\lambda_{Second}$ at 1.53 μ m was estimated to be about 3.79nm, which is broader than that of the main hole at 1.53 μ m. In addition, the main hole width was found to become broader even at 77K as the saturating signal wavelength became longer whereas the second hole width did not show the saturation signal wavelength dependence and was about 3.85nm.

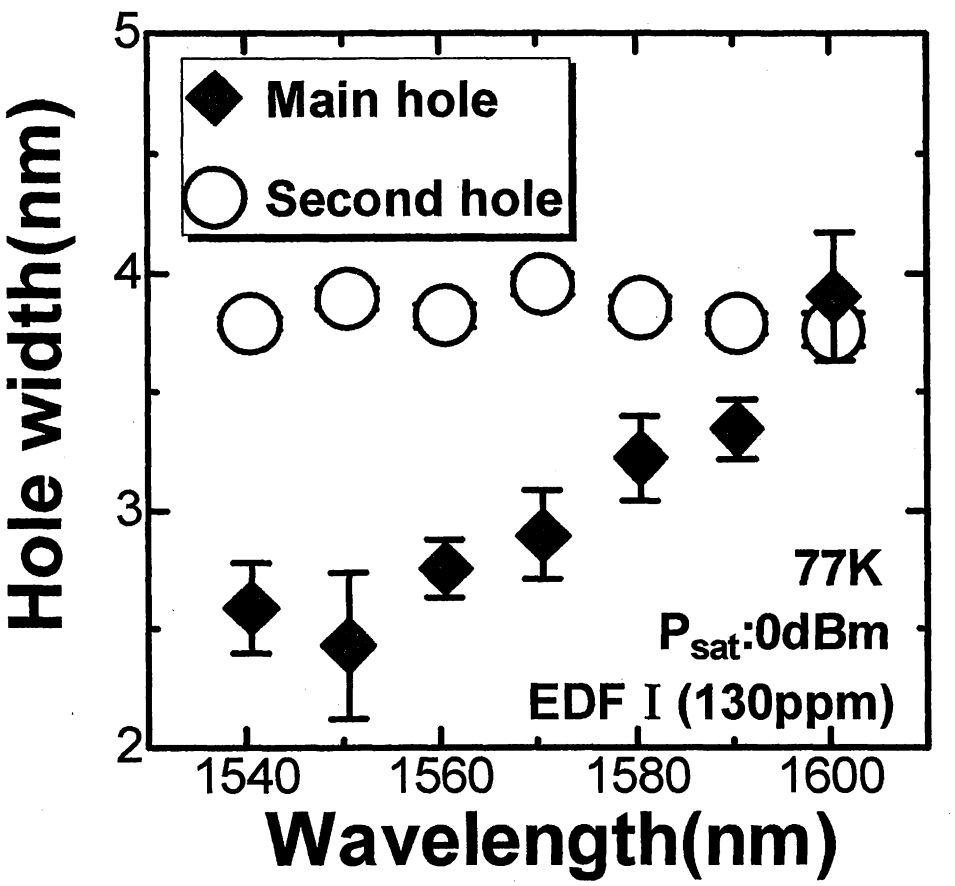

Figure 5-6 Relationships between the main and second hole widths and the saturating signal wavelength (P_{sat}=0dBm).

5-3-3. Er^{3+} ion concentration and saturation signal input power dependence of the second hole character

Fig. 5-7(a) and 5-7(b) show GSHB spectra for four EDF samples with different saturating signal power (P_{sat}=-5.3dBm, 0dBm). The wavelength of saturating signal is 1550.5nm. When the input power of saturation signal was -5.3dBm, the second hole showed almost the same shape and depth regardless of the Er^{3+} ion concentration (Fig. 5-7(a)). On the other hand, in the case of the saturation signal power 0dBm, the second hole depth showed the Er^{3+} ion concentration dependence (Fig. 5-7(b)). Fig. 5-8 shows the Er^{3+} ion concentration dependence of the second hole depth at 77K (P_{sat}=-5.3dBm, 0dBm). In the case of EDF I (Er^{3+}:130ppm), the second hole depth became deeper as the saturating signal input power increased. However, the second hole depth of EDFIV (Er^{3+}:1600ppm) shows little power dependence at 77K. With decrease of the Er^{3+} ion concentration in EDF samples, the second hole depth for saturating signal power 0dBm became deeper. Fig. 5-9 shows the saturation signal wavelength dependence of the second hole depth of GSHB for four EDF samples ((a) P_{sat}=-5.3dBm, (b) P_{sat}=0dBm). When the saturating signal power was -5.3dBm, there was little difference among the second hole depth of four EDF samples. On the other hand, Er^{3+} ion concentration dependence of the second hole depth was observed when the saturating signal power was 0dBm. Second hole depth became deeper in the EDF sample that had higher Er^{3+} ion concentration. This Er^{3+} ion concentration dependence was verified to be observed when the saturation signal wavelength was varied form 1540nm to1580nm.

Fig. 5-10(a) and 5-10(b) show the second hole spectra of GSHB with different saturating signal input power for EDF I (Er^{3+}:130ppm) and EDF IV(Er^{3+}:1600ppm), respectively.

Fig. 5-11 shows the relationships between saturating signal input power and the second hole depth for EDF I (Er^{3+}:130ppm) and EDF IV (Er^{3+}:1600ppm). The difference between the second hole depths of two samples did not occur in the low input power region than –5dBm and high input power region than 5dBm.

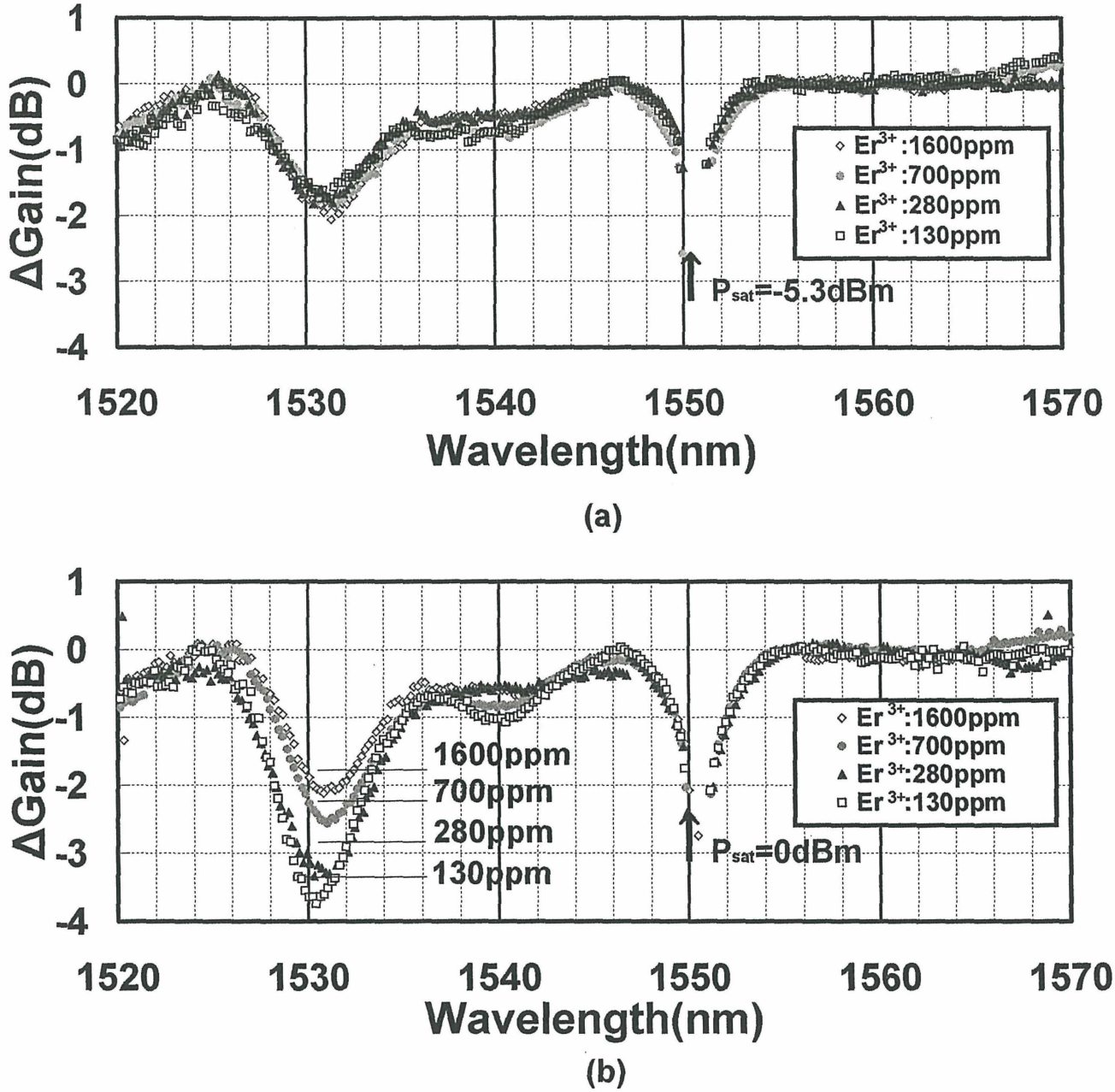

Figure 5-7 GSHB spectra for four EDF samples with different saturating signal power (P_{sat}=-5.3dBm, 0dBm).

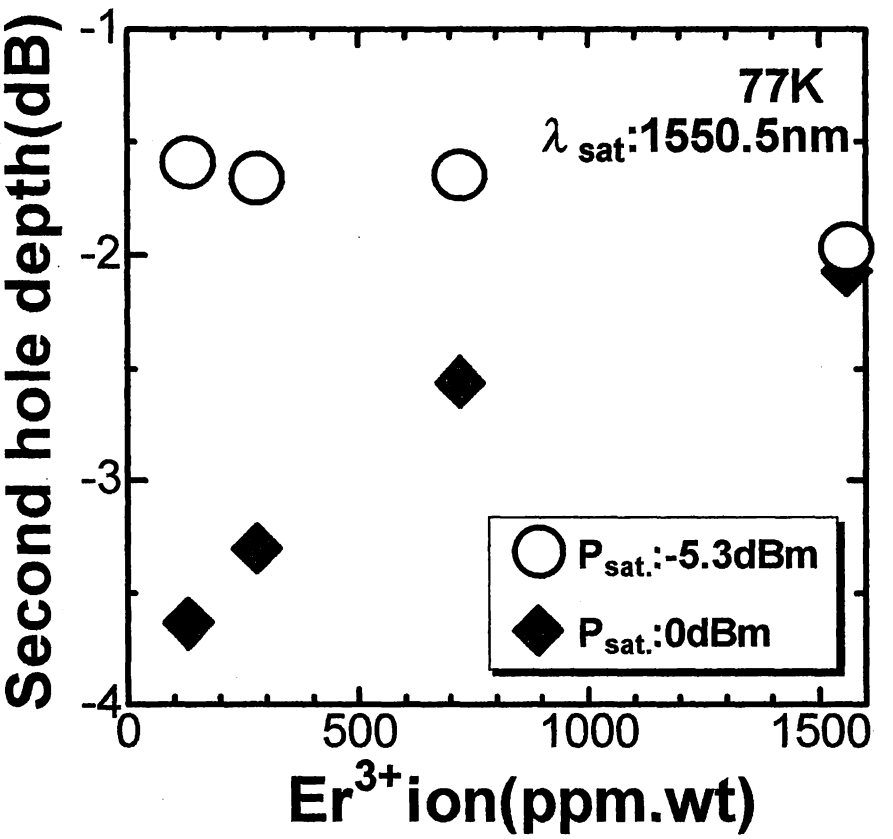

Figure 5-8 Er^{3+} ion concentration dependence of the second hole depth at 77K (P_{sat}=-5.3dBm, 0dBm).

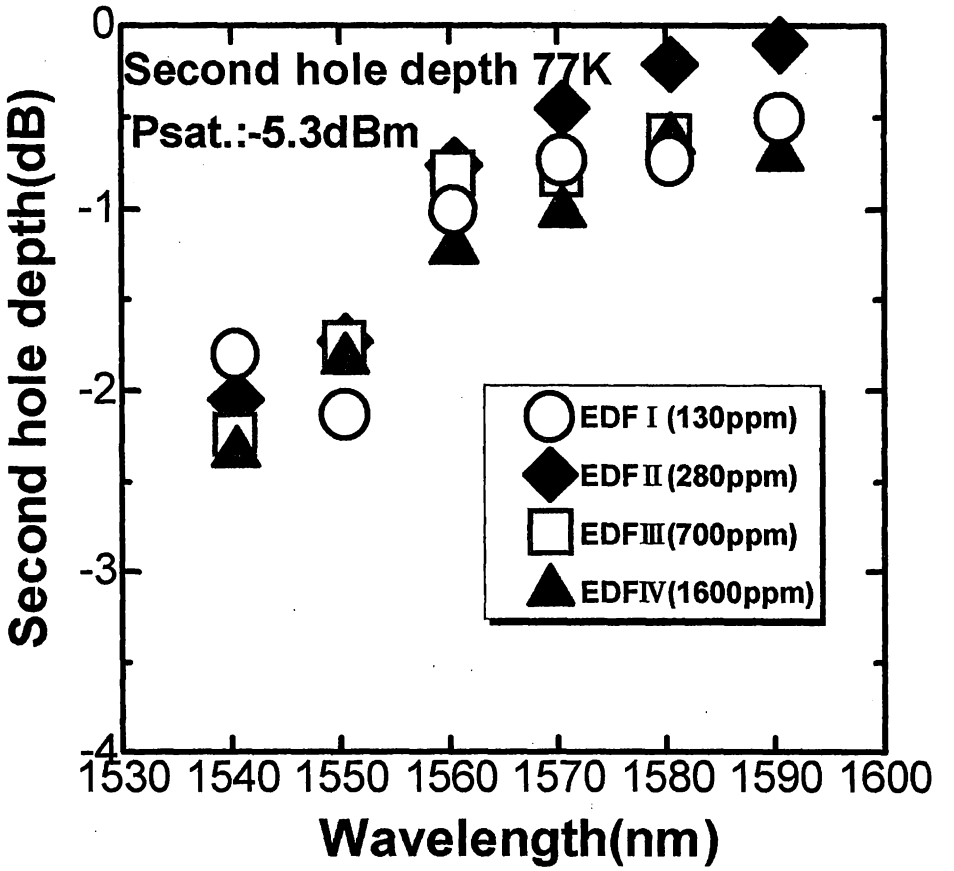

Figure 5-9(a) Saturation signal wavelength dependence of the second hole depth of GSHB for four EDF samples (P_{sat}=-5.3dBm).

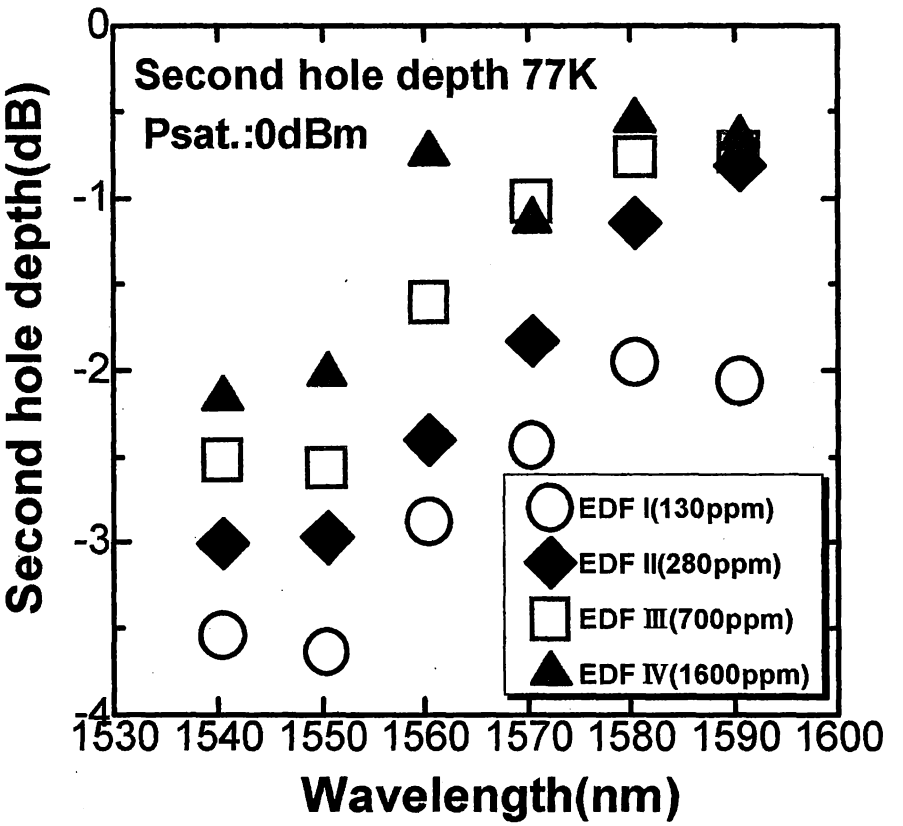

Figure 5-9(b) Saturation signal wavelength dependence of the second hole depth of GSHB for four EDF samples (P_{sat}=0dBm).

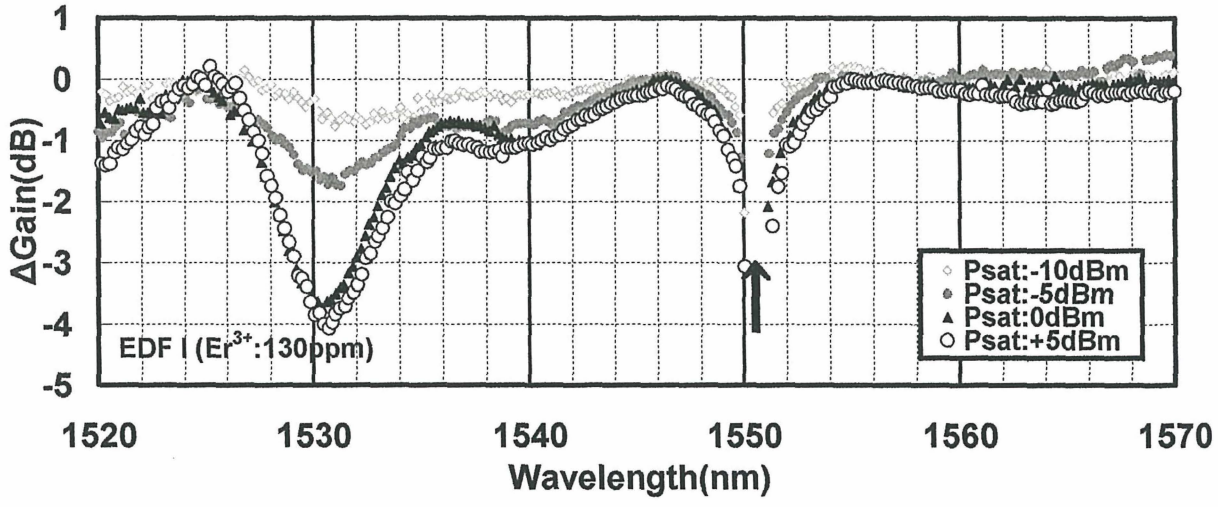

(a)

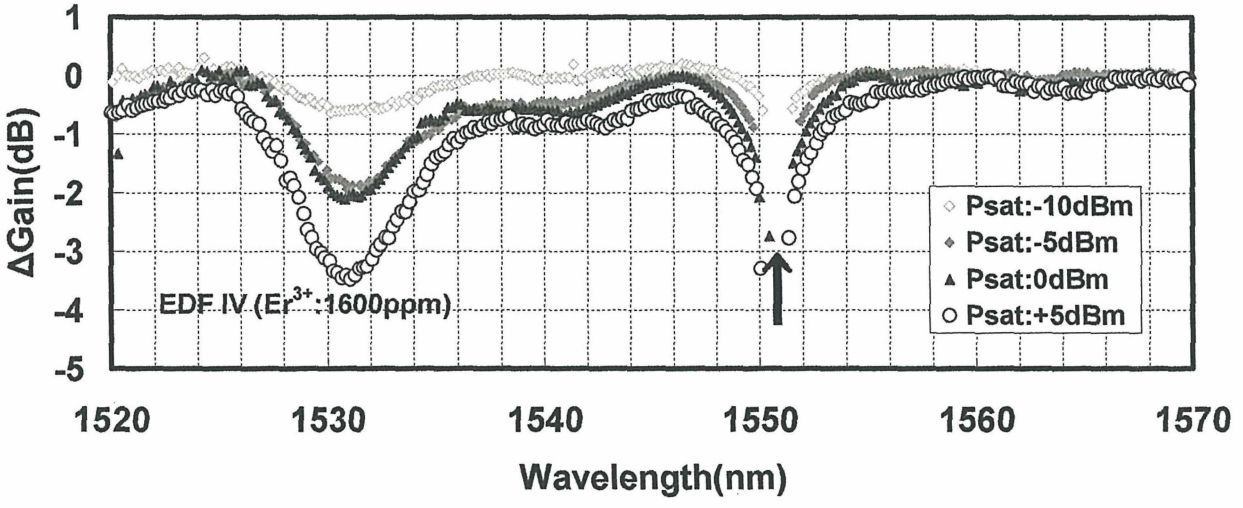

(b)

Figure 5-10 Second hole spectra of GSHB with different saturating signal input power ((a)EDF I (Er^{3+}:130ppm), (b)EDF IV(Er^{3+}:1600ppm)).

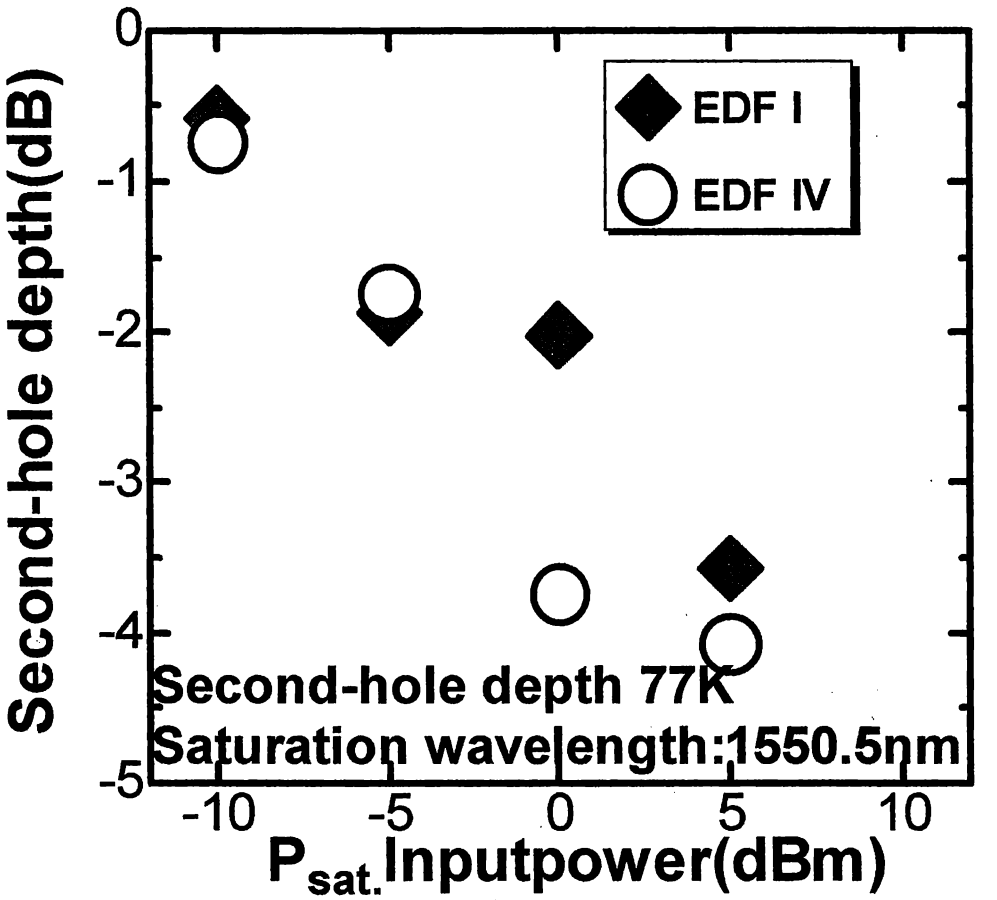

Figure 5-11 Relationships between saturating signal input power and the second hole depth for EDF I (Er^{3+}:130ppm) and EDF IV (Er^{3+}:1600ppm).

The Er^{3+} ion concentration dependence of the second hole depth became more evident when the saturating signal power of 0dBm was input into EDF.

5-4. Discussion

In our measurements, very deep and sharp second and main holes were observed at 77K compared with those at room temperature. The second hole and main hole depth became deeper as the wavelength of saturating signal became longer. In addition, the main hole width was found to become broader at 77K as the saturating signal wavelength became longer whereas the second hole width did not show the saturation signal wavelength dependence.
Moreover, the second hole depth showed the Er^{3+} concentration dependence and was found to become deeper in the silica-based EDF that had higher Er^{3+} concentration, although four EDF samples have the same total Er^{3+} ion number. Therefore, we discuss the physical dynamics of hole formation process, mainly focusing on the anomalous characteristics of Er^{3+} concentration dependence of the second hole.

5-4-1. Characteristics of the gain spectral holes at low temperature

The origin of deep second and main holes at low temperature is most likely due to the change of the thermal relaxation rate to the Boltzmann distribution over the Stark manifolds of Er^{3+} ions. Since the thermal relaxation to the Boltzmann distribution at low temperature achieved more slowly, the crude population density of ions in the excited state $^4I_{13/2}$ remains almost unchanged as in the initial state until the induced emission from the $^4I_{13/2}$ level occurs, which suggests that Er^{3+} ions in the Stark manifolds within the $^4I_{13/2}$ level can be depopulated more stably at 77K than that at room temperature. On the other hand, at room temperature, the thermal equilibrium over the Stark manifolds within the $^4I_{13/2}$ and the $^4I_{15/2}$ level is achieved very fast before the induced emission from the $^4I_{13/2}$ level to the $^4I_{15/2}$ level occurs. Therefore, the

Boltzmann distribution in the excited state is build up in very short time at room temperature, which leads to the shallow second hole at room temperature as mentioned above.

5-4-2. Saturating wavelength dependences of the main and second hole depths

The main and second hole depths decreased as the wavelength of saturation signal became longer. These characteristics of the main and second hole depths can be explained by the energy structure model as shown in Fig. 5-12 (a) and 5-12 (b). The solid bars show the region over the Stark manifolds that can contribute to the formation of the second hole. The dashed bars show that can contribute to the formation of the main hole. In addition, the length of solid bars and that of dashed bars correspond to the energy of the second and main hole, respectively. The population of the half-toned Stark manifolds can be depopulated by a saturating signal. Fig. 5-12(a) and 5-12(b) show the burned areas by the saturating signal whose wavelength is longer and shorter, respectively. As shown in Fig. 5-12, the population of the Stark manifolds within the $^4I_{13/2}$ state decreases when the wavelength of saturating signal became longer due to the decrease of the population of the Stark manifolds within the $^4I_{13/2}$ state.

5-4-3. Saturating wavelength dependences of the main and second hole widths

The main hole width was found to become broader as the saturating signal wavelength became longer whereas the second hole width did not show the saturation signal wavelength dependence as mentioned above. These characteristics of the main and second hole widths give an important information on the relaxation process between the Stark manifolds relating the formation of the main and second holes because the relaxation process is directly correlated with the linewidth.

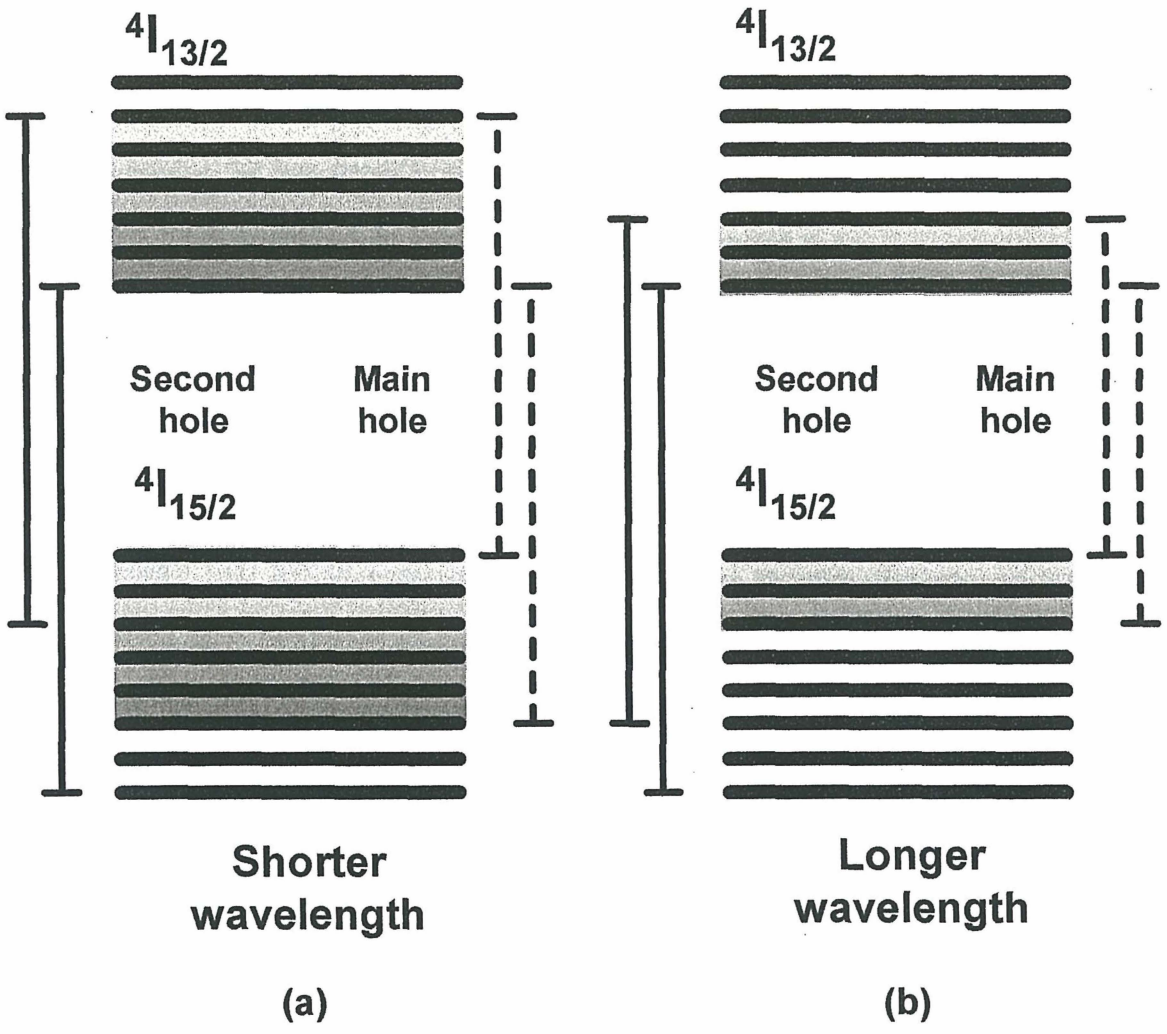

Figure 5-12 Depopulated energy state region of the Er^{3+} ion energy structure by the saturating signals ((a) shorter wavelength, (b) longer wavelength).

Judging from the saturating signal wavelength-independent character of the second hole, the relaxation process relating the formation of the second hole is supposed not to change when the saturating signal wavelength was varied. On the other hand, the difference between the main hole widths in the C-band and the L-band region as shown in Fig. 5-5 is possibly caused by the difference between the relaxation processes in the C-band and the L-band regions. Actually, it has been reported that the temperature dependence of the homogeneous broadening in C-band region indicated $T^{1.5}$ over the temperature range 30-150K, which indicates that both direct one-phonon process (which leads to T^1 temperature dependence) and Raman process (which leads to T^2 temperature dependence) are included into the relaxation process of the transitions in the C-band wavelength region [10]. $T^{1.73}$ law has been also reported for the homogeneous broadening at 1.53 μ m over the temperature range 20-77K [1]. Therefore, one reason for the decrease of the second and main hole depth is considered to be homogeneous broadening in C-band region indicated $T^{1.5}$ over the temperature range 30-150K, which indicates that both direct one-phonon process (which leads to T^1 temperature dependence) and Raman process (which leads to T^2 temperature dependence) are included into the relaxation process of the transitions in the C-band wavelength region. On the other hand, the temperature dependence of the homogeneous broadening in the L-band region has been reported to follow the temperature law, T (which indicates that direct one-phonon process is dominant). In addition, the homogeneous linewidth in the L-band region is broader than that in the C-band region at low temperature. (T<120K) [10]. Taking these into account, the observed main hole width broadening in the L-band wavelength region at 77K can be originated from the homogeneous contributions to the transitions in the L-band wavelength region.

5-4-4. Er^{3+} ion concentration dependence of the second hole depth

For an explanation of the Er^{3+} ion concentration dependence of the second hole depth, we propose the contribution of Er^{3+}-Er^{3+} energy transfer mechanism to thermal relaxation rate as a

hole formation mechanism. The rate of relaxation is delayed at low temperature because of the decrease of the number of thermally activated phonons that contribute to the relaxation. On the other hand, the direct energy transfer between Er^{3+} ions such as migration is not largely affected by the change in temperature. In the case of electric dipole interaction, the energy transfer probability on the separation between Er^{3+} ions has been well known to be inversely proportional to six power of average distance between Er^{3+} ions [11].

Therefore, the effect of the direct energy transfer among Er^{3+} ions is more likely dominant in the EDF sample that has higher Er^{3+} ion concentration. In the case of the EDF samples with higher Er^{3+} ion content, the delayed thermal relaxation rate at 77K is expected to be compensated by the contribution of the direct Er^{3+}-Er^{3+} energy transfer mechanism to thermal relaxation rate. The migration process between donor and accepter has been reported to contribute to make the homogeneous distribution of Er^{3+} ions excited to $^4I_{13/2}$ state by energy transfer [12]. Therefore, the second hole depth of the EDF sample with higher Er^{3+} ion content such as EDF IV (Er^{3+}:1600ppm) is considered not to change even in high saturation signal power because of the rapid energy transfer among Er^{3+} ions. On the other hand, in the case of the EDF sample with lower Er^{3+} ion concentration like EDF I (Er^{3+}:130ppm), the second hole depth becomes deeper because of the slow energy transfer mechanism among Er^{3+} ions.

5-5. Conclusion

The saturating power, the wavelength and Er^{3+} ion concentration dependence of GSHB in silica-based EDFA at 77K were reported. The depth of main and second hole decreased as the wavelength of the saturating signal became longer. The main hole width was found to become broader even at 77K in the L-band region than that in the C-band region. On the other hand, the second hole width did not show the saturation signal wavelength dependence in the C-band and the L-band regions. In addition, the second hole depth of GSHB showed the Er^{3+} ion concentration dependence and increased with decreasing of the Er^{3+} ion concentration when a high saturating signal was input. The contribution of the energy transfer mechanism among Er^{3+} ions to the relaxation mechanism of GSHB is also proposed for this Er^{3+}-dependent GSHB characteristic. This Er^{3+} concentration dependence of GSHB and the physical mechanism is considered to be the same for other emission systems which exploit the 1.5 μ m emission of Er^{3+} ion. As far as we know, this is the first report of the Er^{3+} concentration effect on the gain spectral hole burning in the Er^{3+} doped fiber.

References

[1]. E.Desurvire, J. L. Zyskind, and J. R. Simpson, "Study of spectral dependence of gain saturation and effect of inhomogeneous broadening in erbium-doped aluminosilicate fiber amplifiers," IEEE Photon. Technol. Lett.,vol. 2, no4, pp. 246-248, 1990.

[2]. E. Rudkevich, D. M. Baney, J. Stimple, D. Derickson and G. Wang, "Nonresonant spectral-hole burning in erbium-doped fiber amplifier," IEEE Photon. Technol. Lett., vol. 11, pp. 542-544, 1999.

[3]. N. S. Bergano, C. R. Davidson, M. A. Mills, P. C. Corbett, S, G, Ecangelides, B. Pederson, R. Menges, J. L. Zyskind, J. W. Sulhoff, A. K. Srivastava, C. Wolf, and J. Judkins, "Long-haul WDM transmission using optimum channel modulation: A 160 Gb/s (32 x 5 Gb/s) 9,300 km demonstra- tion," *in Proceedings of Optical Fiber Conference 1997,* OFC97, PD16, 1997.

[4]. M. Nishihara, Y. Sugaya, and E. Ishikawa, "Characterization and new numerical model of spectral hole burning in broadband erbium-doped fiber amplifier," *in Proceedings of Optical Amplifiers and Their Applications 2003*, OAA 2003, Tud3, 2003.

[5]. J. Chung; S. Yong Kim; C. J. Chae, "Performances of all optical gain-clamped EDFAs with different feedback wavelengths for use in multiwavelength optical networks" *in Proceedings of Optical Fiber Conference 1997,* OFC97, TuE5, pp. 22-24, 1997.

[6]. G. Luo, J.L. Zyskind; Y. Sun, A.K. Srivastava, J.W. Sulhoff; M.A. Ali, "Relaxation oscillations and spectral hole burning in laser automatic gain control of EDFAs," *in Proceedings of Optical Fiber Conference 1997,* OFC97, WF4, pp. 130-131, 1997.

[7]. M. Bolshtyansky, "Spectral hole burning in erbium-doped fiber amplifiers," IEEE Photon. Technol. Lett., vol. 21, no4, pp. 1032-1038, 2003.

[8]. J. W. Sulhoff, A. K. Srivastava, C. Wolf, Y. Sun, and J. L. Zyskind, "Spectral-hole burning in erbium-doped silica and fluoride fibers," IEEE Photon. Technol. Lett., vol. 9, no12, pp. 1578-1579, 1997.

[9]. I. Joindot and F. Dupre, "Spectral hole burning in silica-based and in fluoride-based optical fibre amplifiers," Electron. Lett., vol. 33, pp. 1239-1240, 1997.

[10] L. Bigot, A. Jurdyc, B. Jacquier, L. Gasca, and D. Bayart, "Resonant fluorescence line narrowing measurements in erbium-doped glasses for optical amplifiers," Phys. Rev., B 66, pp. 1-9, 2002.

[11] D. L. Dexter, "A theory of sensitized luminescence in solids," J. Chem. Phys., vol. 21, pp. 836-850, 1953.

[12] V. P. Gapontsv, and N. S. Platonov, "Migration-Accelerated Quenching in Glasses Activated by Rare Earth Ions", in Dynamical Processes in Disordered Systems, Material Science Forum, vol. 51, 1990.

Chapter 6

Evidence of existence of side holes induced by gain spectral hole burning in erbium-doped fiber at 77K

6-1. Introduction

One of the limiting factors to the performance of the long haul optical transmission system using dense wavelength-division-multiplex (DWDM) technique is gain spectral hole burning (GSHB) in erbium-doped fiber amplifier (EDFA). Since the transmission distance of long haul optical transmission system becomes much longer than ever, which includes over 150 EDFAs, the degradation of the gain spectrum of an EDFA is accumulated over a hundred times in the system and the effect of gain spectral hole burning on the gain spectral shape after transmission becomes much more critical problem [1].

As well known, GSHB is the phenomenon that causes the gain spectral deviation in the wavelength region when some strong signals are input into EDFA [2]. It has also been reported that an additional hole ("second hole" or "nonresonant hole") can be burned at around

1530nm independent of the wavelength of the saturating signal, where the main hole is burned [3, 4]. The effect of these holes is large enough to degrade the gain flatness. Therefore, GSHB in EDFA has become a serious problem for the precise design of the long haul optical transmission system. At this moment, the characteristics of GSHB in the C-band wavelength region has been considered to be dominated mainly by the inhomogeneous broadening attributed to the site-to-site variations of the local ligand fields that surround Er^{3+} ions in the amorphous glass host of EDF. On the other hand, it was recently reported that the characteristics of GSHB in the L-band wavelength region at low temperature can be strongly dominated by the homogeneous broadening induced by Raman and one phonon processes [5].

Like this, the origin of these gain spectral holes seems to vary in different wavelength regions and the whole physical mechanism of the formation of these holes is being investigated now. So far, no complete physical interpretation of GSHB has been formulated, although many numerical and experimental measurements have been performed to clarify and model the mechanism of GSHB [6-10]. Above all, the second hole characteristics has not been sufficiently investigated. Therefore, we investigated the saturating signal wavelength dependence of the second hole depth of GSHB in silica-based EDFA at 77K using the saturating signal whose wavelength regions were in the C-band and the L-band. Low temperature was required to suppress the contribution of the phonons that promotes the rapid relaxation to the thermal equilibrium over the Stark levels within the $^4I_{13/2}$ and the $^4I_{15/2}$ manifolds and prevents the clear observation of hole shape. As a result, we observed the second hole accompanied with side holes burned at around 1520nm and 1540nm at 77K for the first time as far as we know. And we obtained an interesting saturating signal wavelength dependence of the second hole at 77K. In addition, the saturation signal wavelength dependence of the gain spectral hole, the relaxation time measurements were also performed to evaluate the relaxation time of the main and second holes. The hole formation mechanism is discussed based on these experimental results.

6-2. Experimental

6-2-1. Characteristics of EDF samples

Three silica-based EDF samples with different Er_2O_3 content were used as the gain medium in GSHB measurements in the C-band and L-band wavelength regions. The Er^{3+} ion concentrations of samples were 130ppm, 700ppm, and 1600ppm. Optical parameters for each EDF are shown in Table 6-1. The fiber length of each EDF was decided to include the same total number of Er^{3+} ions in EDF, which leads to the same attenuation for all EDF samples. The absorption spectra in the wavelength region from 1420nm to 1640nm for each EDF are shown in Fig. 6-1. Each spectrum has the peak value 38dB at about 1531.8nm.

Table 6-1. Parameters for silica-based EDF samples.

Sample	Er^{3+} ion (ppm.wt)	Fiber Length (m)	$n_{1.3\mu m}$ (-)
EDF I	130	30.0	1.469
EDF II	700	4.8	1.468
EDF III	1600	2.9	1.470

6-2-2. GSHB measurement scheme at 77K

Fig. 6-2 shows the experimental setup of GSHB measurement at 77K. EDF sample was cooled directly by liquid nitrogen in a dewar. The saturating signal and the probe signal were coupled with two 3dB couplers. We used the subtractive technique to measure gain spectral hole burning shapes in over 130nm bandwidth (1510nm-1645nm). Three tunable laser sources were used for the probe and signal light source, (Santec, TSL210). The coupled signals were input finally into the polarization scrambler to cancel the effect of polarization hole burning. The gain spectrum was measured with an optical spectrum analyser, OSA (Anritsu, MS9780A). EDF was forwardly pumped with a 980nm LD and the pump power of LD was stabilized in order to maintain a constant gain at the gain locking signal when the saturating signal was input into EDF. The gain locking signal wavelength was 1570nm in order to avoid the influence of the saturation signal on the population inversion ratio. The wavelength 1540nm signal was temporary used as gain locking signal when the saturating signal was 1570.5nm. The power of the gain locking signal was -30dBm. The power of probe signal was -30dBm. To examine the saturating wavelength dependence of the second hole, the wavelength of saturating signal was varied in the range from 1540.5nm to 1640.5nm. GSHB was measured at the saturating power of 0dBm. The GSHB spectrum was calculated by subtracting a gain spectrum without the saturating signal from that with the saturating signal. The gain spectrum without saturating signal was set to have the same gain 11.1dB at 1531.8nm, which corresponds to the second hole peak wavelength, to keep the same population inversion ratio in order to compare the degradation of population inversion ratio caused by GSHB.

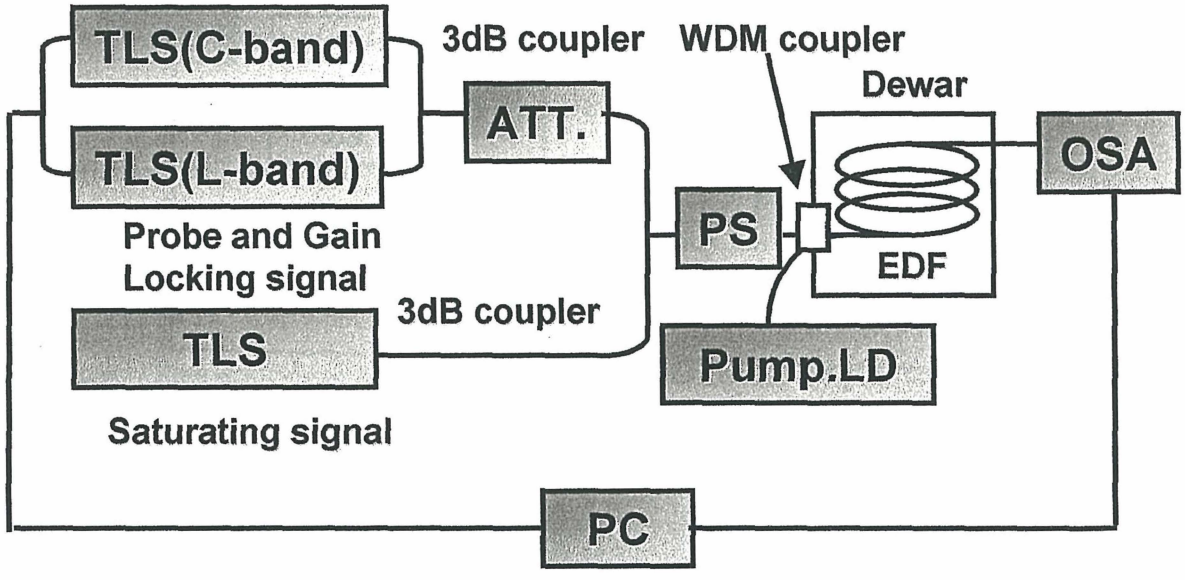

Figure 6-1 Experimental set up of GSHB measurement at 77K.

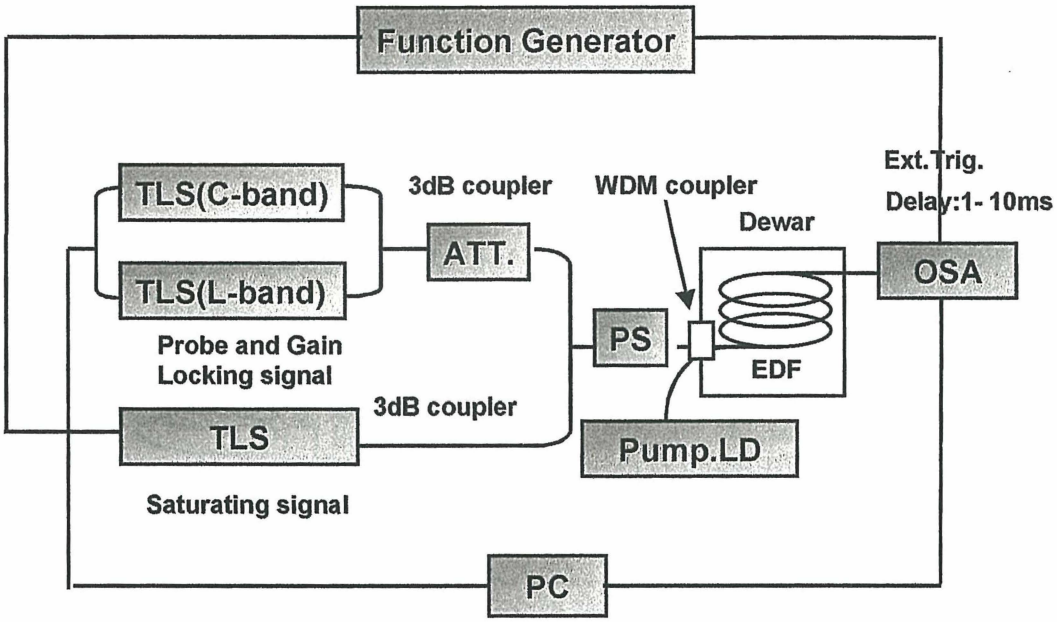

(a)

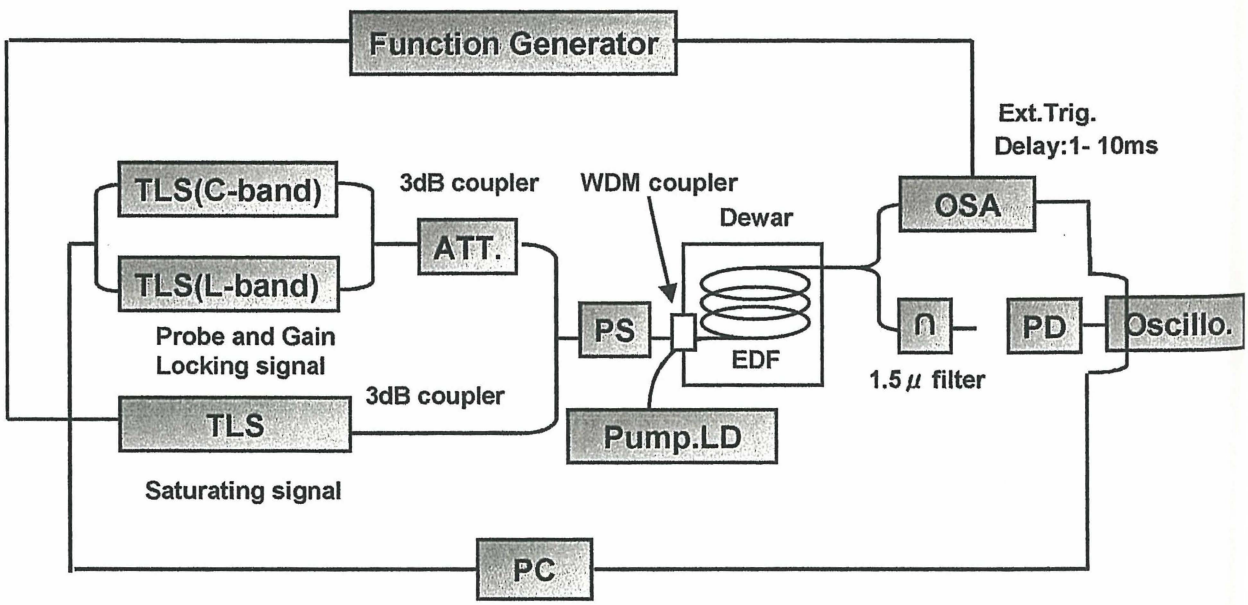

(b)

Figure 6-2 Experimental set up of the relaxation characteristics measurement of holes at 77K

(a)Gain measurement set up, (b)Intensity (signal+ASE) measurement set up.

6-2-3. Relaxation time measurement of GSHB at 77K

In addition to the GSHB measurement, the relaxation time measurements were performed in order to evaluate the relaxation time of the main and second holes. Fig. 6-3(a) and 6-3(b) show the relaxation time measurement scheme. As shown in Fig. 6-3(a) and 6-3(b), two tunable laser sources were used for the probe light source, in the C-band and the L-band wavelength regions and the other laser source was used for saturating signal (Santec, TSL210). A saturating signal was modulated by the function generator to output 150μs rectangular optical pulse. Pulse interval was decided to be 10ms (repetition time:100Hz) . As shown in Fig. 6-3(a), Optical spectrum analyser, OSA (Anritsu, MS9780A), was triggered by the function generator. Data acquisition of OSA was set to be started within 0-5(ms) after a trigger event occurred in order to observe the relaxation characteristics of the main and the second holes.
In Fig. 6-3(b), the output signal from the edge of EDF was filtered with a tunable optical filter (Santec, TSL210). And the filtered output signal was detected with a photo detector connected to an oscilloscope to compare the relaxation characteristics of the signal intensity level with a saturation signal with that without a saturation signal. GSHB was measured at the saturating power of 0dBm and the wavelength of the saturation signal was 1550.5nm in both cases.

6-3. Results and Discussion

6-3-1. Main hole with side holes

Fig. 6-4 shows the gain spectral hole shape observed at 77K for and EDF sample (EDF I). The saturation signal wavelength was 1530.5nm. Two side holes were burned at 1520nm and 1540nm in addition to the main hole at 1530.5nm. We call the side hole in shorter wavelength region than 1530nm "third hole" and that in the longer wavelength region than 1530nm "fourth hole". The depth of the main hole was about four times as deeper as that of the side holes. So far, these side holes haven't been reported to exist. Instead, the "uplift" of the gain at room

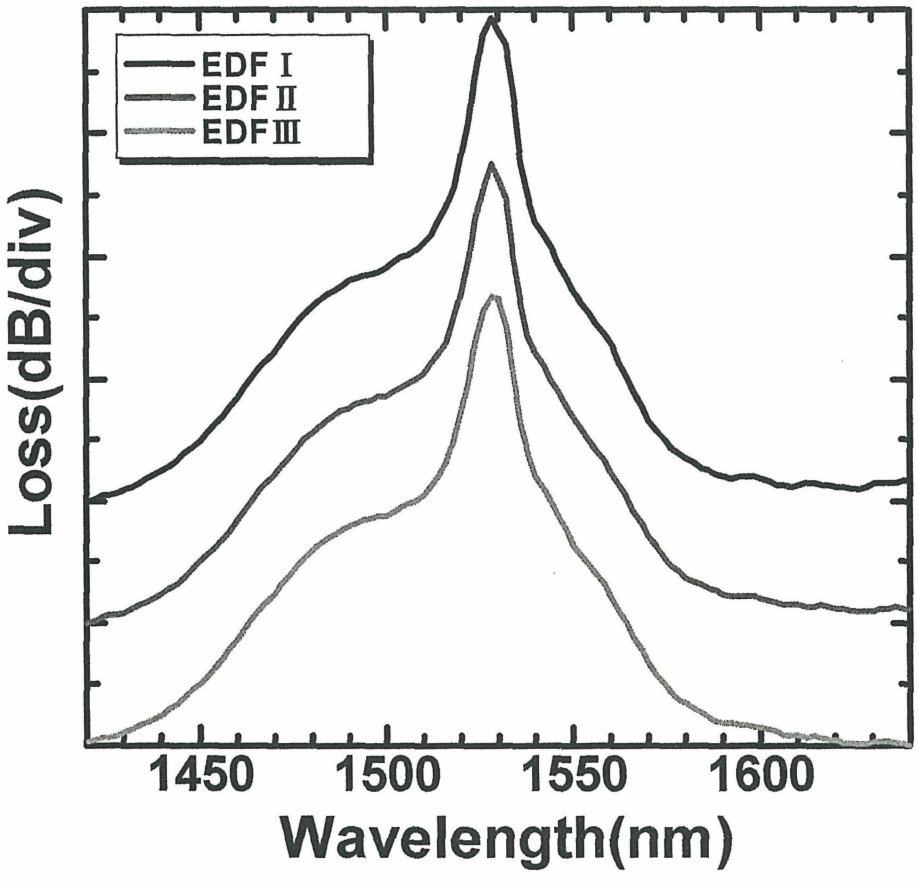

Figure 6-3 The absorption spectra of EDF in the wavelength region from 1420nm to 1640nm.

temperature has been reported. However, this uplift should not be considered to be the intrinsic character of the gain spectral hole burning. It seems like an artifactual result due to the difference between the population inversion ratio of the reference gain and that of the gain with saturation signal input.

In our measurements, the spacing between the side and main hole was about 10nm which corresponds to 43.3cm^{-1} and 42cm^{-1} in wavenumber for the third and fourth hole, respectively. The values of these spacings almost correspond to the reported energy separation between the lowest Stark level and the first excited Stark level of the $^4I_{15/2}$ manifold [6].
Generally, at 77K, it is enough to consider only the depopulation of the first excited and the lowest Stark level within the $^4I_{13/2}$ manifold because about 90% of the excited Er^{3+}ion are populated in the lowest two Stark level within $^4I_{13/2}$ manifold at 77K. Therefore, these side holes indicate that the induced emission from the first excited and the lowest Stark levels of the $^4I_{13/2}$ manifold are suppressed by the increase in the population of the lowest and the first excited Stark levels of the $^4I_{15/2}$ manifold in particular. Thus, it is shown that the depopulation of the lowest two Stark levels within the $^4I_{13/2}$ manifold has influences on the other emissions whose wavelength is not 1530.5nm.

Moreover, the side holes seem to be observed when the broadening of the emission line that corresponds to the transitions between the Stark levels of Er^{3+} ion becomes small.
Comparing GSHB in Er^{3+}-doped silica-based fiber with that in Er^{3+}-doped fluoride fiber, the gain spectral hole width in Er^{3+}-doped silica fiber has been reported to be narrower than that in Er^{3+}-doped fluoride fiber [7]. Generally, the broadening of the emission line that corresponds to the transitions between the Stark levels of Er^{3+} ion is smaller in Er^{3+}-doped silica-based fiber than that in Er^{3+}-doped fluoride fiber. This indicates that inhomogeneity plays more dominant role in Er^{3+}-doped silica-based fiber than that in Er^{3+}-doped fluoride fiber.

So far, it has been considered that the saturation signal whose wavelength is 1530nm can burn only a main hole at 1530nm at room temperature. However, if the emission line

broadening mentioned above is small, there is a possibility to burn the side holes in addition to the main hole even at room temperature. Actually, "uplift" was clearly observed in Er^{3+}-doped silica-based fiber [7], which seems to be the side holes.

Fig. 6-5 shows the hole shapes for the sample EDFI (Er^{3+}:130ppm) at 77K when the wavelength of saturating signal was varied from 1540.5nm to 1640.5nm. The saturating signal power was 0dBm in all measurements. As in the case of the main hole, very deep and sharp second hole at around 1530nm was observed compared with those at room temperature. So far, the second hole depth of GSHB observed at around 1530nm has been reported to be about 1dB at room temperature even if a strong saturating signal was input into EDF [8]. This is because the thermal relaxation assisted by phonons occurs more rapidly at room temperature than that at low temperature, which suppresses the formation of the gain spectral hole. Generally, the number of the phonons that are excited thermally decreases at low temperature. Therefore, second hole should be deeper and narrower at 77K than at room temperature.

As shown in Fig. 6-5, the wavelengths of the second and side holes were independent of the saturating signal wavelength (1535.5nm–1640.5nm). This character has been reported for the second hole at room temperature in the C-band wavelength region [3, 4] and indicates that the formation mechanism of the second and side holes are originated from the Stark energy structure of Er^{3+} ion. The second and side hole depths became shallower as the saturating signal wavelength became longer. These characters of the holes indicate the decrease of the Stark levels of Er^{3+} ion, which correspond to the wavelength of the saturation signal, with the wavelength of the saturation signal varying.

6-3-2. Second hole characteristics with the saturation signal wavelength varied

Fig. 6-6 shows the wavelength dependence of second hole depth and 980nm LD input power in

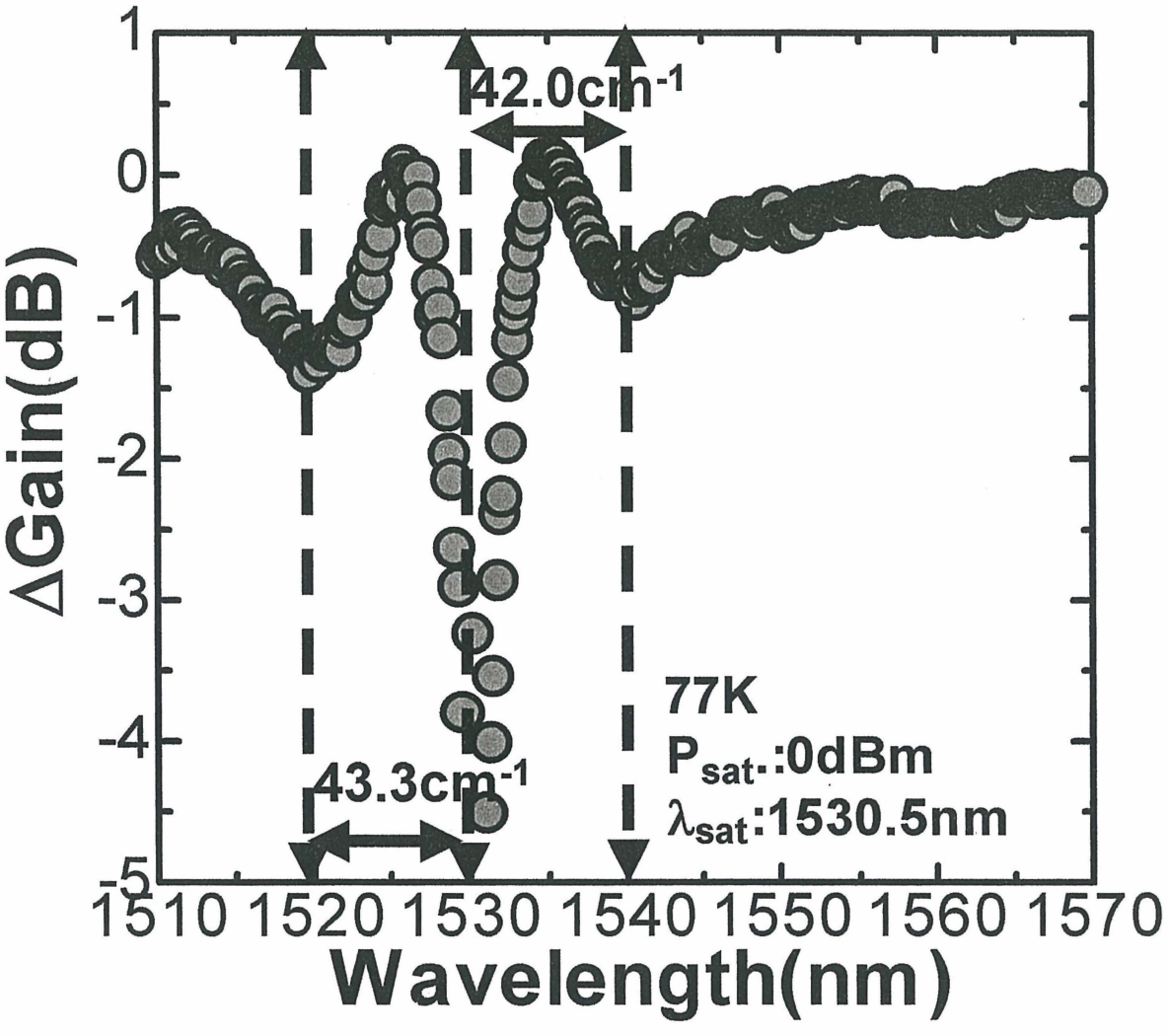

Figure 6-4 Gain spectral hole at 77K of EDF I sample (Er^{3+}:130ppm).

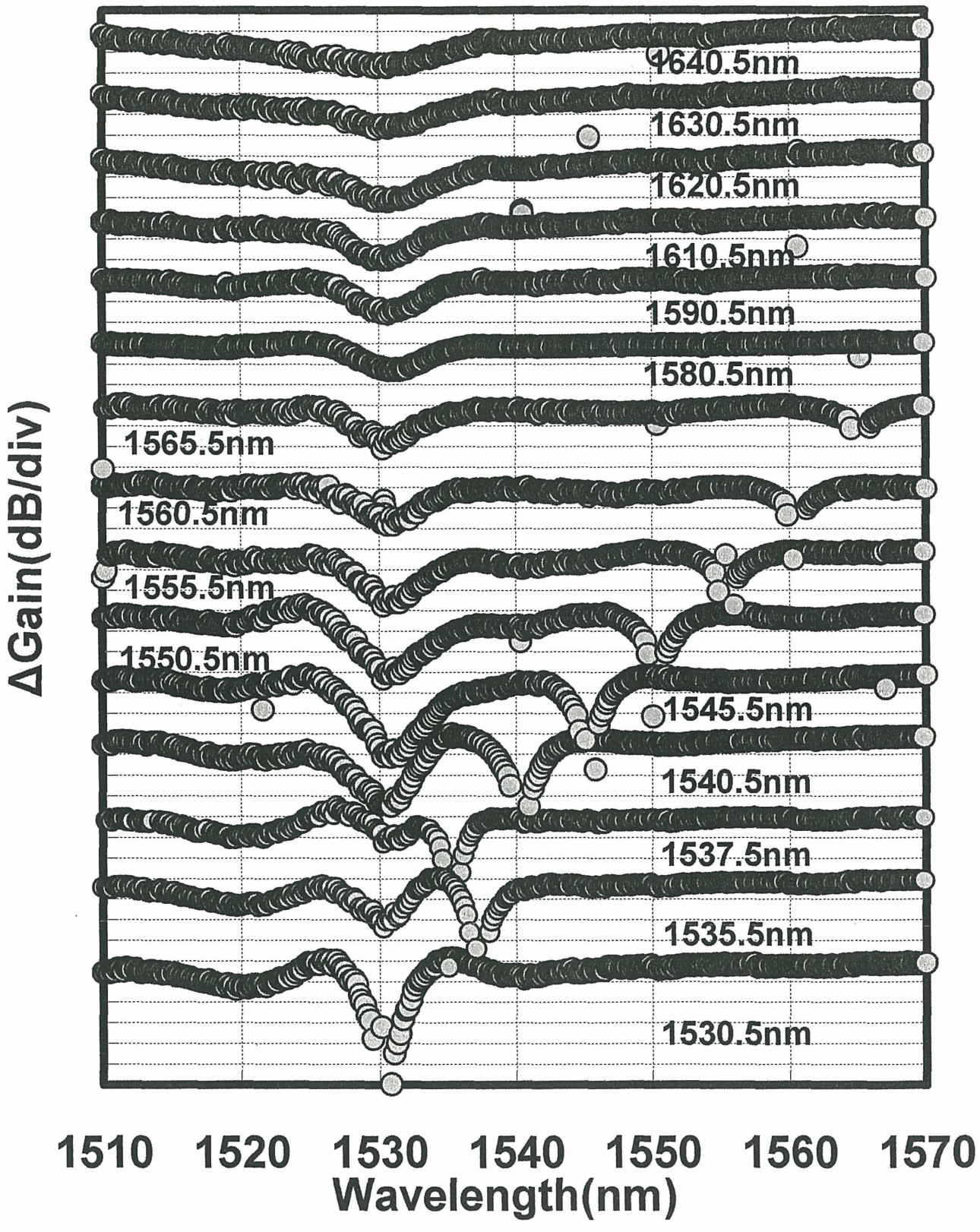

Figure 6-5 Hole shapes of the sample EDFI (Er^{3+}:130ppm) at 77K with various saturating signal.

the C-band wavelength region. The second hole depth increases with increasing the LD input power. Fig. 6-7 shows the LD input power dependence of the second hole depth. Clearly, there is a negative correlation between the LD input power and the second hole depth.

Fig. 6-8 shows the relationship between the second hole depth and the saturating signal wavelength of EDF I (Er^{3+}: 130ppm) in the C-band and the L-band wavelength regions when the saturating signal power is 0dBm. The second hole depth is found to show the two local peaks at around 1545nm and 1590nm. This character of the second hole depth at 77K is not consistent with that observed at room temperature in the C-band wavelength region [3].
This character suggests that the saturation signal wavelength satisfied the resonance condition with the energy gap, which correspond to about 1545nm, between the first excited or lowest Stark level within the $^4I_{13/2}$ manifold and the lower Stark levels within the $^4I_{15/2}$ manifold, which leads to the occurrence of the frequent induced emission.

The second hole depth at 77K decreased again until the wavelength of the saturation signal became 1580nm. In much longer wavelength region than 1580nm, the second hole depth became deeper again and showed the second local peak at around 1590nm. Thus, the depth of the second hole at 77K was found to show the two peaks and not to decrease monotonically when the wavelength of the saturating signal becomes longer. The mechanism of this second hole character of in the L-band wavelength region is not unclear yet and now under consideration in connection with the Stark energy structure of Er^{3+}.

6-3-3.Er^{3+} concentration dependence of the second hole depth

Fig. 6-9(a) and 6-9(b) show the saturation signal wavelength dependences of the second and the side holes for EDF II (Er^{3+}:700ppm) and EDF III (Er^{3+}:1600ppm), respectively.

In both cases, the saturation signal powers were 0dBm. A third hole in the shorter wavelength region is observed in EDF II and EDF III as in the case of EDF I.

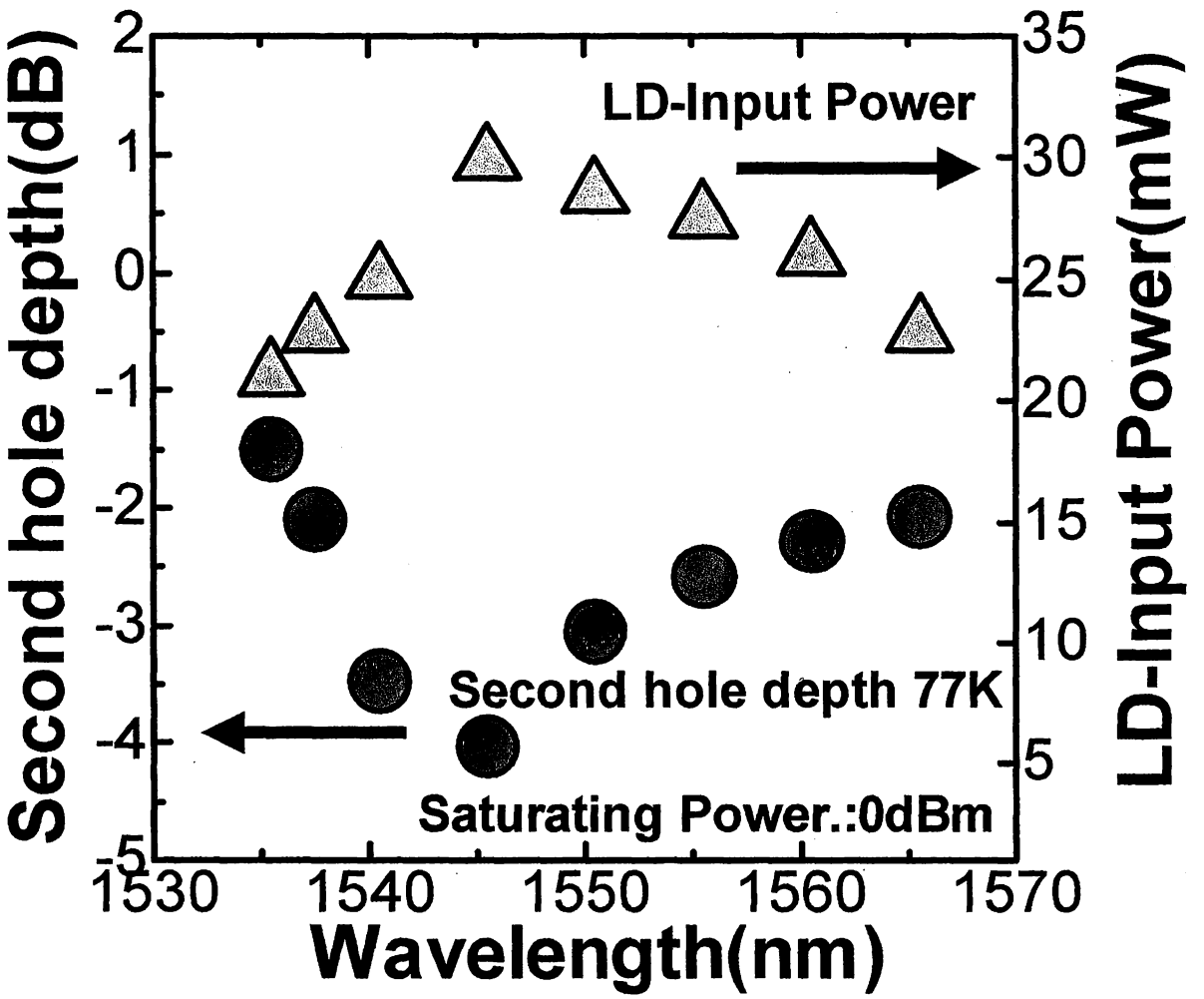

Figure 6-6 Wavelength dependences of the second hole depth and 980nm LD input power in the C-band wavelength region (EDFI).

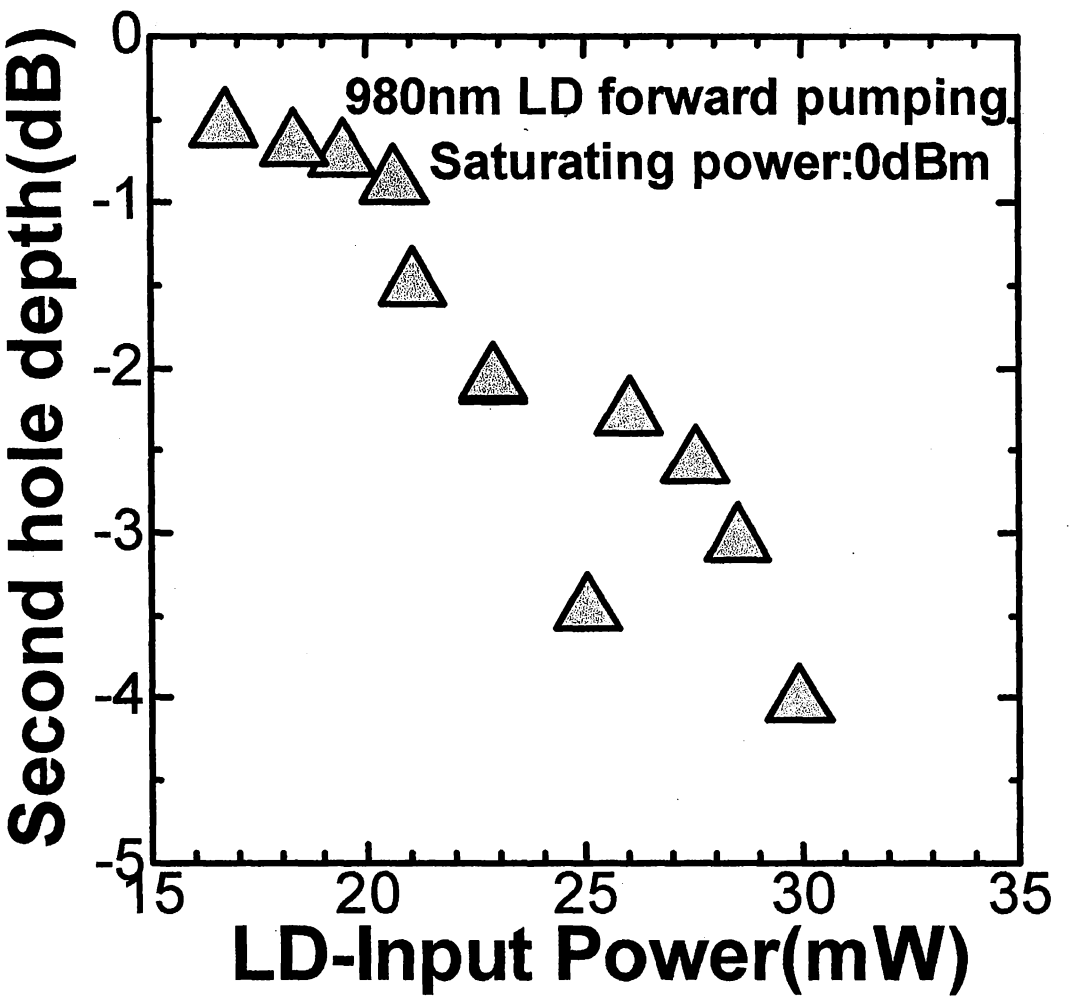

Figure 6-7 LD input power dependence of the second hole depth.

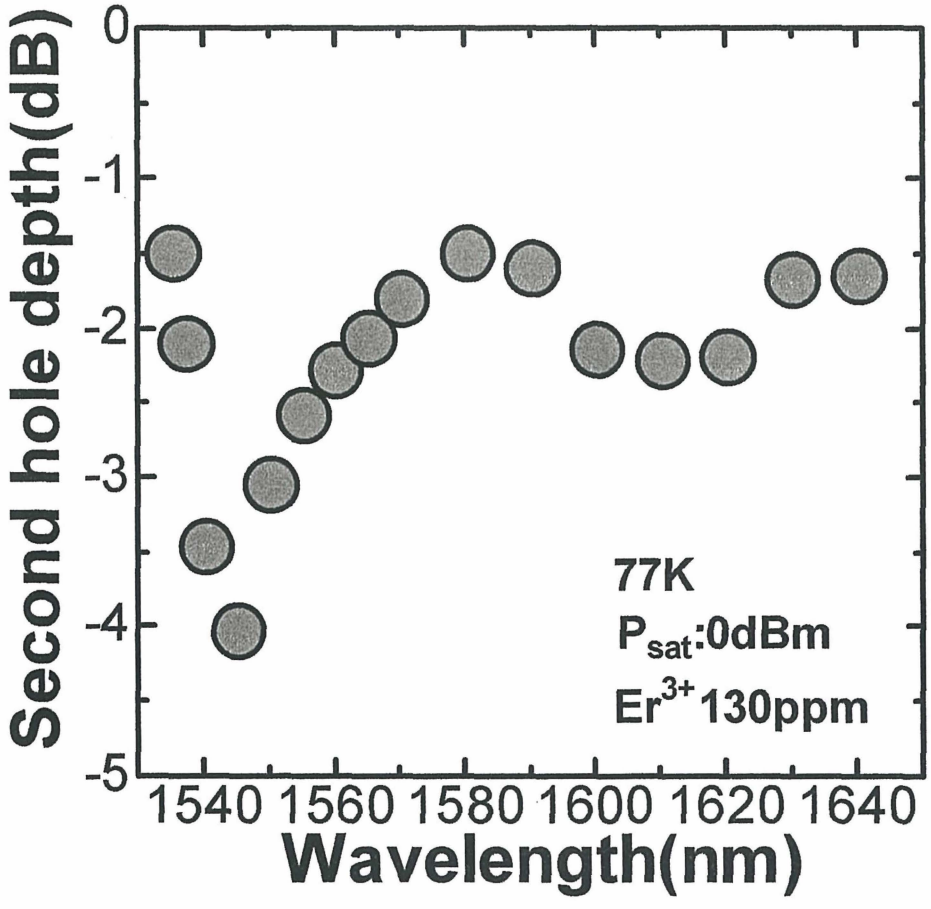

Figure 6-8 Relationship between the second hole depth and the saturating signal wavelength of EDF I (Er^{3+}: 130ppm) in the C-band and the L-band wavelength regions (P_{sat}=0dBm).

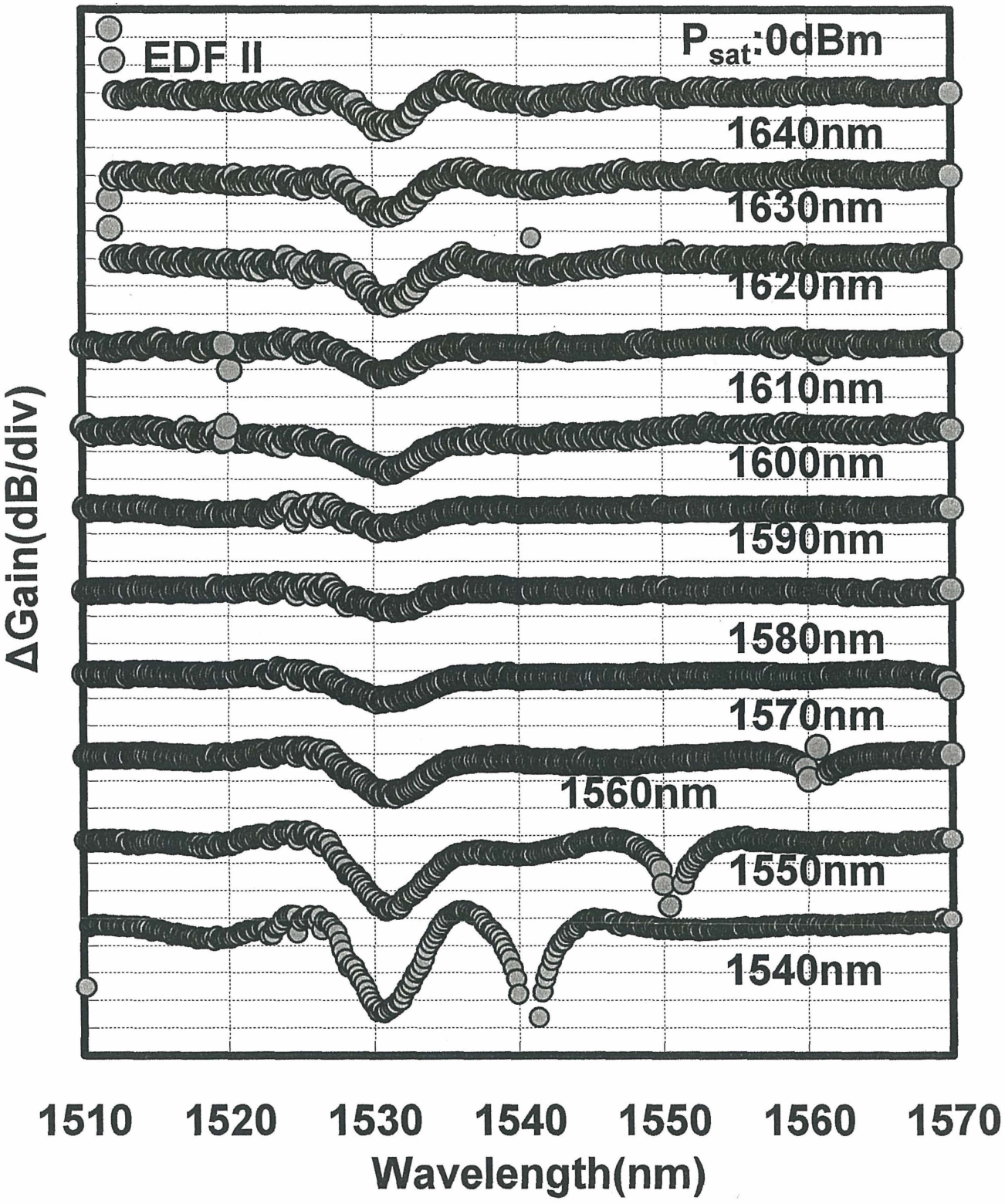

Figure 6-9(a) Hole shapes of the sample EDFII (Er^{3+}:700ppm) at 77K with various saturating signal.

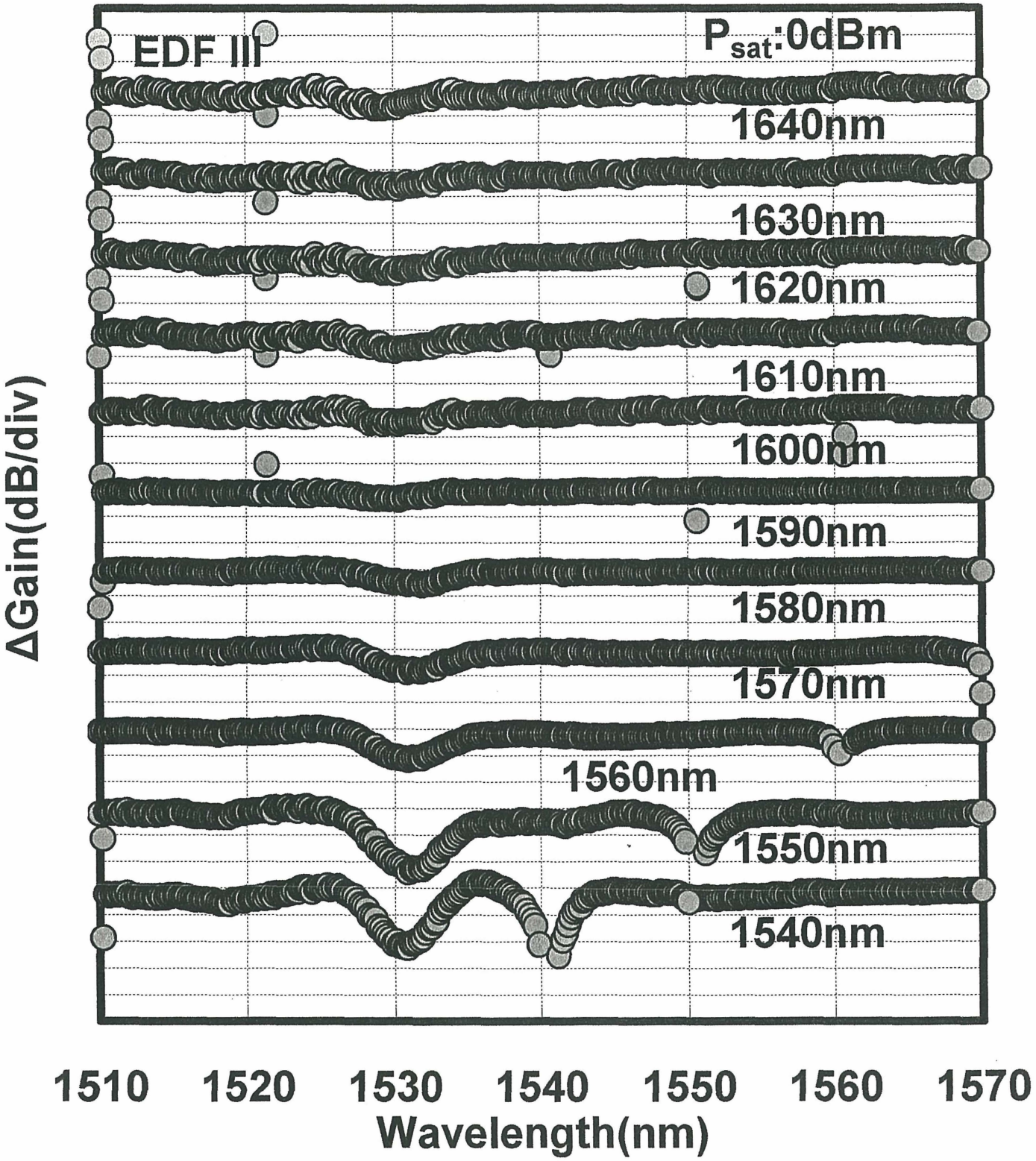

Figure 6-9(b) Hole shapes of the sample EDFII (Er^{3+}:700ppm) at 77K with various saturating signal

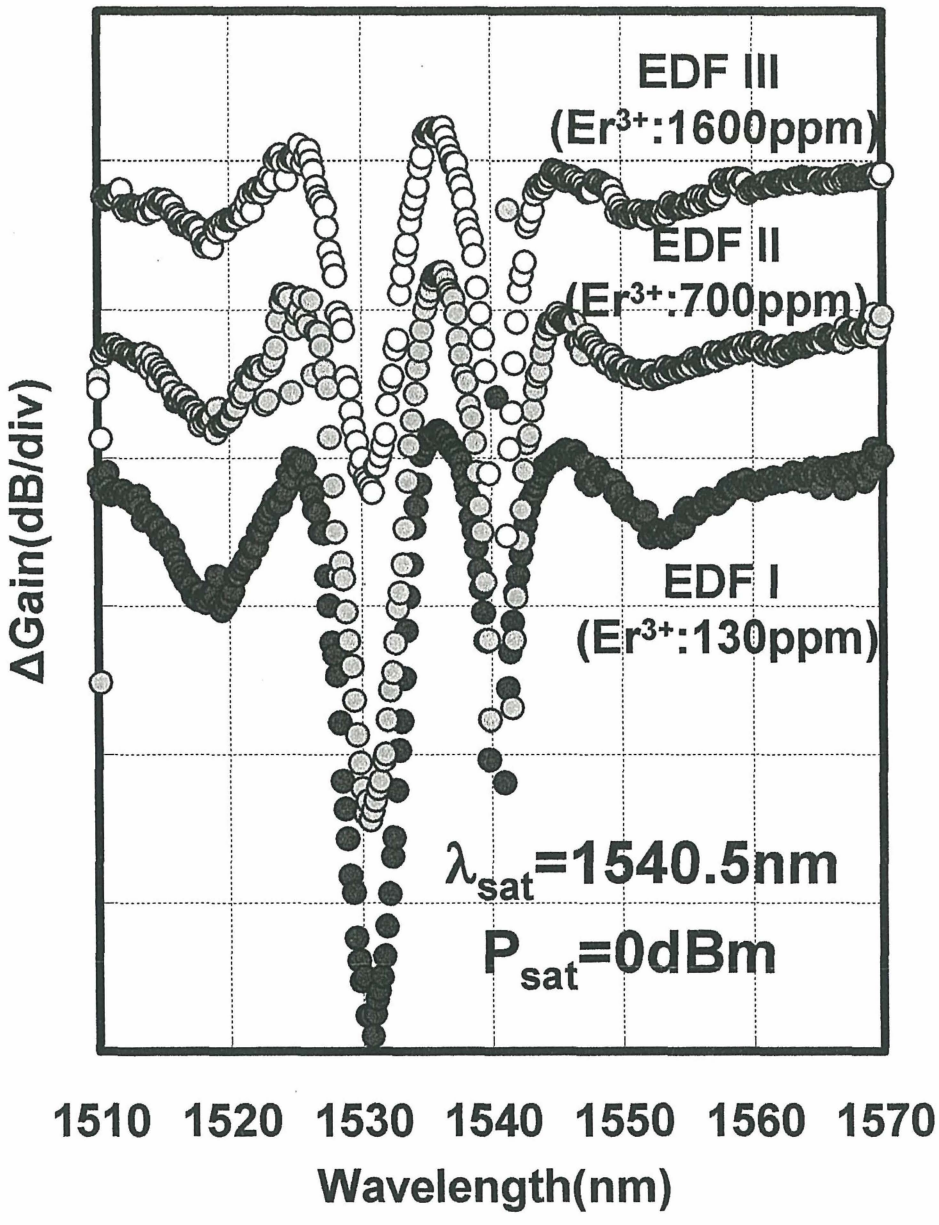

Figure 6-10 Comparison among the hole depths of three EDF samples (λ_{sat}=1540.5nm, Psat=0dBm).

Fig. 6-10 shows the comparison among the hole depths of three EDF samples. The saturation signal wavelength is 15405nm and the saturation signal power is 0dBm.

Compared with the depth of the third hole at around 1530nm in EDFI, the depth of the third hole became shallower in EDF II and EDF III, which have lower Er^{3+} ion concentration than that in EDF I. This Er^{3+} ion concentration dependence of the third hole depth is consistent with that of the second hole, which was found in our pervious GSHB study using the saturations signal wavelength of 1550.5nm. At 77K, about 90% of the excited Er^{3+}ion are populated in the lowest two levels within $^4I_{13/2}$ manifold at 77K. Therefore, the emission which corresponds to the wavelength of 1520nm seems to be induced by the transition between the second lowest Stark level within the $^4I_{13/2}$ manifold and the lowest Stark level within the $^4I_{15/2}$ manifold. The population density of the second lowest Stark level within the $^4I_{13/2}$ manifold can be affected and compensated by the Er^{3+}-Er^{3+} ion interaction.

In addition, additional hole at around 1550nm was also observed. This additional hole depth seems to have the Er^{3+} ion concentration dependence as in the case of the second and third hole depth. Taking account of these characteristics of holes, the gain spectral hole seems to be burned periodically in about 10nm steps, which indicates the Stark level structure within the $^4I_{15/2}$ manifold of Er^{3+} ion. Therefore, we would like to propose the gain spectral hole shape model shown in Fig. 6-11, which is different from the gain spectral hole shape that has been reported to have the a second hole burned around 1530nm. In this model, the hole width becomes wider with increasing temperature. As a result, the hole shape at 1530nm become wider and seems to form a second hole at around 1530nm at room temperature.

Fig. 6-12 shows the relation ships between the second hole depth and the saturation signal wavelength for three EDF samples. The saturation signal was varied from 1550.5 nm to 1640.5nm in 10nm steps. The Et^{3+} ion concentration dependence of the second hole depth, which is that the second hole depth becomes deeper in the EDF that has shallower Er^{3+} ion concentration is verified to be maintained in both the C-band and the L-band wavelength

regions. A peak observed at around 1590nm in EDF I was also observed in EDF II and EDFIII.

Therefore, these second hole characteristics of in the L-band wavelength region may be intrinsic.

6-3-4.Relaxation characteristics of the main and the second hole

Fig. 6-13 shows the relaxation characteristics of intensity level at 1530nm. At 77K, the intensity level recovered its initial condition after 12ms had passed.

Fig. 6-14 shows the relaxation characteristic of the gain of EDF I after 150μs rectangular optical pulse falls. The wavelength of pulsed saturation signal was 1550.5nm. Main hole burned at 1550.5nm was found to remain even when 2ms second has passed after trigger event occurred.

Fig. 6-15 shows the relaxation characteristics of the main and second holes at 77K. These hole shapes were calculated by subtracting a gain spectrum without the saturating signal from that with the saturating signal. As far as we know, this is the first observation of the relaxation characters of the main and second holes. Both gain spectral holes are found to remain even when 5ms has passed after optical pulse falls. However, it cannot be judged whether the difference between the relaxation times of the main holes and second holes occurs or not. Since the relation between the hole formation mechanism and the depopulation of the Stark level within the $^4I_{13/2}$ manifold are indicated by the existence of the second holes, there should occur the difference between the relaxation times of the main hole and second hole. Therefore, further studies on the relaxation time of the main and second holes are needed to make progress in the understanding of the origin of the hole formation.

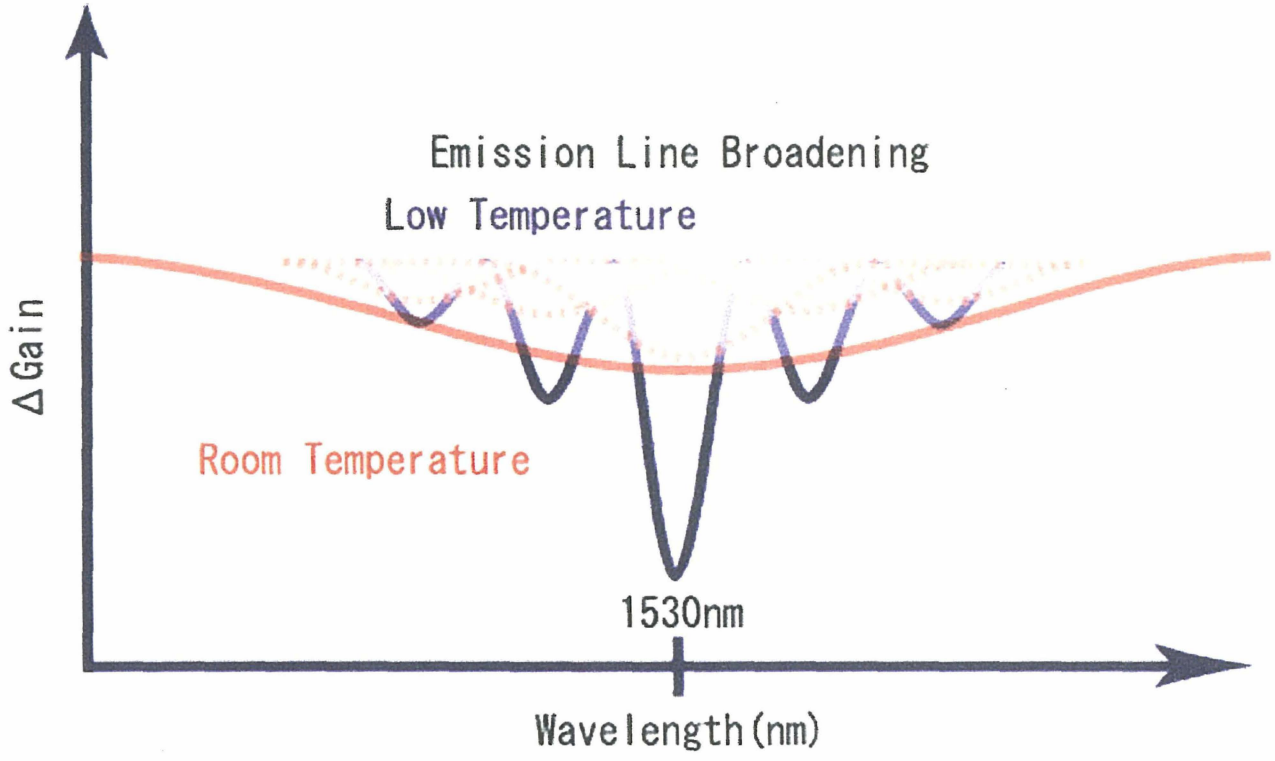

Figure 6-11 Gain spectral hole shape models at high and low temperature.

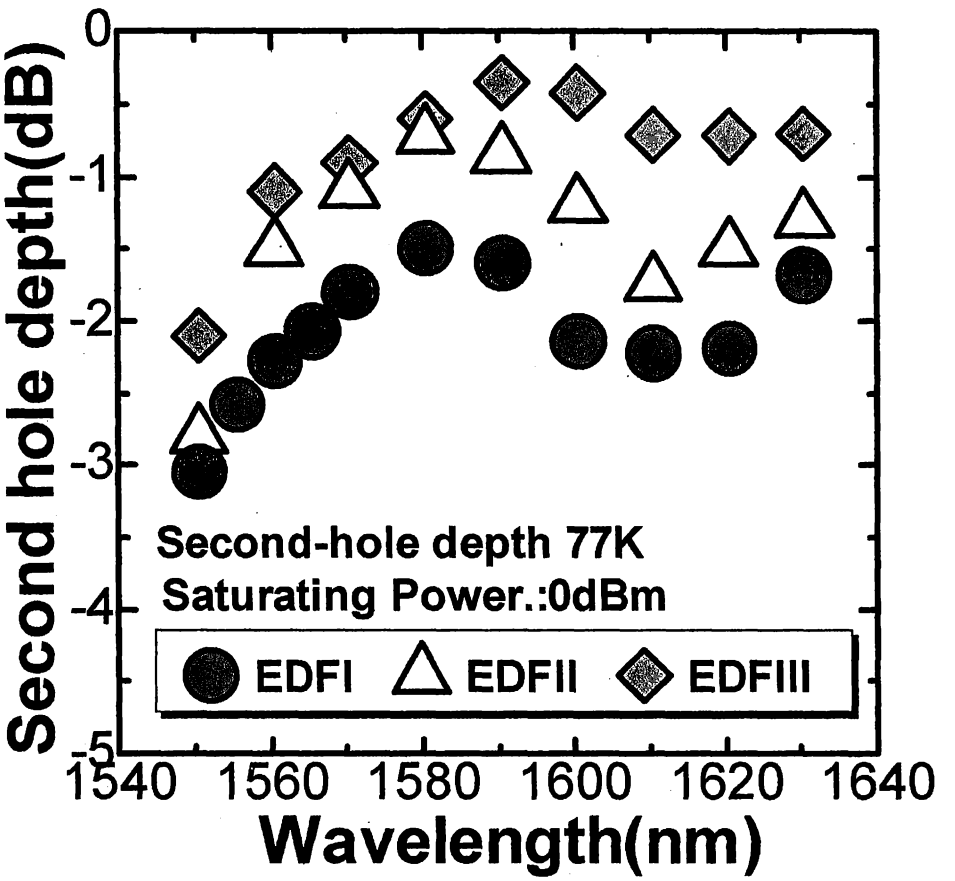

Figure 6-12 Comparison of the relation ships between the second hole depth and the saturation signal wavelength of three EDF samples.

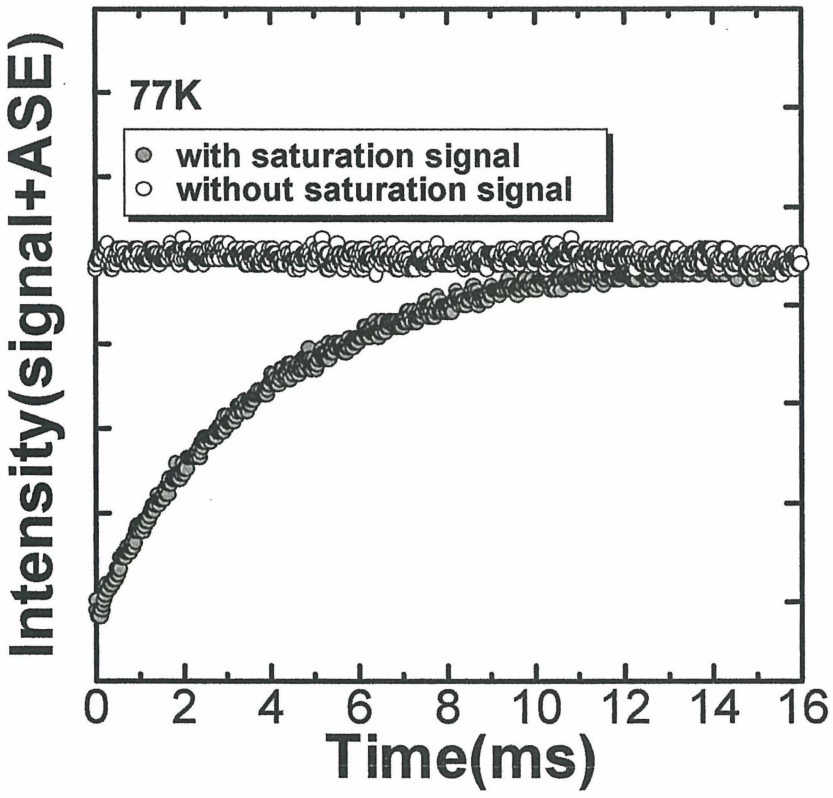

Figure 6-13 Relaxation characteristic of the intensity level (signal + ASE) at 1530nm.

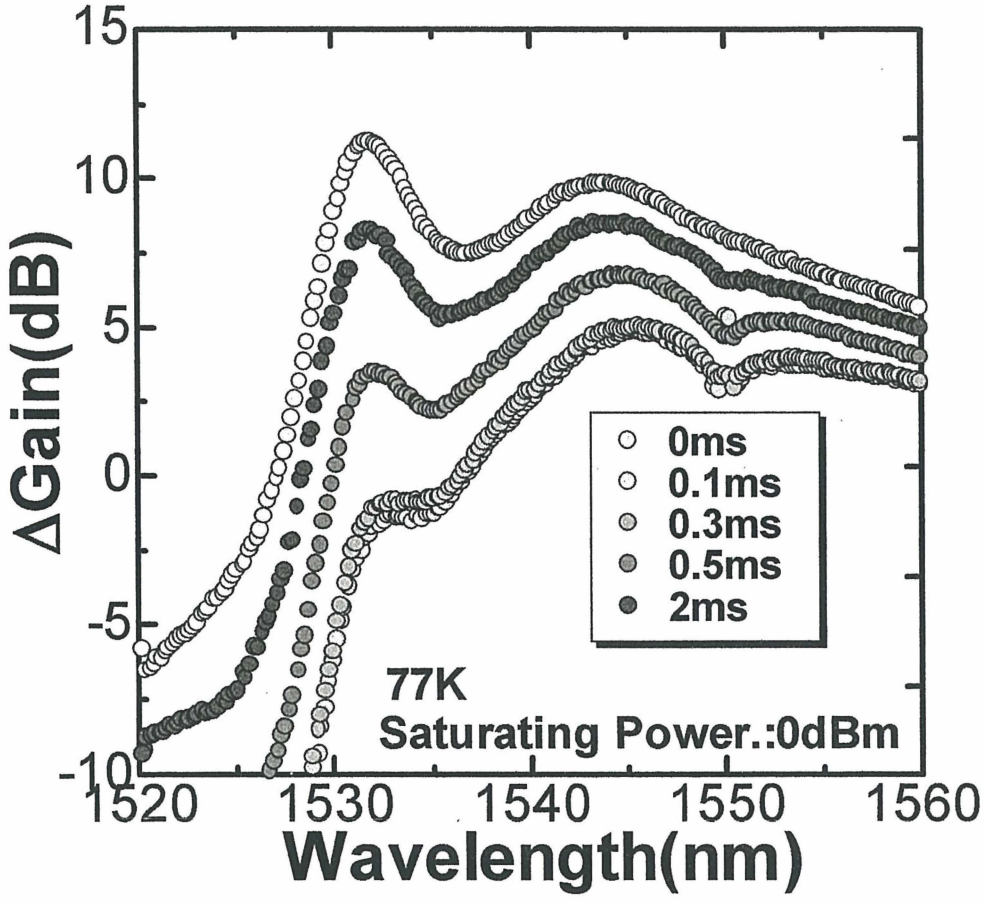

Figure 6-14 Relaxation characteristic of the gain in the C-band wavelength region.

(P_{sat}=0dBm, λ_{sat}=1550.5nm).

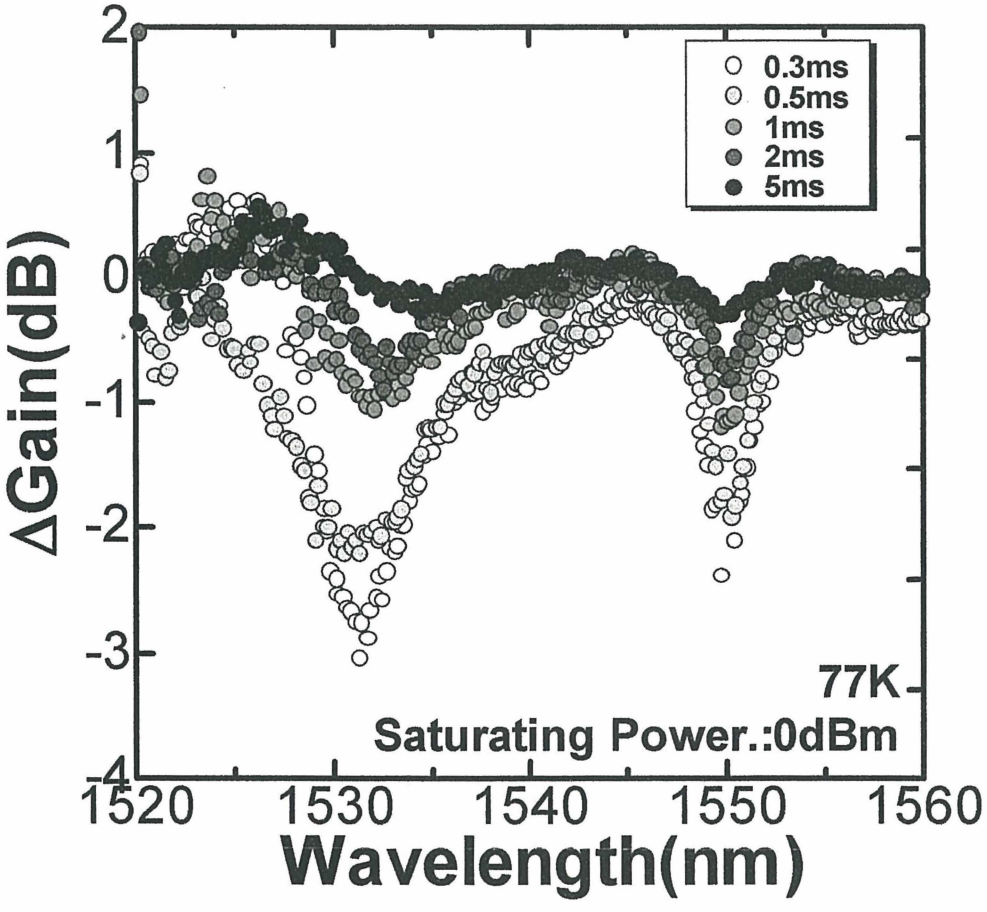

Figure 6-15 Relaxation characteristic of the main and second hole shapes

(P_{sat}=0dBm, λ_{sat}=1550.5nm)..

6-4.Conclusion

The existence of the additional holes and the wavelength dependence of the gain spectrum holes in a silica-based EDFA at 77K were reported. The main hole accompanied with two side holes was observed at 77K for the first time. These two side holes were separated form the main hole by about 10nm which almost corresponds to the energy gap between the first excited and lowest Stark level within the $^4I_{15/2}$ manifold of Er^{3+} ion. The wavelengths of the second and side holes were independent of that of the main hole. These characters of holes indicate that the formation mechanism of holes is closely-linked to the Stark level structure of Er^{3+} ion. So far, gain spectral hole has been considered to be burned and localised at around 1530nm and the wavelength of saturation signal. And the effect of the gain spectral hole burning on the gain characteristics is also considered to be confined to the localised wavelength region. However, from our experimental results at 77K, it was shown that there can be additional holes in much wider wavelength region than expected at 77K. When the wavelength of the saturating signal were varied, the depth of the second hole at 77K was found to show the two peaks at around 1545nm and 1590nm and not to decrease monotonically with increasing the saturating signal wavelength. This saturating signal wavelength dependence was observed for the first time and was verified to be quite different from that observed at room temperature. In addition, the Er^{3+} ion concentration dependence of the second hole depth was investigated for three EDF samples with different Er^{3+} content and verified that the Er^{3+} ion concentration dependence of the second hole depth was also maintained even when the wavelength of the saturation signal was varied in the C-band and the L-band wavelength regions. Relaxation characteristics of the holes were also measured for the first time. It was found that main and second holes remained even when 5ms had passed after optical pulse vanished. However, it cannot be judged precisely whether the difference between the relaxation times of the main holes and second holes occurs or not. Therefore, further studies on the relaxation time of holes are awaited for the better understandings of the gain spectral hole characteristics in the future.

References

[1]. F. I. Kharti, D. G. Duff, M. Vaa and A. L. Simons, "Spectral hole burning effects on partially loaded, 19 nm bandwidth, 6246 km long EDFA lightwave transmission system,"Electron. Lett., vol. 36, no. 8 pp. 739-740, 2000.

[2]. E.Desurvire, J. L. Zyskind, and J. R. Simpson, "Study of spectral dependence of gain saturation and effect of inhomogeneous broadening in erbium-doped aluminosilicate fiber amplifiers," IEEE Photon. Technol. Lett., vol. 2, no4, pp. 246-248, 1990.

[3]. E. Rudkevich, D. M. Baney, J. Stimple, D. Derickson and G. Wang, "Nonresonant spectral-hole burning in erbium-doped fiber amplifier," IEEE Photon. Technol. Lett., vol. 11, pp. 542-544, 1999.

[4]. M. Nishihara, Y. Sugaya, and E. Ishikawa, "Characterization and new numerical model of spectral hole burning in broadband erbium-doped fiber amplifier," *in Proceedings of Optical Amplifiers and Their Applications 2003*, OAA 2003, Tud3, 2003.

[5] L. Bigot, A. Jurdyc, B. Jacquier, L. Gasca, and D. Bayart, "Resonant fluorescence line narrowing measurements in erbium-doped glasses for optical amplifiers," Phys. Rev., B 66, pp. 1-9, 2002.

[6]. E. Desurvire and J. R. Simpson, "Evaluation of $^4I_{15/2}$ and $^4I_{13/2}$ Stark-level energies in erbium-doped aluminosilicate glass fibers," Opt. Lett., vol.15, no10, pp. 547-549, 1990.

[7]. J. W. Sulhoff, A. K. Srivastava, C. Wolf, Y. Sun, and J. L. Zyskind, "Spectral-hole burning in erbium-doped silica and fluoride fibers," IEEE Photon. Technol. Lett., vol. 9, no12, pp. 1578-1579, 1997.

[8]. I. Joindot and F. Dupre, "Spectral hole burning in silica-based and in fluoride-based optical fibre amplifiers," Electron. Lett., vol. 33, pp. 1239-1240, 1997.

[9]. M.J. Yadlowsky, "Pump Wavelength-Dependent Spectral-Hole Burning in EDFA's," J. Light wave. Technol., vol. 17, pp. 1643-1648, 1999.

[10]. M. Bolshtyansky, "Spectral hole burning in erbium-doped fiber amplifiers," IEEE Photon. Technol. Lett., vol. 21, no4, pp. 1032-1038, 2003.

Appendix

Review of Gain Performance for Erbium-Doped Fiber by Numerical Simulation Model

In chapter 2 and chapter 3, the temperature dependent and the Er^{3+} ion concentration dependent numerical simulation were build to analyze the gain performance of silica-based EDFA. These simulation models were based on the rate equation for the three level system, the propagation equation, and the McCumber theory. Here, in Appendix, the review of the numerical simulation is made to clear its procedure.

A-1 Theory for the numerical simulation based on the rate and propagation equations

Considering the energy level diagram for four level system with pump excited absorption as shown in Fig. 1, with the population conservation law, the rate equations for the populations N_1, N_2, N_3, and N_4 of levels 1, 2, 3 and 4 are given by,

$$N_1 + N_2 + N_3 + N_4 = N_{total}, \tag{1}$$

$$\frac{dN_1}{dt} = A_{21}N_2 + W_{21}N_2 - W_{12}N_1 - RN_1 + RN_3, \tag{2}$$

$$\frac{dN_2}{dt} = W_{12}N_1 + A_{32}N_3 - R'N_2 + R'N_4 - A_{21}N_2 - W_{21}N_2, \tag{3}$$

$$\frac{dN_3}{dt} = A_{43}N_4 - A_{32}N_3 + RN_1 - RN_3, \tag{4}$$

$$\frac{dN_4}{dt} = R'N_2 - R'N_4 - A_{43}N_4, \tag{5}$$

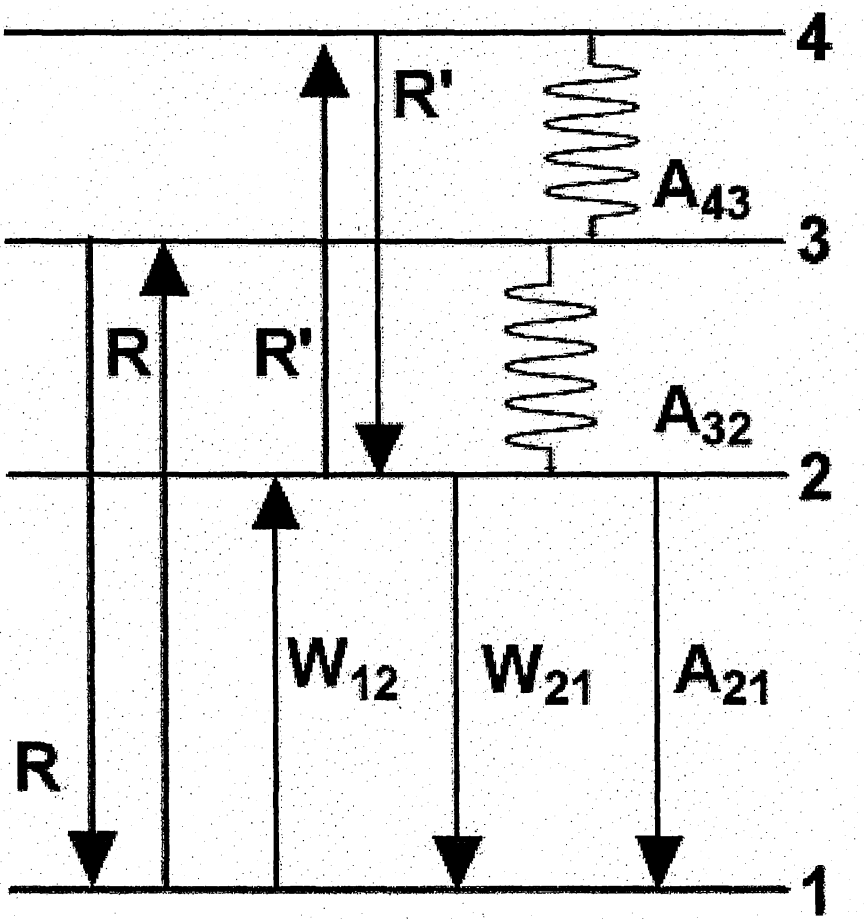

Figure 1 Energy level diagram for four level system with pump excited absorption.

where R and R' is the pumping rates corresponding to ground state absorption (GSA) and excited absorption (ESA) which take place between levels 1 and 3, and 2and 4, respectively. This four level system corresponds to that of Er^{3+} ion, which consists of the $^4I_{15/2}$, $^4I1_{3/2}$, $^4I_{11/2}$ and $^4I_{9/2}$ level. We assume $R=R_{13}=R_{31}$ and $R'=R_{24}=R_{42}$. The nonradiative decay rate from the levels 3 and 4 are A_{32} and A_{43}, respectively, while the radiative decay rate from the metastable level, level 2, is A_{21}; the stimulated emission rates are W_{12} and W_{21}. Using the steady state condition ($dN_i/dt=0$, i=1, 2, 3, 4), we obtain the steady solutions as follows:

$$N_1 = N_{total}\frac{(1+\varepsilon R\tau)[1+W_{21}\tau+R'\tau(1-\frac{1}{1+A_{43}/R'})]-R''}{(1+2\varepsilon R\tau)[1+W_{21}\tau+R'\tau(1-\frac{1}{1+A_{43}/R'})]+(1+\frac{1}{1+A_{43}/R'})[(1+\varepsilon R\tau)W_{12}\tau+R\tau]+R''\tau(\varepsilon W_{12}\tau-1)} \tag{6}$$

$$N_2 = N_{total}\frac{(1+\varepsilon R\tau)W_{21}\tau+R\tau}{(1+2\varepsilon R\tau)[1+W_{21}\tau+R'\tau(1-\frac{1}{1+A_{43}/R'})]+(1+\frac{1}{1+A_{43}/R'})[(1+\varepsilon R\tau)W_{12}\tau+R\tau]+R''\tau(\varepsilon W_{12}\tau-1)} \tag{7}$$

$$N_3 = N_{total}\frac{\varepsilon R\tau[1+W_{21}\tau+R'\tau(1-\frac{1}{1+A_{43}/R'})]+\varepsilon R'\tau}{(1+2\varepsilon R\tau)[1+W_{21}\tau+R'\tau(1-\frac{1}{1+A_{43}/R'})]+(1+\frac{1}{1+A_{43}/R'})[(1+\varepsilon R\tau)W_{12}\tau+R\tau]+R''\tau(\varepsilon W_{12}\tau-1)} \tag{8}$$

$$N_4 = \frac{1}{1+A_{43}/R'}N_2 \tag{9}$$

where we use next definition for simplicity;

$$\tau = 1/A_{21} \tag{10}$$

$$\varepsilon = A_{21}/A_{32} \tag{11}$$

$$\varepsilon' = A_{21}/A_{43} \tag{12}$$

$$R'' = R' / (1 + \varepsilon' R' \tau) \qquad (13)$$

We consider the case of Er^{3+} ion in silica-based glass where the spontaneous decay rate A_{21} is negligible compared to the nonradiative decay rates. In this case, $A_{21}/A_{32} \ll 1$, and $A_{21}/A_{43} \ll 1$ are satisfied. Therefore, we can apply the condition that $\varepsilon \fallingdotseq \varepsilon' \fallingdotseq \kappa \fallingdotseq 0$ to the equations (6) – (9), which leads to $N_3 \fallingdotseq N_4 \fallingdotseq 0$. Consequently, the almost of all population density exists in the fast excited state 2 and the ground state 1 stably. Then equations (6) and (7) become:

$$N_1 = N_{total} \frac{1 + W_{21}\tau}{1 + W_{21}\tau + W_{12}\tau + R\tau} \qquad (14)$$

$$N_2 = N_{total} \frac{R\tau + W_{12}\tau}{1 + W_{21}\tau + W_{12}\tau + R\tau} \qquad (15)$$

This shows that the second and third excited levels are very weekly populated because of fast nonradiative decay. Therefore, considering $N_3 \fallingdotseq N_4 \fallingdotseq 0$, the rate equations (2) and (3) are rewritten as follows:

$$\frac{dN_1}{dt} = A_{21}N_2 + W_{21}N_2 - W_{12}N_1 - RN_1 \qquad (16)$$

$$\frac{dN_2}{dt} = W_{12}N_1 - R'N_2 - A_{21}N_2 - W_{21}N_2 \qquad (17)$$

$$W_{21(12)} = \int \frac{\sigma_{as(es)}(\nu)P_s(\nu)}{h\nu\pi b^2} d\nu \qquad (18)$$

$$R' = \int \frac{\sigma_{ESA}(\nu)P_s(\nu)}{h\nu\pi b^2} d\nu \qquad (19)$$

$$R = \int \frac{\sigma_{ap}(\nu)P_p(\nu)}{h\nu\pi b^2} d\nu \qquad (20)$$

where h is Plank's constant, $h\nu$ is the photon energy, b is the radius of the uniformly erbium-doped region, P_s and P_p are the signal and pump power, σ_{as}, σ_{es}, σ_{ESA} and σ_{ap} are the absorption, emission and excited state absorption cross section for the signal and pump, respectively. In addition, the propagation equations for the signal and the pump are given by,

$$\frac{dP_s(z)}{dz} = (\sigma_{sa}N_2 - \sigma_{sa}N_1 - \sigma_{sESA})P_s(z) \qquad (21)$$

$$\frac{dP_p(z)}{dz} = (\sigma_{pe}N_2 - \sigma_{pa}N_1)P_p(z) \qquad (22)$$

$$\frac{dP_{ASE}(z)}{dz} = \pm(\sigma_{se}N_2 - \sigma_{sa}N_1 - \sigma_{sESA})P_{ASE}(z) \pm mh\nu\Delta\nu\sigma_{se}N_2 \qquad (23)$$

Usually, the σ_{ESA} is very small and can be neglected in the C-band wavelength region because the signal ESA between the $^4I_{13/2}$ and the $^4I_{9/2}$ level occurs in the L-band wavelength region longer than 1680nm.

A-2 Performance of numerical simulator for the gain and loss characteristics of EDFA

A-2-1 Simulation model for the two level system

Based on the propagation equation and rate equations mentioned above, numerical simulator was build. We assume the two level system consists of the $^4I_{13/2}$ level and the $^4I_{15/2}$ level of Er^{3+} ion c which leads to the conservation law for the total population density ,

$$N_{total} = N_1 + N_2 \qquad (24)$$

In addition, the ESA from the $^4I_{13/2}$ level to the $^4I_{9/2}$ is neglected in the numerical simulation because the ESA has the effect on the gain performance in the longer wavelength region than about 1670nm. Therefore, we obtain R'=0, and the rate equations and propagation equations for the two level system of Er^{3+} ion is given by,

$$\frac{dN_2}{dt} = -\frac{dN_1}{dt} = -(A_{21} + W_{21})N_2 + (W_{12} + R)N_1 \qquad (25)$$

$$\frac{dP_p(z)}{dz} = -\sigma_{pa}N_1P_p(z) \qquad (26)$$

$$\frac{dP_s(z)}{dz} = (\sigma_{se}N_2 - \sigma_{sa}N_1)P_s(z) \qquad (27)$$

$$\frac{dP_{ASE}(z)}{dz} = \pm(\sigma_{se}N_2 - \sigma_{sa}N_1)P_{ASE}(z) \pm mh\nu\Delta\nu\sigma_{se}N_2 \qquad (28)$$

where P_s, P_p and P_{ASE} show the power of signal, pump, and amplified spontaneous emission,

respectively. m is the number of guided modes, normally 2 (number of polarization) , propagating at the signal wavelength and $\Delta \nu$ is the ASE bandwidth. For the ASE bandwidth, the resolution of the optical spectrum analyzer was chosen uniformly for all wavelengths in the numerical simulation. Equations (26)-(28) are a set of nonlinear differential equations that can be solved only numerically by means of an iterative propagate procedure. Fig. 2 shows the numerical simulation procedure. Initial values for the simulation are σ_{as}, σ_{es}, σ_{ap}, P_s, P_p, P_{ASE} and the iteration number n which defines the EDF length. Propagation equations (26)-(28) are solved in each step to decide the signal, pump and ASE power in next step. When the iteration procedure is once finished, other procedure starts calculating the gain or loss at other wavelength using other $\sigma_{as}(\lambda_i)$ and $\sigma_{es}(\lambda_i)$. Finally, Gain or Loss is given by,

$$Gain(\nu, z)(Loss(\nu, z)) = \exp[\int (N_2(z)(\sigma_e(\nu) + \sigma_a(\nu)) - N_{total}\sigma_a(\nu))dz] \quad (29)$$

Absorption or Gain coefficient is defined by,

$$\alpha = -[N_2(z)(\sigma_e(\nu) + \sigma_a(\nu)) - N_{total}\sigma_a(\nu)] \quad (30)$$

A-2-2 Fiber length dependences of Gain and Loss characteristics of EDFA

Gain and loss characteristics of EDFA are shown, which are calculated by the numerical simulation model based on the two level system of the excited and ground state of Er^{3+} ion Numerical simulation parameter for the absorption and loss characteristics were performed at 1530nm.

Fig. 3 shows the fiber length dependence of the signal power ratio $P_s(z)/P_s(0)$ with various input signal powers (Ps=-40dBm, -5dBm, 0dBm, 10dBm) without LD pumping. As shown in Fig. 3, the signal power ratio has the power dependence, which means the saturating absorption of the signal. This is because that the population density of the $^4I_{13/2}$ level increases due to the excitation by the signal itself with the increasing input signal power.

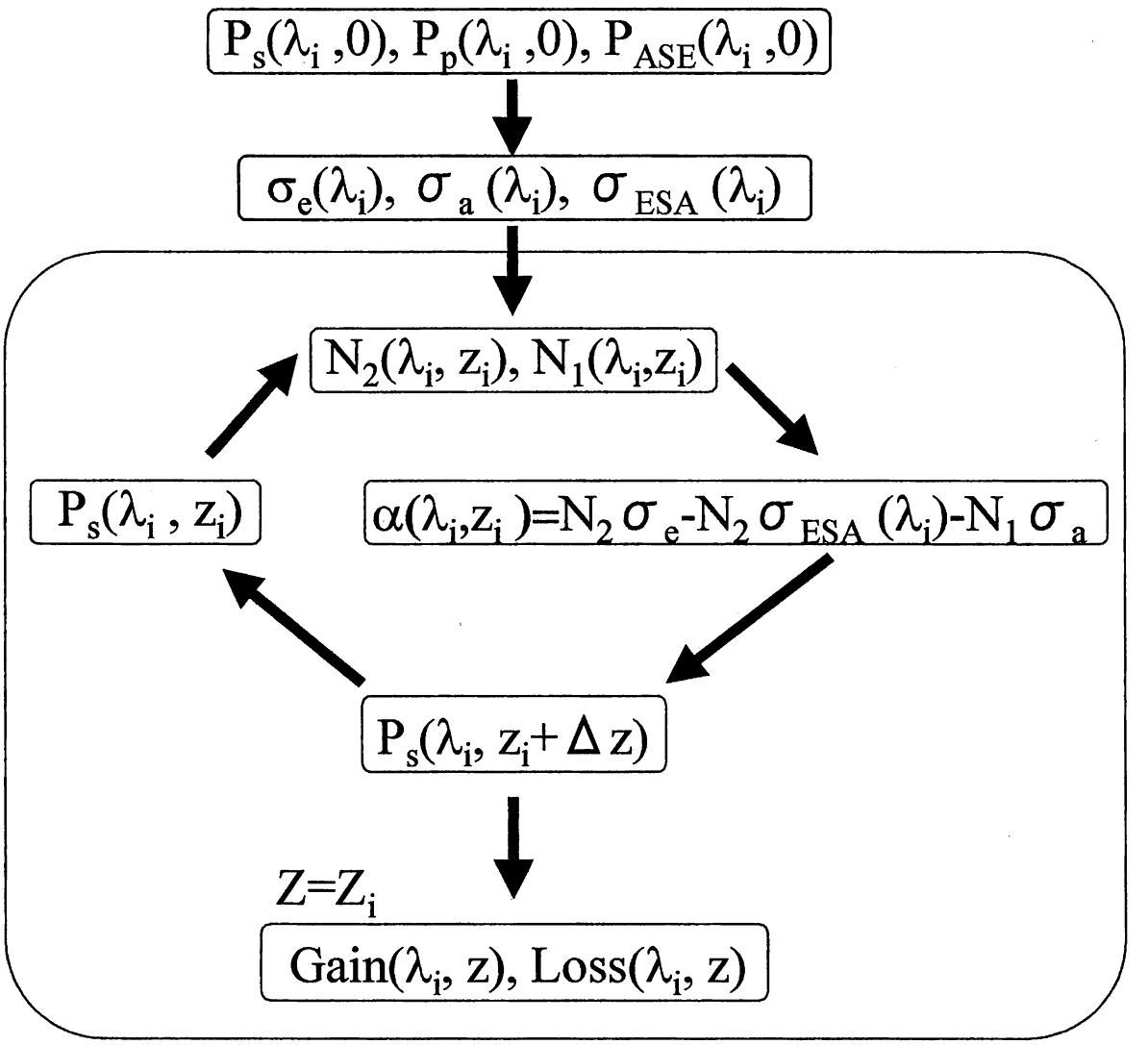

Figure 2 Numerical simulation procedure for the gain and loss characteristics of EDFA.

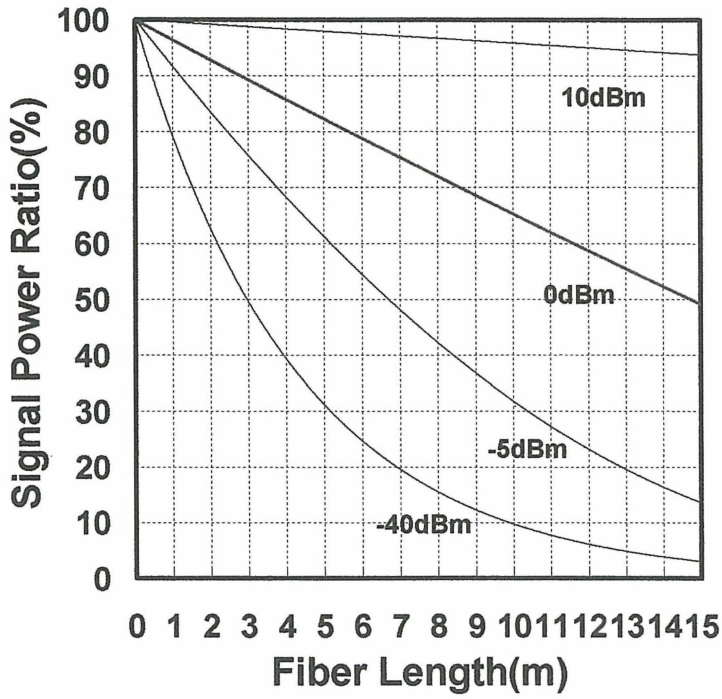

Figure 3 Fiber length dependence of the signal power ratio $P_s(z)/P_s(0)$ with various input signal powers (Ps=-40dBm, -5dBm, 0dBm, 10dBm).

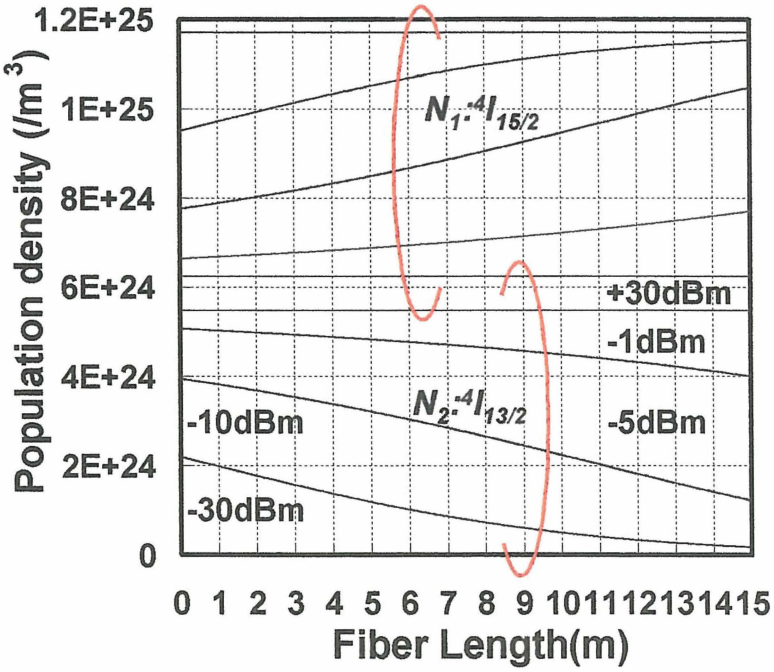

Figure 4 Fiber length dependence of the population densities of the $^4I_{13/2}$ and the $^4I_{15/2}$ level with various input signal powers (Ps=-30dBm, -10dBm, -5dBm, -1dBm, +30dBm).

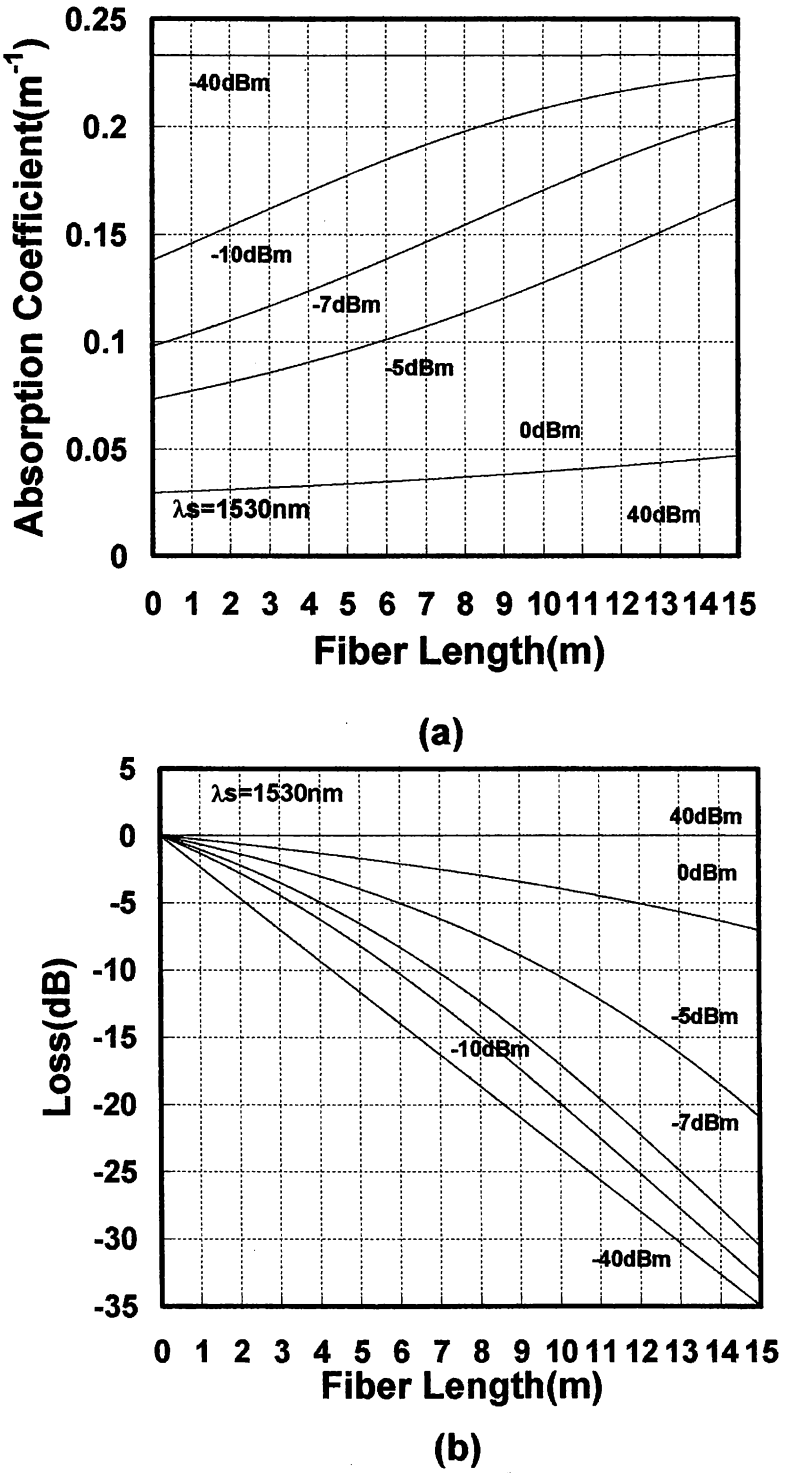

Figure 5 Fiber length dependence of the absorption coefficient (a) and the loss characteristic (b) with various signal input power (-40dBm, -10dBm, -7dBm, -5dBm, 0dBm, 40dBm).

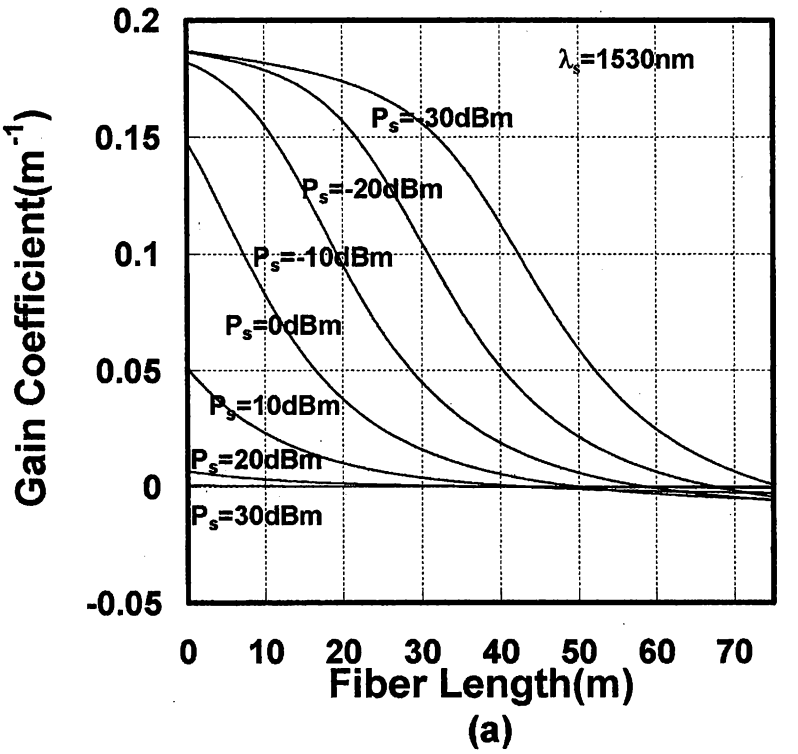

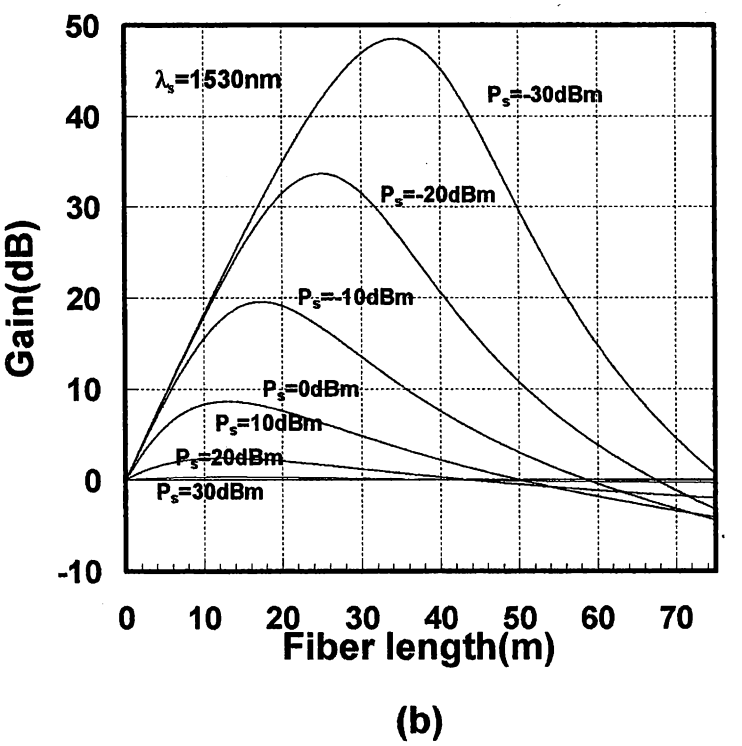

Figure 6 Fiber length dependence of the gain coefficient (a) and the gain characteristic (b) of EDFA with various signal input powers (-30dBm, -10dBm, 0dBm, 10dBm, 30dBm).

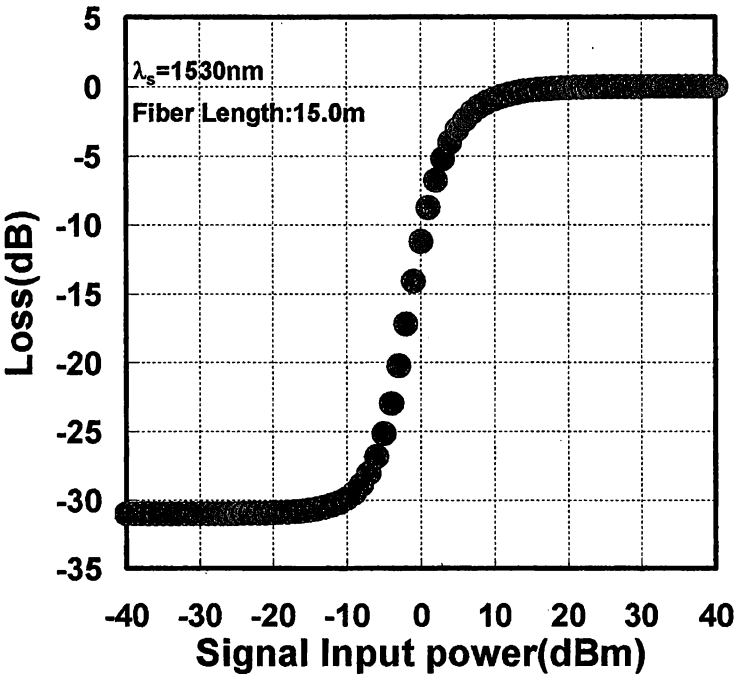

(a)

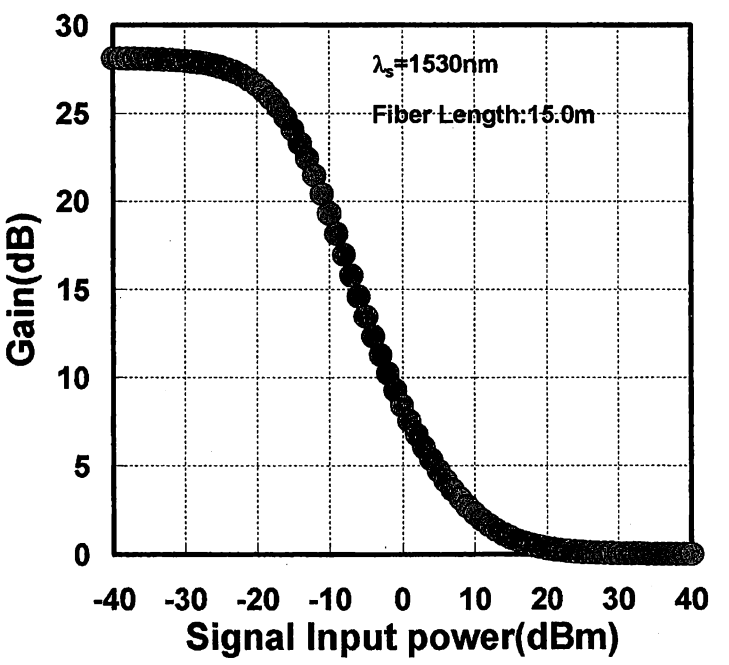

(b)

Figure 7 Signal input power dependence of the saturating loss (a) and the gain (b) characteristics of 15m fiber length EDF

Fig. 4 shows the fiber length dependence of the population densities of the $^4I_{13/2}$ and the $^4I_{15/2}$ with various input signal powers (Ps=-30dBm, -10dBm, -5dBm, -1dBm, +30dBm). The population density of the $^4I_{13/2}$ level becomes almost equal to that of the $^4I_{15/2}$ level with the increasing signal power. This means that the signal absorption comes not to occur as the signal power increases, which corresponds to the signal power dependence of the signal power ratio. Fig. 5(a) and Fig 5(b) show the fiber length dependence of the absorption coefficient and the loss of EDFA wavelength of 1530nm with various input signal power (-40dBm, -10dBm, -7dBm, -5dBm, 0dBm, 40dBm).

On the other hand, Fig. 6(a) and Fig 6(b) show the fiber length dependence of the gain coefficient and the gain characteristics of EDFA at the wavelength of 1530nm with various signal input powers (-30dBm, -10dBm, 0dBm, 10dBm, 30dBm). As shown in Fig. 8, with decreasing signal input power, gain shows a peak value, which shows that there exists optimum fiber length as optical amplifier. In the fiber length region over the optimum length, the gain characteristics of EDFA become to be dominated by the ground state absorption (GSA) of Er^{3+} ion. In the numerical simulation, very high gains are obtained for the low signal input power. However, in experiment, lasing occurs usually in such high output power region to prevent the achieving of the theoretical gain. Fig. 7(a) and Fig. 7(b) show the signal input power dependence of the saturating loss and the gain characteristics of 15m fiber length EDF, respectively. In the two level system, the gain and loss come close to zero in very high signal input power region due to the induced emission and the induced absorption, respectively.

A-2-3 Wavelength dependence of Gain and Loss characteristics of EDFA

Fig. 8 shows the experimental absorption and the theoretical emission cross section. The emission cross section was obtained thorough the McCumber theory using the absorption cross section obtained by the absorption measurement. The McCumber theory, which describes an relation between the emission cross section and the absorption cross section very accurately, are

given by,

$$\sigma_e(\nu) = \sigma_a \exp[(E_0 - h\nu)/kT] \cdot \frac{1 + \sum_{j=2}^{8} 7\exp(-\Delta E_{1j}/kT)}{1 + \sum_{j=2}^{7} 6\exp(-\Delta E_{2j}/kT)} \quad (31)$$

where E_0 is the separation energy between the lowest components of each manifold, which is assumed to be 1530nm. ΔE_{1j} and ΔE_{2j} is the difference in energy between the jth and the lowest components of the $^4I_{13/2}$ and the $^4I_{15/2}$ level. Fig. 9 shows a comparison of an experimental gain with theoretical one. Theoretical gain shape calculated by the numerical simulation recreates experimental gain shape fairy well.

Fig. 10(a) and Fig. 10(b) show the signal input power dependence of the gain and loss characteristics. With increasing signal input power, the gain and loss become close to zero in all wavelength regions from 1420nm to 1640nm, which shows that the population density of the $^4I_{13/2}$ level becomes equal to that of the $^4I_{15/2}$ level. Namely, it indicates that saturation of the $^4I_{13/2}$ level is induced by the strong signal power input. Fig. 11(a) and Fig. 11(b) show the fiber length dependence of the gain and the gain coefficient in the wavelength region from 1420nm to 1640nm. The gain and the gain coefficient are calculated for the 100m length EDFA. As EDF length becomes longer, EDF becomes the absorption media in the wavelength region shorter than 1530nm due to the absorption of Er^{3+} ion. Gain coefficient comes to show the negative value as the fiber length becomes longer in the wavelength region shorter than 1530nm. L-band EDFA, which is used to amplify the signal the wavelength region from 1580nm to 1640nm, exploits this absorption of Er^{3+} ion in the shorter wavelength region than 1530nm.

Fig. 12(a) and Fig. 12(b) show the gain shape in the wavelength region from 1420nm to 1640nm at the beginning and the end of fiber, respectively. At the beginning of the fiber, the gain characteristic becomes that in the C-band EDFA. On the other hand, at the end of the fiber, the gain characteristic becomes that in the L-band EDFA mentioned above.

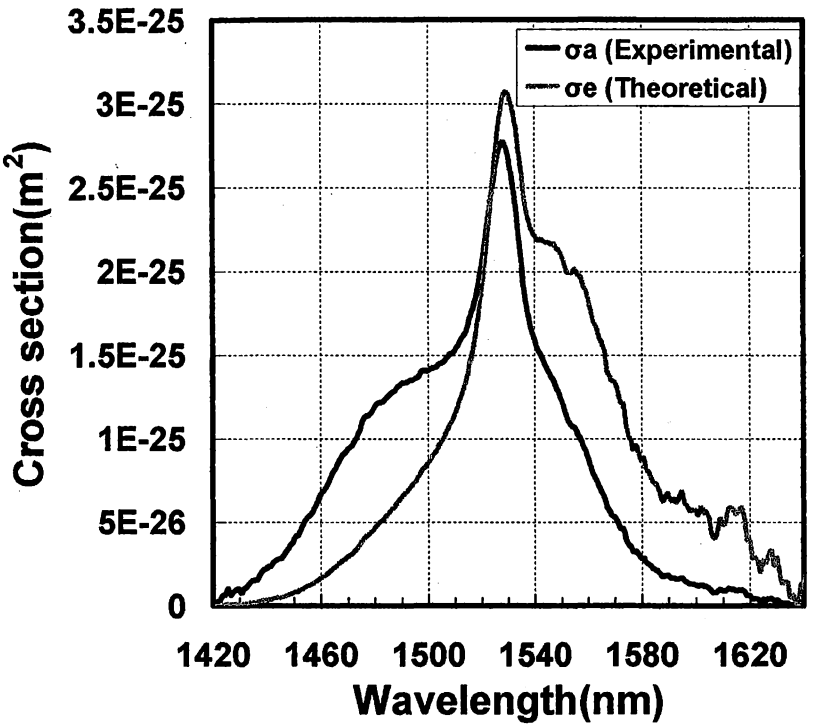

Figure 8 Experimental absorption and the theoretical emission cross section.

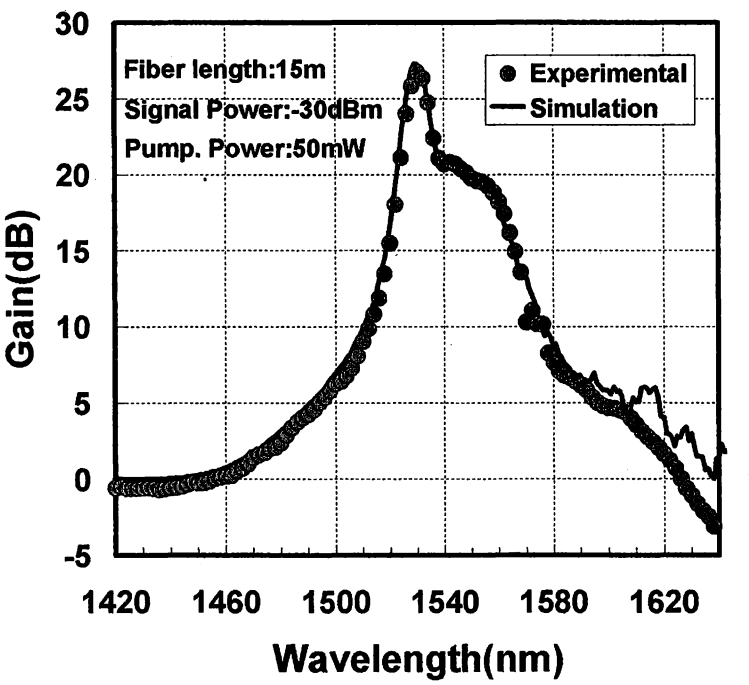

Figure 9 Comparison of an experimental gain with theoretical one calculated by the numerical simulation based on two level system model.

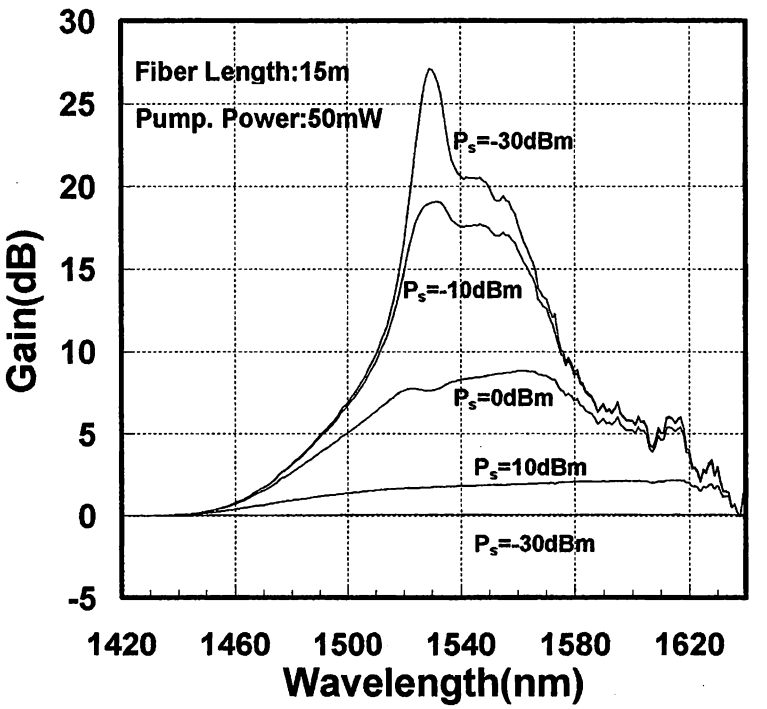

(a)

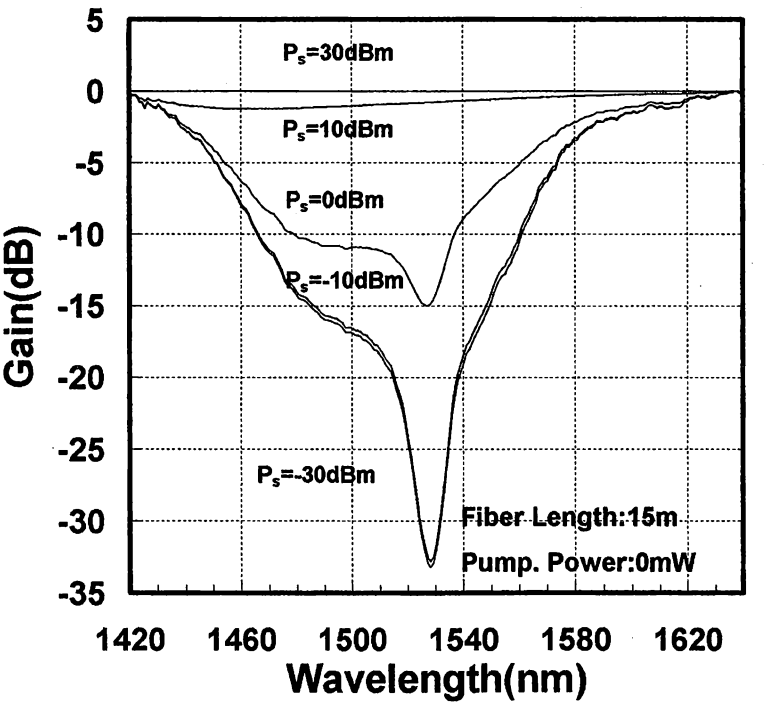

(b)

Figure 10. Signal input power dependence of the gain (a) and loss (b) characteristics.

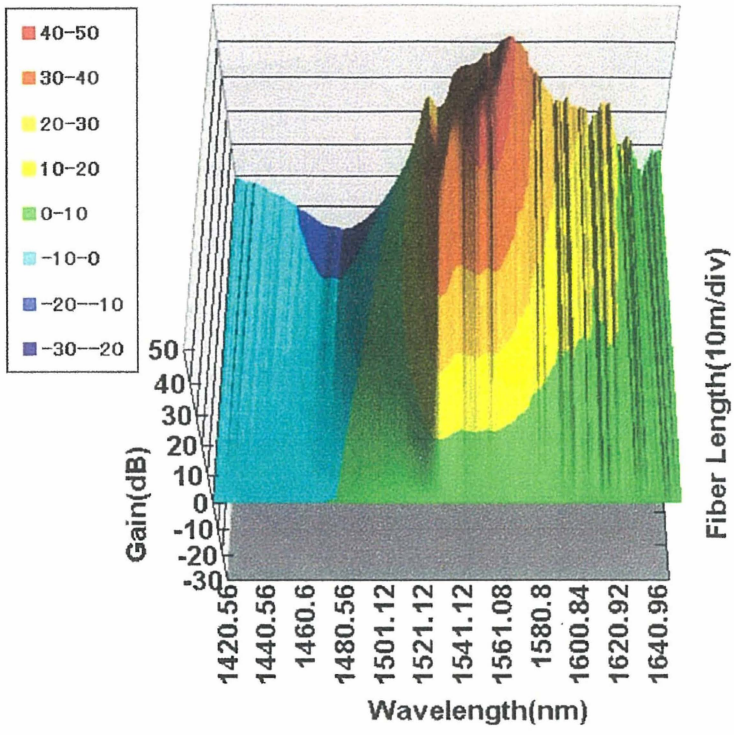

(a)

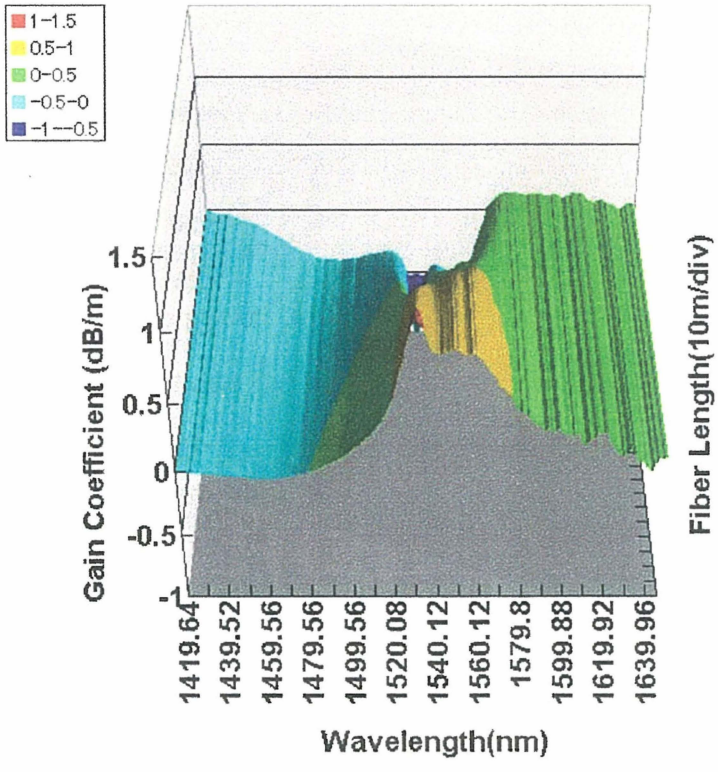

(b)

Figure 11 Fiber length dependence of the gain (a) and the gain coefficient (b) in the wavelength region from 1420nm to 1640nm.

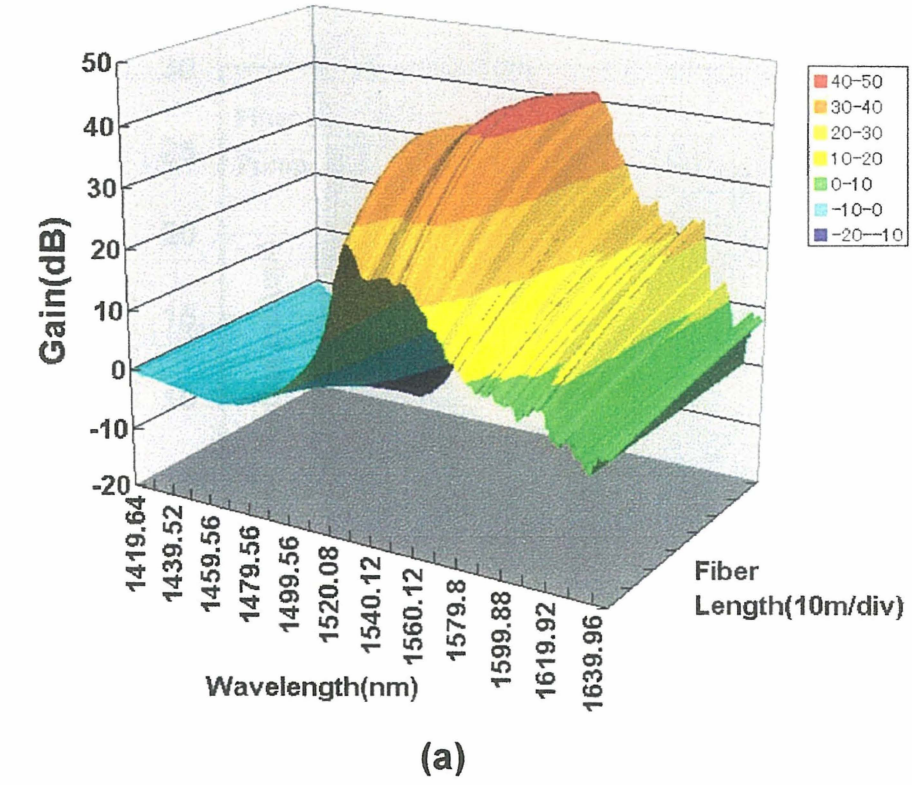

(a)

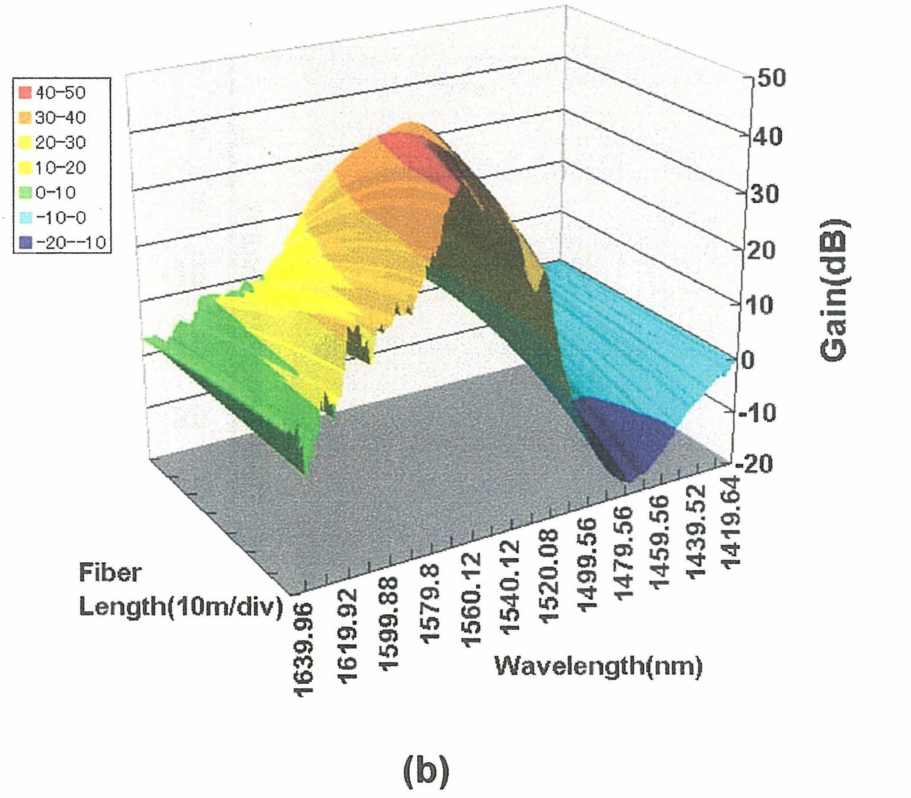

(b)

Figure 12 C-band like (a) and L-band like(b) gain characteristics of EDFA.

Summary

In this thesis, the gain characteristics and optical properties of silica-based erbium-doped fiber amplifier (EDFA) were investigated from many angles based on the spectroscopic studies using the 4f electron transition theory in order to propose the possibility of the realization of advanced EDFA for new optical transmission systems.

In Chapter 1, as the fundamental back ground of this thesis, the development of the optical transmission systems and the optical amplifiers were related with relation to the evolution of laser using the rare earth doped glass host. The promising candidates of the new optical amplifiers that can bring the new transmission bands for the optical telecommunication system were also introduced considering their merits and demerits in the optical transmission system. In addition, the application scheme of advanced EDF to the next high bit rate optical system was also reviewed.

In Chapter 2, the effect of Al_2O_3 doping on the optical properties of EDF was investigated precisely using the Judd-Ofelt analysis. From the 1.5μm absorption measurements of EDF samples, the spontaneous probability $A_{JJ'}$ and line strength $S_{JJ'}$ of the 1.5μm transition increased with increasing Al_2O_3 content in EDF. From the analysis of the1.5μm absorption spectra of EDF samples based on Judd-Ofelt analysis, it was found hat the Ω_6 parameter increases with increasing Al_2O_3 content. The increases of $A_{JJ'}$ and $S_{JJ'}$ are considered to be cause by the increase of the Ω_6 parameter with increasing Al_2O_3 content because the line strength of 1.5 μm ($^4I_{13/2}$-$^4I_{15/2}$) is mainly dominated by Ω_6 parameter. This result indicates that the decrease of local basicity around Er^{3+} ion site occurs with increasing Al_2O_3 content in fibers. In addition, from the Judd-Ofelt analysis, the Ω_2 parameter in fiber form was found to be about three times as large as those in alumino-silicate bulk glasses. This shows that the polarization or asymmetric distortion at Er^{3+} ion site is enhanced in the fiber form than in the bulk glass. The increase of the four-coordinated Al^{3+} ion in alumino-silicate EDF with increasing Al_2O_3 content

was proposed for one explanation about the decrease of local basicity and symmetry of the Er^{3+} ligand field in fiber form.

In Chapter 3, the S-band gain (1480nm-1530nm) characteristics of alumino-silicate EDF were investigated using the numerical and experimental measurements. Firstly, the temperature dependence of the gain property of 10m-lengh silica-based EDFA was investigated experimentally. As a result, about 2dB increase of the S-band gain was observed as temperature increased up to 373K. To examine the origin of the increase of gain in the S-band wavelength region, the temperature-dependent McCumber simulation model was built up for the two level energy system of Er^{3+} ion using McCumber theory. In comparison with the experimental result, it was verified that the temperature-dependent McCumber simulation model could explain well the experimental gain characteristics in the S-band wavelength region numerically. Therefore, the increase of experimental S-band gain observed with increasing temperature is considered to be caused by the change of the population density in the Stark manifolds of the $^4I_{13/2}$ and the $^4I_{15/2}$ state, which could bring about 0.2dB/m improvement in S-band gain coefficient. In addition, it was proved that the temperature-dependent McCumber simulation model is applicable to the prediction for the S-band gain characteristics of EDF. On the other hand, the gain spectrum in the C-band and the L-band wavelength regions showed different temperature dependence from that of the temperature-dependent McCumber simulation model. The origin of these temperature-dependent gain characteristics in the C-band and the L-band wavelength regions is not made clear at present.

In Chapter 4, the effect of Er^{3+} concentration quenching on the gain characteristics of silica-based EDF was investigated, particularly focusing on the effect of pair induced quebching (PIQ). From the 1.5μm absorption measurements of silica-based EDF samples, it was found that the nonradiative decay rate increases significantly with increasing Er^{3+} ion concentration. This significant increase of nonradiative decay rate can be ascribe to the enhancement of the nonradiative energy transfer between Er^{3+} ions due to the increasing Er^{3+} ion concentration.

The nonradiative energy transfer to some defects or OH in EDF samples is also considered to be enhanced with increasing Er^{3+} ion concentration. The Er^{3+} ion concentration dependences of the power conversion efficiency (PCE) and quantum efficiency (QE) were also evaluated. And both of them increase with increasing Er^{3+} ion concentration. About 20% degradation of PCE and 26% of QE occurred in highly-erbium doped. These Er^{3+} ion concentration dependence of spontaneous emission probability, nonradiative decay rate, PCE and QE indicate that the degradation of the gain characteristics is expected to occur in highly erbium doped fiber.

To evaluate the effect of concentration quenching on the gain characteristics of EDFA precisely, the gain simulator considering the clustered and isolated ions was built up. As a result of the analysis on the experimental gains using this numerical gain simulator, it was estimated that even about 2% paired Er^{3+} ions in silica-based EDF can cause about 10% degradation of the population densities of the $^4I_{13/2}$ level, which leads to about 1dB degradation of the gain spectrum. In addition, Er^{3+} concentration dependence of the normalized population density of the $^4I_{13/2}$ state and the paired Er^{3+} ion number were evaluated. As results of the evaluation, it was found that the paired Er^{3+} ion number increases linearly with increasing Er^{3+} ion concentration. On the other hand, the population density of the first excited state was found to degrade with increasing Er^{3+} ion concentration.

In Chapter 5, the characteristics of gain spectral hole burning (GSHB) were investigated at 77K, focusing on Er^{3+} ion concentration dependence of the gain spectral hole depth.

At 77K, as expected, sharper and deeper main and second holes were observed compared with that at room temperature. In addition to a main hole burned at the wavelength of a saturating signal, the second hole was also burned at around 1530nm. The wavelength of the second hole was independent of that of main hole. These characteristics of holes are consistent with those at room temperature. The main and second hole depths decreased as the saturating signal wavelength became longer in all EDF samples with different Er^{3+} ion concentration. The main and second hole characteristics indicate the decrease of the population inversion ratio

and the number of the transitions between the Stark manifolds of Er^{3+} ion, which have resonant wavelength with that of the saturation signal. At 77K, about 90% of the excited Er^{3+}ion are populated in the lowest two Stark levels within the $^4I_{13/2}$ state. Therefore, the decrease of the population inversion ratio between the Stark manifolds of Er^{3+} ion is considered to be mainly caused by the increase of the population density of the lower Stark manifolds within the $^4I_{15/2}$ state. The main hole width was found to become broader even at 77K in the L-band region than that in the C-band region. On the other hand, the second hole width did not show the saturation signal wavelength dependence in the C-band and the L-band regions. In this thesis, the explanation for this saturation wavelength dependence of the main and second hole width was tried to made in terms of the difference among the relaxation times of the Stark manifolds of Er^{3+} ions. However, the origin of the difference between the saturation wavelength dependence of the main and second hole width is not made clear completely at present.

In addition, the second hole depth was found to show the Er^{3+} ion concentration dependence and become deeper with decreasing Er^{3+} ion concentration when a high saturating signal was input. As far as we know, this is the first report of the Er^{3+} concentration effect on the gain spectral hole burning in the Er^{3+} doped fiber. For this Er^{3+} ion content dependent hole depth characteristics, the nonradiative energy transfer mechanism among Er^{3+} ions was proposed.

These gain spectral hole characteristics are considered to be common in other gain media which exploit the 1.5 μ m emission of Er^{3+} ion such as erbium-doped waveguide and erbium-doped fiber ring laser because these Er^{3+} ion concentration dependent GSHB characteristics is considered to be originated from the Stark manifolds structure of Er^{3+} ions and the nonradiative energy transfer between Er^{3+} ions.

In Chapter 6, the main hole accompanied with two side holes was reported to be observed at 77K for the first time as far as we know. These two side holes were separated form the main hole by about 10nm which almost corresponds to the energy gap between the first excited and lowest Stark manifold within the $^4I_{15/2}$ state of Er^{3+} ion. The existence of side holes indicates

that the formation mechanism of holes is closely-linked to the Stark manifold structure of Er^{3+} ion. At 77K, almost of all the excited Er^{3+}ion are populated in the lowest two Stark levels within the $^4I_{13/2}$ state. Therefore, in addition to a main hole, these side holes also seem to be induced by the depopulation of the population density of the lowest two Stark levels within the $^4I_{13/2}$ state. So far, gain spectral hole has been considered to be burned and localised at around 1530nm and the wavelength of saturation signal. And the effect of the gain spectral hole burning on the gain characteristics is also considered to be confined to the localised wavelength region. However, from our experimental results at 77K, it was shown that there can exist additional holes in much wider wavelength region than expected. Therefore, gain spectral hole burning seems to have more wide-raging impact on the gain shape and the gain fluctuation of EDF.

As a continuation of the previous work, the Er^{3+} ion concentration and wavelength dependence of the gain spectrum holes at 77K were also investigated. From the comparison among side hole depths in three EDFs, side holes was found to show the same Er^{3+} ion concentration dependence as that of the second hole depth when the wavelength of the saturation signal was varied in the C-band and the L-band wavelength regions.

When the wavelength of the saturating signal were varied, the depth of the second hole at 77K was found to show the two peaks at around 1545nm and 1590nm and not to decrease monotonically with increasing the saturating signal wavelength. This saturating signal wavelength dependence was different from that observed at room temperature.

Relaxation characteristics of the holes were also measured for the first time. It was found that main and second holes remained even when 5ms had passed after optical pulse vanished. However, it cannot be judged precisely whether the difference between the relaxation times of the main holes and second holes occurs or not. Therefore, further studies on the relaxation time of holes are awaited for the better understandings of the gain spectral hole characteristics in the future.

List of Publications

Chapter. 2 S. Ono and S. Tanabe, "Evidence of enhanced hypersensitive transition in erbium-doped fibers with different Al_2O_3 content," IEEE Journal of Quantum Electronics, vol. 40, no. 12, pp. 1704-1708, 2004.

S. Ono and S. Tanabe, "Precise characterization of Er^{3+} ions in fibers with different Al_2O_3 content," OSA Trends in Optics and Photonics (TOPS), Optical Amplifiers and Their Applications 2003, November, 2003,vol. 92, pp. 8-12.

Chapter. 3 S. Ono and S. Tanabe, "Evaluation of the quenching effect on gain characteristics in alumino-silicate erbium doped fiber using numerical simulation," Journal of Alloys and Compounds, in press.

Chapter. 4 S. Ono and S. Tanabe, " Numerical and experimental evaluation of S-band gain characteristics of erbium-doped fiber," IEEE Journal of Quantum Electronics, submitted.

Chapter. 5 S. Ono, S. Tanabe, M. Nishihara and E. Ishikawa, "Study on the dynamics of gain spectral hole in silica-based erbium-doped fiber at 77K," Journal of Optical Society of America B, submitted.

S. Ono, S. Tanabe, M. Nishihara and E. Ishikawa, "Effect of erbium ion concentration on gain spectral hole burning in silica-based erbium-doped fiber," Optical Fiber Communication Conference (OFC 2005), OThL1, Anaheim, USA, 2005, accepted.

Chapter. 6 S. Ono, S. Tanabe, M. Nishihara and E. Ishikawa, "Saturating signal wavelength dependence of gain spectral hole burning in erbium-doped fiber at 77K," Optics Letters, submitted.

Acknowledgements

First of all, the author would like to express special thanks to Associate Prof. Setsuhisa Tanabe (Kyoto University), who supervised the present work, for his directions, arrangement of the experimental set-up and of a collaborative study with FUJITSU LABORATORIES LTD.

Author would like to express his sincere gratitude to Ms. Etsuko Ishikawa and Mr. Masato Nishihara (FUJITSU LABORATORIES LTD) for their technical supports and fruitful discussions filled with implication in the collaborative meeting. Author could never finish this thesis without their helpful supports. Author also would like to appreciate the sample supply by Optical Devices Development Department, FUJITSU LTD.

Grateful acknowledgements are made to Prof. Tetsusuke Hayashi (Kyoto University) and Dr. Masayuki Watanabe (Kyoto University) for his valuable suggestions, helpful discussions.

Author wishes to specially thank Dr. Jack Stoneman (Columbia University) for his warm encouragements and his advice based on his deep insight into Japanese culture.

Author also wishes to thank Mr. Masayuki Nishi, Mr. Hiroshi Yamazaki, Mr. Masafumi Onishi, Mr. Yuki Kishi, Ms. Haruko Horiguchi, Mr. Takeshi Tamaoka and all members of related laboratories for their helpful discussions and excellent assistance in the experimental work. Last but not least, author express to sincere gratitude to my parents, Mr. Masao Ono and Ms. Masako Ono for their encouragements.

Sakyo, Kyoto

January, 2005

Shunsuke Ono